Institut für Erd- und Umweltwissenschaften
Mathematisch-Naturwissenschaftliche Fakultät
Universität Potsdam

East African monsoon variability since the last glacial

Kumulative Dissertation

zur Erlangung des akademischen Grades

doctor rerum naturalium (Dr. rer. nat.)

eingereicht an der

Mathematisch-Naturwissenschaftlichen Fakultät

der Universität Potsdam

von

Christian Wolff

Potsdam, Juli 2011

Principal supervisor:

Prof. Dr. Gerald H. Haug
Universität Potsdam - DFG Leibniz Center for Surface Process and Climate Studies
ETH Zürich - Geologisches Institut

Co-supervisors:

Prof. Dr. Dirk Verschuren
Ghent University - Department of Biology, Research group Limnology

Prof. Dr. Achim Brauer
Universität Potsdam
Helmholtz-Zentrum Potsdam, Deutsches GeoForschungsZentrum GFZ

Published online at the
Institutional Repository of the University of Potsdam:
URL http://opus.kobv.de/ubp/volltexte/2012/5807/
URN urn:nbn:de:kobv:517-opus-58079
http://nbn-resolving.de/urn:nbn:de:kobv:517-opus-58079

In East Africa, rainfall is never right – there is either too much or too little!

Table of contents

Abstract

The impact of global warming on human water resources is attracting increasing attention. No other region in this world is so strongly affected by changes in water supply than the tropics. Especially in Africa, the availability and access to water is more crucial to existence (basic livelihoods and economic growth) than anywhere else on Earth. In East Africa, rainfall is mainly influenced by the migration of the Inter-Tropical Convergence Zone (ITCZ) and by the El Niño Southern Oscillation (ENSO) with more rain and floods during El Niño and severe droughts during La Niña. The forecasting of East African rainfall in a warming world requires a better understanding of the response of ENSO-driven variability to mean climate.

Unfortunately, existing meteorological data sets are too short or incomplete to establish a precise evaluation of future climate. From Lake Challa near Mount Kilimanjaro, we report records from a laminated lake sediment core spanning the last 25,000 years. Analyzing a monthly cleared sediment trap confirms the annual origin of the laminations and demonstrates that the varve-thicknesses are strongly linked to the duration and strength of the windy season. Given the modern control of seasonal ITCZ location on wind and rain in this region and the inverse relation between the two, thicker varves represent windier and thus drier years. El Niño (La Niña) events are associated with wetter (drier) conditions in east Africa and decreased (increased) surface wind speeds.

Based on this fact, the thickness of the varves can be used as a tool to reconstruct a) annual rainfall b) wind season strength, and c) ENSO variability. Within this thesis, I found evidence for centennial-scale changes in ENSO-related rainfall variability during the last three millennia, abrupt changes in variability during the Medieval Climate Anomaly and the Little Ice Age, and an overall reduction in East African rainfall and its variability during the Last Glacial period. Climate model simulations support forward extrapolation from these lake-sediment data, indicating that a future Indian Ocean warming will enhance East Africa's hydrological cycle and its interannual variability in rainfall.

Furthermore, I compared geochemical analyses from the sediment trap samples with a broad range of limnological, meteorological, and geological parameters to characterize the impact of sedimentation processes from the in-situ rocks to the deposited sediments. As a result an excellent calibration for existing µXRF data from Lake Challa over the entire 25,000 year long profile was provided.

The climate development during the last 25,000 years as reconstructed from the Lake Challa sediments is in good agreement with other studies and highlights the complex interactions between long-term orbital forcing, atmosphere, ocean and land surface conditions. My findings help to understand how abrupt climate changes occur and how these changes correlate with climate changes elsewhere on Earth.

Zusammenfassung

Änderungen des Klimas in einer sich erwärmenden Erde haben große Auswirkungen auf den globalen und lokalen Wasserhaushalt und rücken anhand starker Extremereignisse immer häufiger in den Fokus der Öffentlichkeit. Besonders die Regionen der Tropen sind von derartigen Einschnitten stark gefährdet. Der jährliche Niederschlag in Ostafrika ist stark mit der saisonalen Wanderung der ITCZ (Innertropischen Konvergenzzone) sowie mit dem El Niño/Southern Oscillation (ENSO) Phänomen verbunden. Extreme Regenfälle und Überschwemmungen während El Niño Jahren stehen Trockenheit und Dürren in La Niña Jahren gegenüber. Prognosen über zukünftige Veränderungen der ostafrikanischen Niederschläge erfordern ein verbessertes Verständnis der ENSO antreibenden Faktoren. Unglücklicherweise sind die vorhandenen meteorologischen Datenreihen nicht lang genug oder besitzen nicht die benötigte Homogenität. Einen hilfreichen Beitrag können jährlich geschichtete Seesedimente des am Fuße des Kilimandscharo gelegenen Lake Challa leisten. Anhand einer monatlich aufgelösten Sedimentfalle konnte ich nachweisen, dass die rund 25.000 Jahre zurückreichenden Sedimente eine jährliche Struktur besitzen sowie die Dicke dieser jährlichen Schichtung (Warve) stark mit der Dauer und Intensität der saisonal windreichen/trockenen Jahreszeit verbunden ist. Dickere Warven repräsentieren windige/trockene Jahre, wohingegen dünnere Warven für windschwache und feuchte Jahre stehen. Stärkere Winde und kaum Niederschläge treten oft im Zusammenhang mit einem La Niña Ereignis in Ostafrika auf, wohingegen während eines El Niño Ereignisses häufig extreme Niederschläge mit wenig Wind zu beobachten sind. Anhand der Vermessung der Warven kann man verschiedene Klimaparameter rekonstruieren: a) den jährlichen Niederschlag b) jährliche Windgeschwindigkeiten und ihre Intensitäten sowie c) ENSO Variabilitäten. Die in meiner Arbeit gewonnenen klimatischen Informationen zeigen starke Änderungen der ENSO Variabilität innerhalb der letzten 3.000 Jahre mit starken Unterschieden während der Kleinen Eiszeit und während der Mittelalterlichen Warmzeit sowie deutlich trockene und windige Bedingungen mit sehr geringen ENSO Aktivitäten im glazialem Zeitraum (18.500 und 21.000 Jahren). Modellberechnungen unterstützen diese Ergebnisse einer Zunahme von Extremereignissen und feuchteren Bedingungen im Zuge einer Erwärmung des Indischen Ozeans. Mittels geochemischer Analysen der Sedimentfallenproben sowie die daraus resultierende Verknüpfung mit limnologischen und meteorologischen Parametern, konnte ich einen entscheidenden Beitrag zur erfolgreichen Interpretation der existierenden 25.000 Jahre langen µXRF Datensätze leisten. Der Anteil an allochthonem und autochthonem Eintrag kann so genau klassifiziert werden. Das dadurch gewonnene Bild der Klimaentwicklung der letzten 25.000 Jahre deckt sich hervorragend mit anderen Studien und ermöglicht Einblicke in das komplexe Zusammenspiel zwischen Ozean-Atmosphäre und Umwelt auf dem afrikanischen Kontinent. Besonders die für die Ostafrikaforschung extrem hohe Auflösung der Daten wird helfen, die abrupten Klimawechsel und Interaktionen besser verstehen zu können.

Acknowledgement

This research was financed by the European Science Foundation (ESF) funded CHALLACEA project, a fellowship from the German Research Foundation (DFG) Graduate School GRK 1364 "Shaping Earth's Surface in a Variable Environment", and the Leibniz Center for Earth Surface Process and Climate Studies at the University of Potsdam.

First of all, I would like to thank Gerald H. Haug for making this project possible and his permanent willingness to support and advice my research. He guided and encouraged me in every possible way and helped me to see my work from a bigger point of view.

I thank the coordinator of the CHALLACEA project Dirk Verschuren to support me during the first field season on the African continent and many stimulating discussions. I will always remember the hot sunny day without sun protection we spent together in a small boat on Lake Challa. In this respect, I would like to thank all members of the CHALLACEA project and all people who helped me with the organization and logistics of my field-work in Kenya, especially Caxton M. Oluseno. Without your straightforward and friendly help this thesis would not be possible.

This thesis would not exist without the indefatigable assignments of all Co-authors on numerous manuscript discussions. Thanks a lot.

Accordingly, I would like to acknowledge the Helmholtz Centre Potsdam **(**GFZ - German Research Centre for Geosciences). Particularly, Achim Brauer and the staff of Section 5.2, they ever gave me the feeling to be a part of this section and not a guest. In this way: Nobert, Ute and Marcus thanks for your daily reminder that a hungry belly does not like to learn.

I am grateful to Manfred Strecker for managing the Graduate School GRK 1364. In this respect I thank all members of the graduate school for fruitful discussion, unprecedented team spirit, funny evenings in Potsdam's "Waschbar", and an unforgettable time during our two excursions to Kenya and the Indian Himalaya.

I am grateful to Tom Johnson and his wife Kate and all members of the Large Lake Observatory in Duluth/Minnesota including the crew of the 'Blue Heron' for an excellent stay. Will, Ryan, Tony, and all the rest from the Woodland Avenue 918. Thanks for a fantastic summer.

A special thank goes to Henry Wichura, Olga Kwiecien, Susanne Stefer, Hans von Suchodoletz, Sebastian Breitenbach, Tina Swierczynski, Clara Mangili, and Andreas Höchner for a wonderful friendship - also outside the scientific walls.

Finally, I express my sincere gratitude for the encouragement and infinite support in so many ways to my family; and last but not least I would not have been able to finish this project without the help and unconditional love from Maria.

1 Introduction

No other region in this world is so strongly faced with water supply than the tropics. Especially in Africa, the availability and access to water is more crucial to existence (basic livelihoods and economic growth) than it is almost anywhere else on Earth.
Over 63 % of sub-Saharan Africa's population is rural (http://data.worldbank.org) and most of them live on small subsistence farms. 95 % of sub-Saharan Africa's farmland relies on rain-fed agriculture (Wani et al., 2009), making most people heavily dependent on annual rainfall pattern. African rainfall variations on seasonal scale are mainly influenced by the migration of the Inter-Tropical Convergence Zone (ITCZ) and the El Niño Southern Oscillation (ENSO) system [chapter 1.2.1].
Unfortunately, the existing instrumental records are too short to evaluate the ITCZ and ENSO system and its long-term response to climate forcing such as global insolation and its interaction between atmospheric and oceanic circulations. This has led to extend the modern records back in time by using historical documents and climate archives. For this reason, an archive is needed which can provide information on temporal pattern of ITCZ migration as well as the qualification to reconstruct processes on annual timescales such as ENSO dynamics at different hydrological conditions.
The study of an annual record from lacustrine sediments from the lower east slope of Mt. Kilimanjaro can give new insights in moisture variabilities since the Last Glacial Maximum (LGM) and may help to characterize a) the rate and timing of climate changes b) global teleconnection patterns with rainfall variability and c) provide new aspects in ENSO activity in a greenhouse-induced warmer future.

1.1 Structure of the thesis

This thesis is organized as a "cumulative thesis" and consists of a series of six chapters (without references and appendix). Chapters 2-5 consist of four individual manuscripts to be published in international peer-reviewed scientific journals. Two manuscripts (chapters 3 and 4) have been already accepted while the other two manuscripts (chapters 2 and 5) have been either submitted or are supposed to be submitted. An outline of each chapter and the contributions of the individual co-authors are provided below. The structure of the thesis (chapter 2-5) is arranged in terms of sample resolution. Chapter 2 focuses on data in monthly resolution via a monthly cleared sediment trap. Chapter 3 is based on annual resolutions, while chapter 4 and 5 discuss data at decadal resolution. Presenting data on different time scales improves the integration of seasonal information in data at millennial time scale and, thus the understanding of seasonal climatic related questions such as seasonality extremes.

CHAPTER 1

Introduction

The first chapter presents the general issue of climate change and the relevance of this thesis for palaeoclimatology and briefly providing an overview about African climate.

CHAPTER 2

Modern seasonality in Lake Challa (Kenya/Tanzania) and its sedimentary documentation in recent lake sediments

From Lake Challa, a hardwater lake on the eastern slope of Mt. Kilimanjaro, a 3-year (November 2006-January 2007) monthly cleared sediment trap was analyzed. In a combined study, microfacies and geochemical data from sediment trap samples were compared with a broad range of limnological, meteorological and geological parameters to characterize the impact of sedimentation processes from the in-situ rocks to the deposited sediments. The first author collected and prepared the samples and helps to analyze the data in cooperation with the head of the relevant laboratory. Based on this data, the first author established a sedimentation model and furthermore led the writing of the first version of the manuscript. All Co-authors provided fruitful discussions and helped in finishing and improving the final manuscript version.

CHAPTER 3

Reduced interannual rainfall variability in East Africa during the last ice age

Chapter 3 is the main part of the thesis and integrates results from chapter 2. Varve thickness data show evidence for interannual to centennial – scale changes in ENSO-related rainfall variability during the last three millennia and an overall reduction in East African rainfall and its variability during the Last Glacial period. The first author developed the varve thickness-ENSO relation model and wrote a first version of the manuscript. All Co-authors provided ideas for discussion and helped in finishing and improving the final manuscript version.

CHAPTER 4

Seasonality in precipitation and evaporation for the last 25,000 years revealed by oxygen isotope records from Mount Kilimanjaro

In this chapter the authors present a continuous 25 ka oxygen isotope ($\delta^{18}O$) record extracted from diatom silica in the sediments of Lake Challa. We use diatom $\delta^{18}O$ as a proxy of annual moisture balance. In comparison with other proxies, annual rainfall reveals previously unknown variation in the seasonality of rainfall and drought during the last 25 ka. In this manuscript, I produced the modern water isotope data and helped to develop the model of annual moisture balance. Furthermore, I helped in finishing and improving the final manuscript.

CHAPTER 5

Lake Challa sediments - Variations of East African wind and rainfall intensities over the past 25,000 years

Chapter five is a part of a manuscript which used results from Chapter 2 to characterize µXRF data over the last 25,000 years. The second author led the writing of the paper and calibrates the existing sediment trap results with µXRF data.

CHAPTER 6

Summary

Chapter six presents the main conclusions of the combined results obtained from this thesis.

1.2 Lake Challa

1.2.1 Location - Modern climate conditions

Lake Challa is a fresh-water crater lake on the lower eastern flank of Mt. Kilimanjaro. It is located at an elevation of ~880 m above sea level (asl) and embedded in igneous rocks of the tertiary Kilimanjaro complex (Bear, 1955). These trachy-basaltic volcanics are covered by calcite cemented tuffaceous breccias that are most likely related to the formation of the Challa crater (Downie and Wilkinson, 1972). As the estimated evaporation of ~1700 mm/yr is significantly higher than the precipitation (~600 mm/yr; (Payne, 1970)), the water budget of this ~98 m deep and 4.2 km² large lake is probably controlled by sub-surface inflow. This sub-surface inflow is presumably driven by the percolation of precipitation falling on or above the forest zone of Mt. Kilimanjaro. Because of its steep crater walls, the catchment area is nearly identical to the lake surface and keeps the surface inflow by direct runoff very limited. However, rainfall in equatorial regions is drastically affected by seasonal shifts of the ITCZ (Intertropical Convergence Zone) (Fig. 1-1), the low-pressure belt between the Hadley cells, where the trade winds of the Northern Hemispheres (Northeasterly Trades) and Southern Hemisphere (Southeasterly Trades) converge.

During the year the position of the ITCZ changes with the zenith position of the sun. This intense radiation and subsequent surface warming heats the air in the ITCZ and increases its humditiy by higher evaporation. Accompanied by the convergence of the trade winds, the heated air rises, cools down with increasing altitude, and finally releases the accumulated moisture. Absence or presence of the ITCZ can cause extreme drought or flooding events in nearby areas. The twice-passage of the ITCZ over tropical East Africa and therefore at Lake Challa induces two rain seasons, from October to December (long rains) and from March to May (short rains).

The temperatures are lowest during the southern hemisphere winter (June-August) and reach its highest values during southern hemisphere summer (November-March) (Fig. 1-1 b). In contrast, the wind speeds show the opposite pattern. Whereas strong winds from May to October are related to the

south-easterly trade winds during the period of a northward displaced ITCZ, weaker winds from November to April are controlled by the north-easterly trade winds, which are generated when the ITCZ is located.south of Lake Challa (Fig. 1-1 a+c).

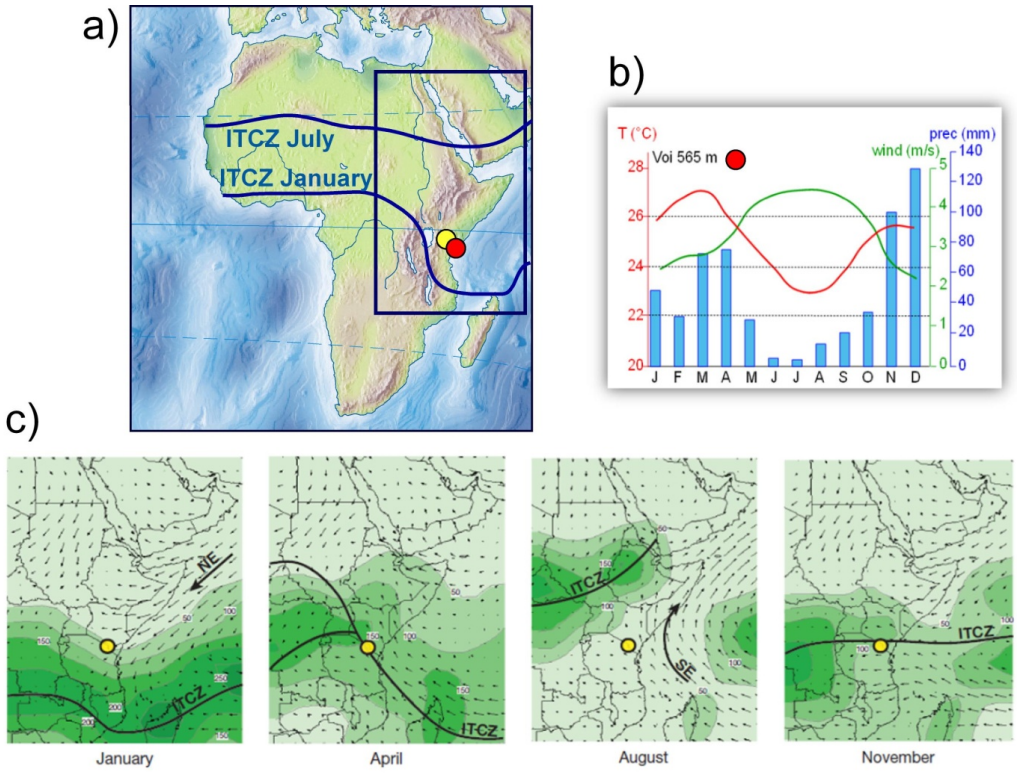

Fig. 1-1: Illustration of modern climate features: a) Location of Lake Challa (yellow dot) and Voi (red dot), blue line indicates the maximum extension of the Inter Tropical Convergence Zone (ITCZ); b) climate diagram from Voi station (red dot) illustrates the two rain seasons, the annual temperature, and wind speed trend; c) Seasonal migration of the ITCZ in relation to Lake Challa (green contours illustrate precipitation at 50 mm intervals; arrows indicate wind direction at 925 hPa and arrow-length show wind-speed vectors (from http://iridl.ldeo.columbia.edu).

Furthermore, the rainfall characteristics in East Africa are tightly linked to the El Niño Southern Oscillation (ENSO) system, with heavy rainfall and flood events during El Niño and extreme drought during La Niña years. This phenomenon is related to an ocean circulation pattern in the Pacific Ocean, which occurs in intervals of 2 to 7 years. Its impact on climate on global scale is only known for the last few decades. Normally, a subtropical high-pressure cell (Fig. 1-2 b), located west of South America, transports warm sea surface water northwards along the coast of South America to the area affected by the southern trade winds. These winds transport warm sea surface water from the equator towards the west, following the east-west pressure contrast in Australia/Indonesia and allow the deeper cold water to well up. The physical nature of these cold waters is that it releases only a few amounts of water vapor. Hence, large parts of South America are influenced by dry conditions. In contrast, the warm surface water in the region around Australia/Indonesia provides an enormous resource for water vapor and induces rainfall in this area. Conditions that differ from this normal state are called El Niño and La Niña and describe the opposite phases of the ENSO system. Specifically, La Niña is sometimes

referred as the cold phase and El Niño as the warm phase of ENSO. During an El Niño event, the weakening of the southern trade winds in the central and western Pacific leads to a depression of the thermocline in the eastern Pacific and an elevation of the thermocline in the west. This process reduces the efficiency of the cool-water upwelling and results in an increase of the sea surface temperature along the coast of South America (Fig. 1-2 c) and a rainfall shift following the warm water from the western Pacific to South- and Central America. The western Pacific is influenced by cooler conditions caused by the loss of warm ocean water and bring drier conditions to the region of Australia and Indonesia. Large changes in global atmospheric circulations are connected to eastward migration of warm water and force weather conditions to change in regions far away from the Pacific Ocean.

The cold counterpart of El Niño is La Niña, basically characterized by a cooler eastern pacific (Fig. 1-2 a). During a La Niña extreme the trade winds become unusually strong, which is an effect of an enhanced pressure gradient between South America and Australia. As a result, an intensified upwelling of the Pacific thermocline occurs along the coast of South America. That means that more deep cold water cools the sea surface waters of the eastern tropical Pacific. As a consequence, extreme dry conditions develop along the coast of South America. Because of stronger trade winds, the sea surface waters in the western tropical Pacific, which are warmer than normal, bring more rainfall in this region.

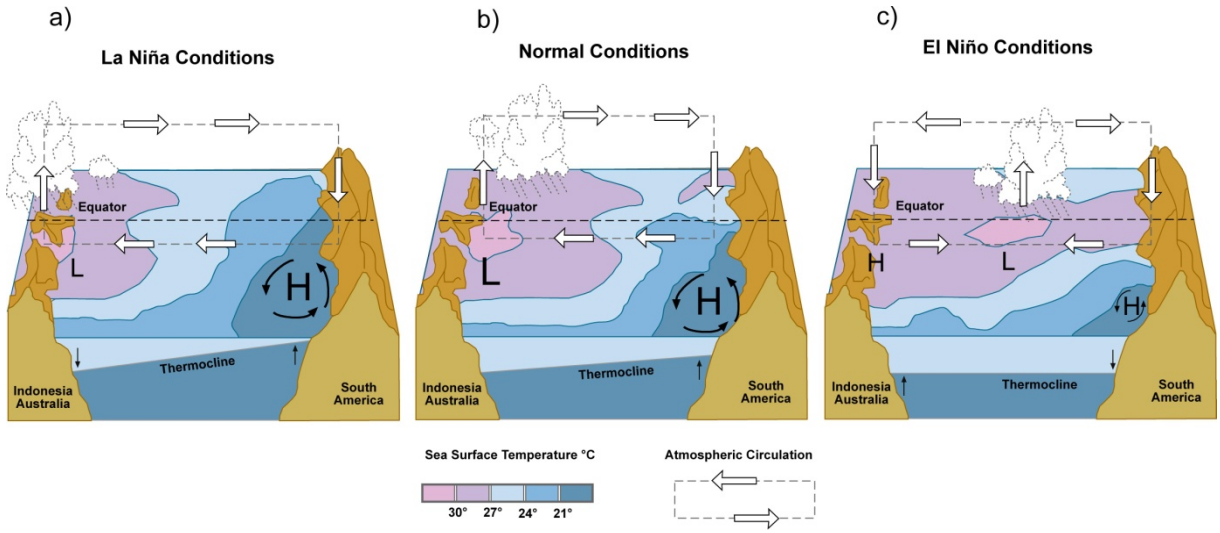

Fig. 1-2: State of the Pacific Ocean during different phases of ENSO a) during La Nina (cold ENSO); b) normal conditions; c) during El Nino (warm ENSO).

Based on its complex nature, it is difficult to define ENSO as a single universal ENSO index, which fully represents all the related complex oceanic and atmospheric conditions (Trenberth, 1997). Currently, many indices are defined to represent ENSO events. The most commons are based on sea surface pressure differences between Darwin and Tahiti (Southern Oscillation index (SOI) back to 1880's) and the Niño 3.4 index (>1950), which is based on sea surface temperature (SST) anomalies on a defined area in the central pacific. Other ENSO indices based on satellite data are often more precise and used to estimate current ENSO events. However, in general they are too short for an identification of the typical ENSO pattern. For a better understanding of this phenomenon, the development of a model, which has the ability to predict ENSO events and its strength, requires more information on past ENSO events. During the last years, numerous studies have been employed to provide a historical perspective of ENSO, for example: (Kaplan et al., 1998) extended the Niño 3.4 index back to the 1850's, (Moy et al., 2002) showed an 12,000 long ENSO record based on lake

sediments, and (Tudhope et al., 2001) gave a first insight in ENSO behavior during glacial periods reconstructed from corals. However, the most paleo-records have not the required resolution for an accurate evolution on the ENSO system. Therfore, more data are required. The Lake Challa sediments have the potential to provide new insights into ENSO dynamics and further information on teleconnections, e.g. how does ENSO influence the global climate.

1.2.2 Lake Challa sediments

Reflection data from a seismic survey (Moernaut et al., 2010) indicate a typical volcanic crater basin morphology (Fig. 1-3) with a flat central lake floor surrounded by near-vertical dipping slopes. This set-up provides perfect conditions to accumulate and preserve sediments. In Lake Challa, the accumulated sediment infill has a thickness of approximately 210 m (Moernaut et al., 2010) but only 10 % are available so far because of drilling equipment limitation. These 20.8 m are composed of several cores (Fig. 1-3). Using magnetic susceptibility and connecting distinct marker layers we reconstructed a composite profile. Wide parts of this profile show a fine laminated succession of light and dark layers. Whereas the dark lamina are primarily composed of organic matter and other allochthonous materials, the light layers mainly contain diatom skeleton (for more information see chapter: *Reduced interannual rainfall variability in East Africa during the last ice age*).

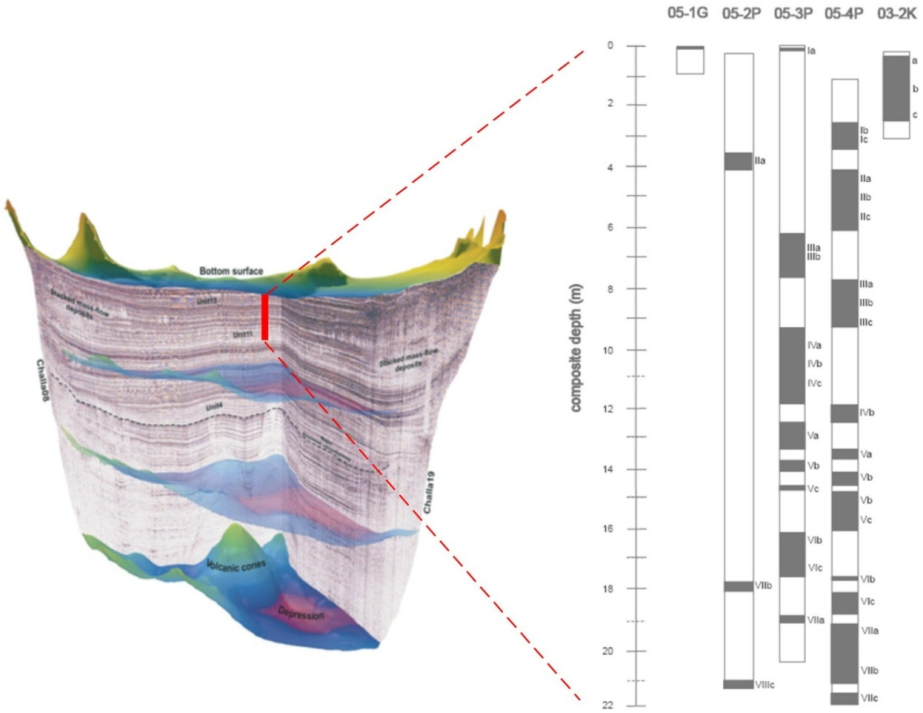

Fig. 1-3: (left) 3D representation of the Lake Challa sediment infill, of which the red bar indicates the cored 21.6m long composite profile; (right) Core sections and composite profile (shaded sections) of the cored sediments from Lake Challa representing the last 25.000 years.

Based on two series of ^{210}Pb and almost 190 ^{14}C geochronological dates, the cored Lake Challa sequence represents a successive period of the last 25.000 years. Bayesian age-modeling was used for calibration and error-weighted smoothed splines were drawn through the ordered calibrated ranges (Fig. 1-4), resulting in 95 % age uncertainties ranging (Verschuren et al., 2009). Based on this well-dated sediment sequence and applied extrapolation methods, the entire 210 m thick profile provide potential palaeo-climate information for the last 140 kyrs (Moernaut et al., 2010).

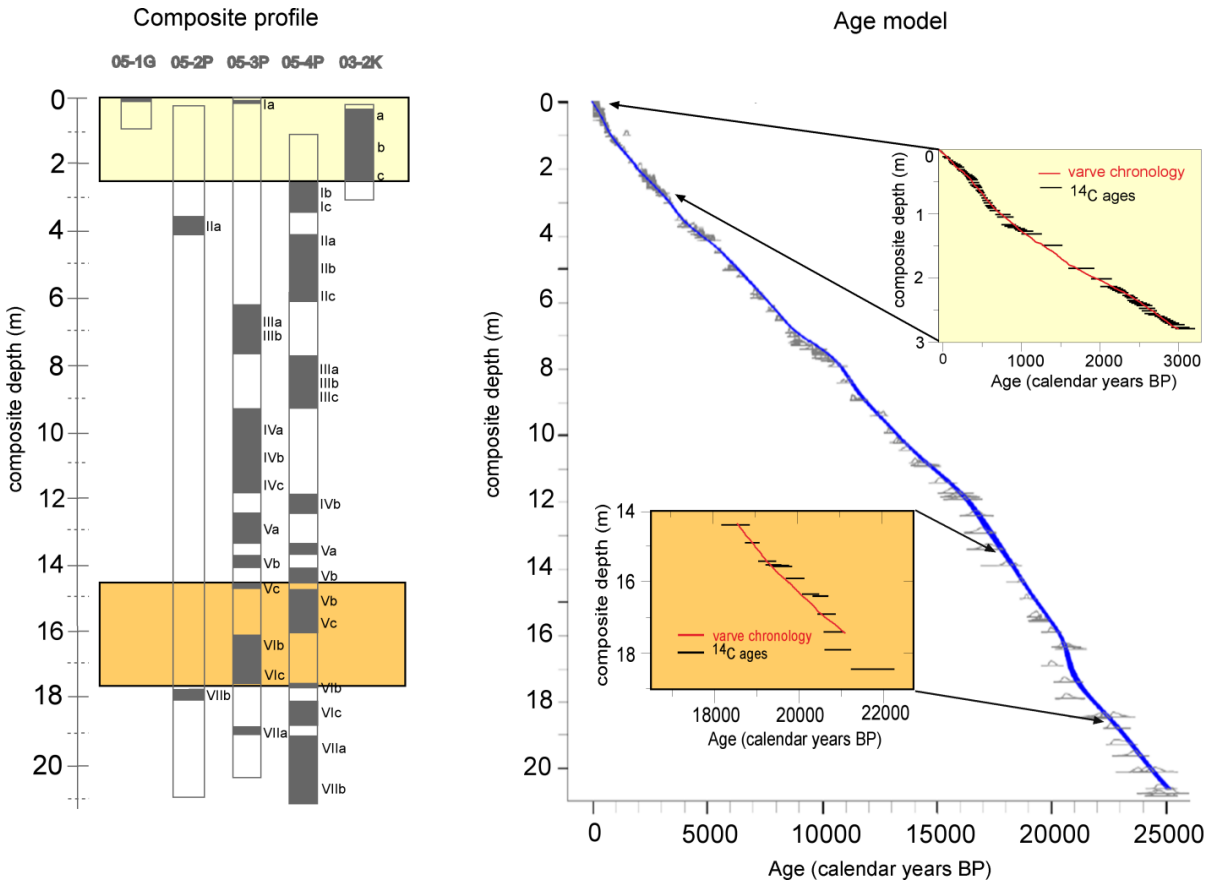

Fig. 1-4: Left panel: Position of the two studied core sections in the composite core sequence, as assembled from the best-quality portions of overlapping gravity- and piston-core sections. Right panel: Varve chronology of the two studied core sections in relation to the ^{14}C-based age-depth curve (Verschuren et al., 2009).

1.3 Objectives of this thesis – How to read a Prehistoric Rain Gauge?

Assessing how tropical climate dynamics might drive or amplify climate change in global and moderate regions is a central point for understanding natural variability and predicting the impact of its future interaction with anthropogenic induced climate change. This study will provide the complete climate history of moisture balance variations since the Last Glacial Maximum from an annually laminated sediment record of Lake Challa (Kenya/Tanzania). This crater lake is located on the eastern flank of Mt. Kilimanjaro which has been under continuous influence of tropical atmospheric dynamics during the last 25,000 years.

In particular, this work will contribute the understanding of tropical variability by addressing the following issues:

- Understanding the formation and meaning of sediment laminations in Lake Challa by comparing samples from a monthly cleared sediment trap with modern climate and limnological conditions

- Using the laminated sequences to evaluate climate changes on an annual time resolution with regard to changes in ENSO dynamics

- Establishing the pattern and timing of moisture-balance fluctuations in East Africa during the last 25,000 years by means of changes in the compositional and elemental inventory of the Lake Challa record

2 Modern seasonality in Lake Challa (Kenya/Tanzania) and its sedimentary documentation in recent lake sediments

To be submitted to: Limnology and Oceanography

Christian Wolff[1,2,6], Iris Kristen[1], Georg Schettler[1], Dirk Verschuren[3], Peter Dulski[1], Rudolf Naumann[4], Birgit Plessen[1], Achim Brauer[1], Gerald H. Haug[5,6]

[1] *Helmholtz Centre Potsdam GFZ German Research Centre for Geosciences, Section 5.2 – Climate Dynamics and Landscape Development, Telegrafenberg, D-14473 Potsdam, Germany*

[2] *DFG Graduate School 1364, University of Potsdam, Institute of Geosciences, Karl-Liebknecht Strasse 24, Haus 27, D-14476, Germany*

[3] *Limnology Unit, Department of Biology, Ghent University, Ledeganckstraat 35, 9000 Gent, Belgium*

[4] *Helmholtz Centre Potsdam GFZ German Research Centre for Geosciences, Section 4.2 – Inorganic and Isotope Geochemistry, Telegrafenberg, D-14473 Potsdam, Germany*

[5] *Geological Institute, Department of Earth Sciences, ETH Zürich, CH-8092 Zürich, Switzerland*

[6] *DFG Leibniz Center for Earth Surface Process and Climate Studies, University of Potsdam, D-14476 Potsdam, Germany*

Abstract

A 3-year (November 2006-January 2007) monthly cleared sediment trap study was deployed in Lake Challa, a hardwater Lake on the eastern slope of Mt. Kilimanjaro in southern Kenya. Microfacies and geochemical data from sediment trap samples were compared with a broad range of limnological, meteorological and geological parameters to characterize the impact of sedimentation processes from the in-situ rocks to the deposited sediments. In combination with XRF data, this study will help to understand how varves and their sublaminae form during the annual cycle to validate existing palaeorecords. The analysis of the sediment trap samples, reveal a sediment mechanism with three components: autogenic calcite, organic matter and diatoms, in which diatoms play the most important role. Main calcite precipitation occurred in southern hemisphere summer (SH) - (November-March), when water temperature is high and the lake is biologically productive (non-diatom algae) and followed by a small amount of organic matter and lithogenic material driven by rainfall during the 'long rain' season (March-May). The rest of the year, during the cool and windy months of the southern hemisphere winter (June-October), a diatom bloom is initiated by upwelling processes. The 3-year trap data provides support for the claim that the light-dark lamination couplets, abundant in lake cores, reflect seasonal delivery to the sediments of diatom-rich particulates during the windy months and diatom-poor material during the wet season. However, interannual and spatial variability in upwelling and productivity patterns, as well as El Niño-Southern Oscillation (ENSO)-related rainfall and drought cycles, appears to exert a strong influence over the magnitude and geochemical composition of particle export to the deep horizons of Lake Challa.

Introduction

The impact of global warming on human water resources in Africa is attracting increasing attention (Cullen et al., 2006; Mölg et al., 2005). Lacustrine sediments from East African lakes provide potential information about changes in the large scale atmospheric circulations and associated moisture-balance variations (Gasse et al., 1989; Johnson et al., 2002; Russell et al., 2007; Verschuren et al., 2009). Palaeoclimatic reconstructions on the basis of lake sediments require the understanding of the lakes response on the seasonality of environmental parameters as temperature and precipitation. Monitoring of the modern lake systems helps to understand sediment formation and preservation in the context of recent seasonal climatic variability. With this study we aim to understand the genesis of the sedimentary record from Lake Challa (Kenya/Tanzania) to provide a reliable mechanistic model for the palaeoclimatic interpretation of sediment records from this lake.

Study site and modern day climate

Lake Challa (3°19'S, 37°42'E), is a crater lake with steep crater walls (up to 170 m) on the lower east slope of Mt. Kilimanjaro (Fig. 2-1). Its maximum depth varies between 92-98 m (1999-2007). The lake surface is approximately 4.5 km² and is located at ~880 m asl within igneous rocks (predominantly trachy-basalts) of the tertiary Kilimanjaro complex (Bear, 1955). These basalts are covered by "calcareous tuffaceous grits", a calcite-cemented tuffaceous breccia (Downie and Wilkinson, 1972). The volcanic complex is underlain by metamorphic rocks (predominantly gneisses) that outcrop east- and southward of Lake Challa and dominate the area up to the coast of the Indian Ocean (Petters, 1991). Seismic surveys detected ~210 m of sediment infill in the crater, which covers the last ~250,000 years (Moernaut et al., 2010).

The water budget of the lake is controlled by sub-surface in- and outflow and the precipitation/evaporation balance (1700 mm/yr evaporation vs. 600 mm/yr precipitation) (Payne, 1970). Groundwater inflow is probably fed by seepage of precipitation falling further uphill in the forest zone at the slopes of Mt. Kilimanjaro. A small creek of ca. 300 m lengths, which breaches the NW corner of the crater rim, is only water-bearing during heavy rainfall events (information from local fishermen).

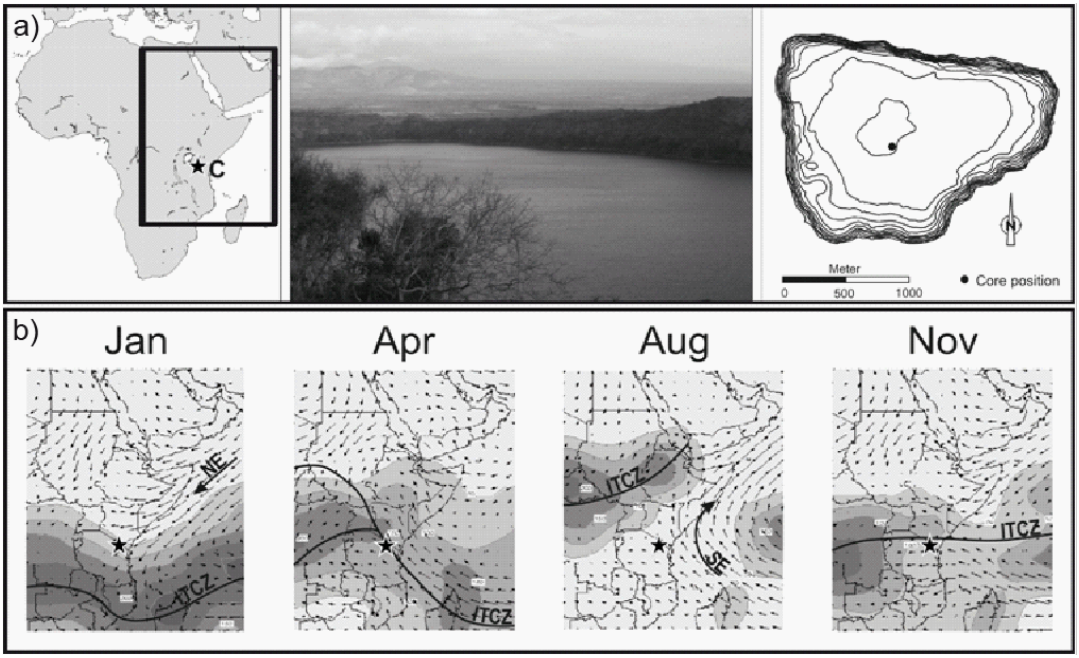

Fig. 2-1: a) Location of Lake Challa (C, 3°19'S, 37°42'E) and bathymetric map (right panel, depth contours at 10 m intervals; (Moernaut et al., 2010). Black outline in the left panel indicates coverage area of Fig. 2-1b). b) Seasonal migration of the ITCZ over Eastern Africa. Monthly precipitation (shading, mm/month) based on satellite precipitation estimates over ocean areas and rain gauge data over land regions, contours are drawn at 50 mm intervals. Large scale wind vectors for the 925 hPa pressure level indicate wind direction with wind speed proportional to the length of the vectors (http://iridl.ldeo.columbia.edu)

Local climate is controlled by the seasonal passage of the Inter-Tropical Convergence Zone (Fig. 2-1) with rainfall occurring predominantly from October to December and March to May (Fig. 2-2) (Nicholson, 2000). These two rainy seasons are referred to as the "long rains" (March – May) usually associated with the major amount of rainfall of the year, and the "short rains" (October – December) with stronger inter-annual variability and presumably respond to changes in Indian Ocean surface temperatures and related atmospheric circulation (Black et al., 2003; Hastenrath et al., 2004). Furthermore, rainfall in East Africa is tightly linked to the El Niño Southern Oscillation (ENSO), with more rain during El Niño years and severe droughts in La Niña years (Nicholson, 2000; Ropelewski and Halpert, 1987). Temperatures in the region just south of the equator are high during northern hemisphere winter (November – March) and slightly decline by about 2 °C during northern hemisphere summer (June – August). Wind speeds show the inverse pattern with prevailing of weak

north-westerly trade winds from November to April and occurrence of strong south-easterly winds from May to October when the ITCZ displaced northward. The north-easterly trade winds are weak and highly variable.

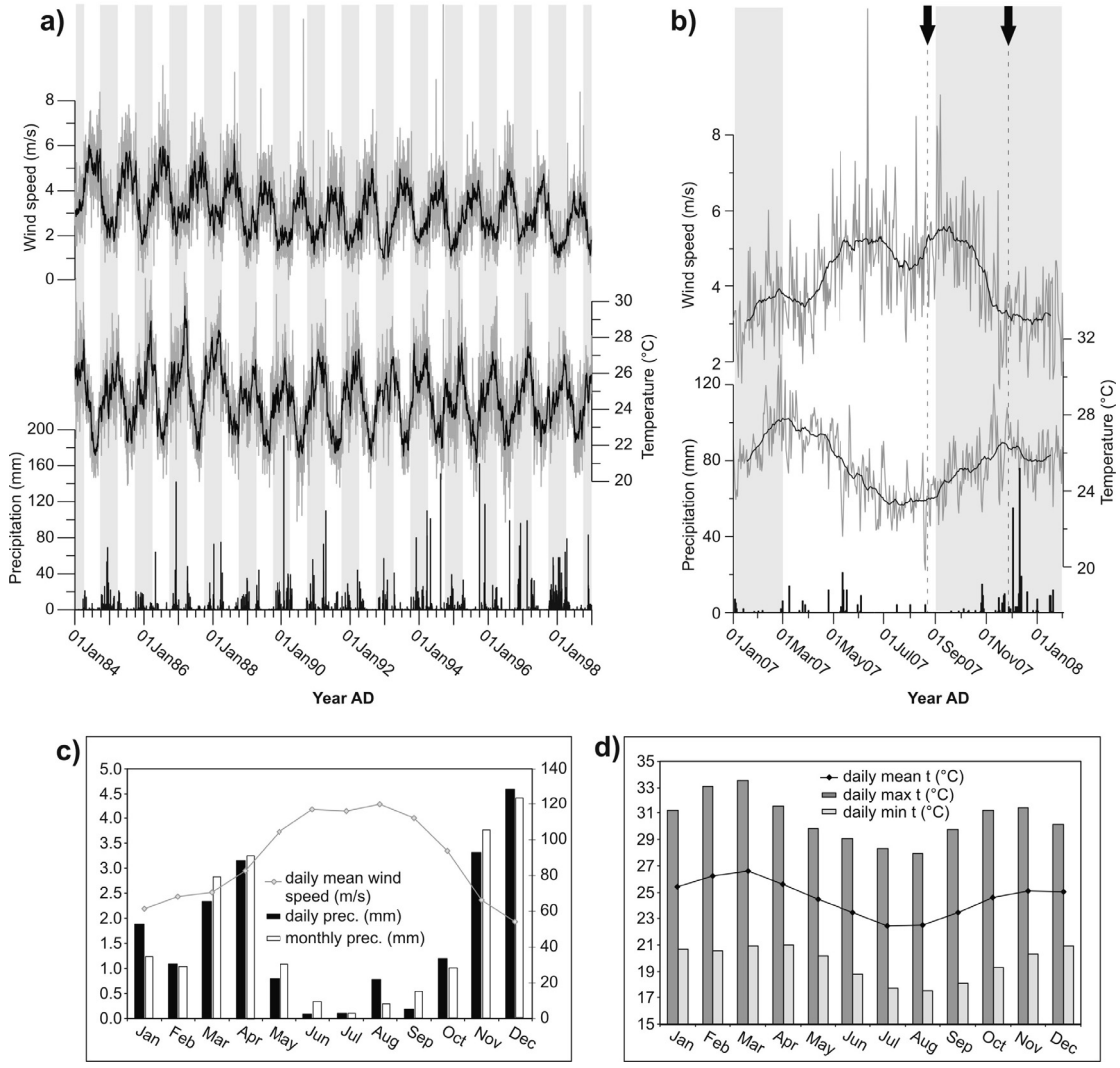

Fig. 2-2: a) + b) Daily meteorological data from Voi, Kenya (~100 km E of Lake Challa), covering the time periods 1984 - 1999 (a), and January 2007 - February 2008 (b) (periods between September and March are shaded, black line in (a) is 11-point running average, black line in (b) is 31-point running average (~ monthly mean), days of sampling for lake water chemistry are marked by arrows in (b), source: http://hurricane.ncdc.noaa.gov/CDO/, global surface summary of day data of the federal climate complex); c) daily precipitation and wind data (left axis), averaged per month (1984-1999), and monthly precipitation data (right axis) from Voi (1904-1990, source: NOAA NCDC GCPS monthly station data); d) daily maximum, minimum and mean temperature data from Voi, averaged per month (1984-1999).

Sampling, field measurements, and laboratory analyses

In-situ monitoring of temperature profiles at 2 hours intervals between November 2006 and January 2010 was based on the installation of eight temperature loggers (Minilog, Vemco, Canada) in various water depths (10, 20, 40, 50, 60, 65, 85m) at a mooring site close to the centre of the Lake.

Water for chemical analyses was sampled along vertical profiles on 23 August 2007 and 28 November 2007 using a Hydro-Bios Plastic Water Sampler (Niskin Type). The water samples (100 ml each) were filtered through 0.2 µm, 25 mm diameter Whatman GD/X PP syringe filters and 50 ml of the samples were acidified with concentrated HNO_3 for analyses of cations. The samples were stored at 4 °C until processing. Chemical analyses closely followed the analytical procedures given in (Eggermont et al., 2007). Profiles of temperature, pH, conductivity and dissolved oxygen were measured using a Hydrolab Quanta CTD profiler and a multi-parameter water quality meter (YSI model: 600XL-B-D), respectively.

In August and November of 2007 water samples from various water depths (0 to 90 m in 10 m steps) were collected for stable isotope analyses in the Alfred Wegner Institute for Marine and Polar Research, Potsdam. The samples were stored in sealed air-tight polypropylene bottles until analysis. A Finnigan MAT Delta-S mass spectrometer equipped with two equilibration units was used for the determination of hydrogen and oxygen isotope composition following the procedures given in (Meyer et al., 2000).

In November 2006 an Uwitec (double funnelled 86 mm diameter) sediment-trap was installed at 35 m water depth at a mooring site close to the centre of the lake. The trap was emptied and redeployed every ~4 weeks, providing 34 monthly samples between December 2006 and January 2010. After settling for one day, the samples were stored frozen until to further preparation in the GFZ laboratories, where the solids were separated by filtration (Schleicher&Schnell RC-L 60, 1µm, 50 mm) and freeze-dried for preservation.

For major and trace element analysis, sample aliquots between 0.0018 and 0.05792 g, depending on the amount of available material, were weighted in a Pt-vessel and transferred into Teflon tubes. After addition of 1 ml HNO_3 (65 %, Merck Suprapur) and complete CO_2 release, organic carbon was oxidized over 3 hours at 130 °C during a first wet-oxidization step in a programmable heating block (TECATOR). The wet-oxidation procedure was continued over 5 hours at 160 °C after addition of 1 ml $HClO_4$ (70 %, Merck Suprapur). After cooling we added 1 ml HF (48 %, Merck Suprapur) and continued the digestion at 70 °C over two days. Excess HF and silica were removed by rising the temperature up to 210 °C. During the entire digestion procedure the tubes were loosely covered with Teflon reflux caps. After cooling the residual (~0.5 ml) was dissolved in 2 ml HCl and filled up on a final volume of 14 ml.

Major and trace elements were measured using an ICP-AES spectrometer equipped with a radial torch (Thermo Elemental Cooperation, ICAP 6000 Series). Four multi-element standards in an acid matrix similar to that of the digestion solutions were prepared for external calibration on the basis of commercial single element standards of Spex and Merck, respectively.

The TC, TOC analyses were performed using an elemental analyser (NC25000 Carlo Erba) at the GeoForschungsZentrum Potsdam. The results were referenced against lab-internal soil standards and a reference sample (Urea). TIC was determined as the difference between TC and TOC.

Saturation indices for calcite were calculated using the USGS program PHREEQC (Parkhurst and Appelo, 1999).

In February 2005, a gravity core (CH05-1G; 49 cm) was taken from the centre of the lake. The sediment surface was undisturbed according to observation of clear bottom water upon retrieval, and comparison with several other short cores all showing the same set of layers. Structures of the sediments were studied under the microscope on thin sections from 10 cm long resin-impregnated blocks. Individual compounds were studied in smear slides, which were prepared with Merck Kaiser's glycerol gelatine for microscopy (molten at 40 °C). Further investigations were done by scanning electron microscopy (SEM).

Changes in the sediment composition and intensities (E_n[cps]/E_m[cps]) of the top 10 cm of the gravity core (~last 100 years) were studied by micro X-ray fluorescence (µXRF) scanning of resin-block surface. Scanning was performed using an EAGLE III XL µXRF spectrometer (Röntgenanalytik, Germany) at GeoForschungsZentrum Potsdam, applying 40 kV tube voltage, 300 µA tube current, 123 µm spot size and 100 µm step size.

Samples of powdered catchment rocks and soils were fused in Li tetraborate-metaborate flux (FLUXANA, FX-X65) and analysed by wavelength-dispersive XRF spectrometry using a Panalytical Axios Advanced XRF spectrometer. Quantification of element concentrations was achieved using calibration curves generated from multiple certified reference samples.

Results and Discussion

Physical and chemical lake water characteristics

Lake Challa is a tropical hardwater lake with 'HCO_3^- + CO_3^{2-}' as the dominant anionic component, followed by Cl^- and SO_4^- (Table A. 8-1). According to (Talling and Talling, 1965), this is the dominant (prevailing) type of lake water in Africa. The DIC (Dissolved Inorganic Carbon) inventory of the lake may originate in a substantial proportion from the chemical dissolution of the local calcite-bearing tuffaceous breccia (c.f., CO2 contents of unweathered and weathered grit Table A. 8-2). Sulfate concentrations in Lake Challa are generally low and decrease in the anoxic bottom water (Fig. 2-3). Soluble reactive phosphorus (SRP) was not detectable in the upper 40 m of the water column (Fig. 2-3), it is obviously limiting for phytoplankton in Lake Challa, in particular for diatom bloom, which would be supported by high Si concentration of the lake. Increase of SRP and NH_4 in the deep water (August 2007) reflects the release of PO_4 and NH_4 from settling particles and the diffusive reflux of both components across the sediment/water interface under anoxic conditions. In November 2007 seasonal depletion of both ions documents oxygenation of the deep water (Fig. 2-3). Nitrate is very low in the top 20 m (August 2007) to 40 m (November 2007), respectively, where it is probably consumed by primary producers. The detection of NO_3^- in 20 to 30 m and 50 to 70 m water depth in August 2007 (Fig. 2-3) and at ~60 m in November 2007 reflects microbially mediated organic matter degradation and nitrification under oxic conditions. However, water profiles of the related period document O_2-depletion below 50 m water depth. The presence of NO_3^- at 50 m water depth may be a relict of previous deep water oxygenation and related nitrifying activity. Alternatively, the presence of NO_3^- and SRP at 60 m water depth in November 2007 could be an indication for groundwater inflow. The absence of coinciding peculiarities in the profiles of inert ions (Na, K, Mg) does not support this hypothesis (Table A. 8-1). In general, Si concentrations are high in Lake Challa (> 20 mg/l). Under stratified conditions in August 2007, higher Si concentrations in the hypolimnion (Fig. 2-3) reflect diatom dissolution in the water column and Si-reflux from the sediments. The profiles of Ca, Sr, and DIC during seasonal stratification (Fig. 2-3) reflect biogenically induced precipitation of low-Sr $CaCO_3$, driven by biogenic uptake of CO_2 in the phototrophic zone, dissolution of settling autochthonous carbonate particles in the deep water, and Ca reflux across the

sediment/water interface. Calcite was oversaturated in the upper 20 m water column on 28 November 2007 and showed under-saturation for the entire water column on 23 August 2007 when an overturn event is documented by water profile data (Table 2-1). Dissolved Fe and Mn concentrations are < 0.01 mg/l down to 40 m water depth in August 2007 and in the whole water column (except at ~60 m and 95 m) in November 2007 (Fig. 2-3) and reflect the precipitation of Fe(Mn)OOH in oxygenated water. Increasing Fe and Mn concentrations downward from the top of the hypolimnion in August 2007 document (probably microbially mediated) reduction of reactive Fe(Mn)OOH probably during settling and in the sediment surface. The higher increase of Mn in comparison to Fe (Mn/Fe maximun at ~50 m water depth, Fig. 2-3) indicate the prevailing of pH/Eh conditions that favoured the precipitation of Fe or the release of Mn2+, respectively, if we exclude inflow of groundwater with high Mn/Fe ratios (Balistrieri et al., 1994; Davison, 1993).

Table 2-1: Calcite saturation indeces during an ongoing mixing event (23.08.2007) and during stratified conditions (28.11.2007).

water samples	HCO_3	CO_3	Alk(HCO_3)	SI (Calcite)
Challa, 23.08.2007, 0 m	37.55	0.56	38.69	-0.09
Challa, 23.08.2007, 10 m	37.40	0.53	38.48	-0.08
Challa, 23.08.2007, 20 m	36.80	0.33	37.48	-0.33
Challa, 23.08.2007, 40 m	37.95	0.24	38.43	-0.46
Challa, 23.08.2007, 60 m	43.64	0.05	43.74	-1.06
Challa, 23.08.2007, 80 m	46.43	0.03	46.50	-1.20
Challa, 28.11.2007, 0 m	37.71	2.22	42.23	0.51
Challa, 28.11.2007, 10 m	37.51	2.43	42.44	0.50
Challa, 28.11.2007, 20 m	37.38	1.56	40.56	0.48
Challa, 28.11.2007, 40 m	38.27	0.28	38.84	-0.25
Challa, 28.11.2007, 60 m	38.49	0.64	39.80	-0.76
Challa, 28.11.2007, 95 m	39.06	0.65	40.39	-0.97

* T °C and pH for SI calculations from 60 m to 80 (95) m were interpolated following the trend of 11. 9 2006 (25. 2. 2005)

Compared to other stratified lakes (Davison, 1993; Schettler and Albéric, 2008; Talling, 1966), Fe concentrations in the anoxic hypolimnion of Lake Challa (in August 2007) are relatively low. Water profiles from 28 November 2007 document the chemical stratification shortly after overturn. The deep water concentrations of Fe^{2+} and Mn^{2+} certainly have increased in the course of the stratification period until to their seasonal precipitation. With dissolved salt content (DSC) concentrations below 200 mg/l (Table A. 8-1), the water of Lake Challa is moderately mineralized (Talling and Talling, 1965). The EC (Electrical Conductivity) profiles between September 1999 and November 2007 show that the salinity of the lake has been rather constant during this period. The obtained maximum variation of the upper 45m water column was ~25 µS/cm. It may largely depend on inter-annual variations in the lake water overturn and calcite precipitation (pH, T°C). The current DSC of Lake Challa may have been built up over a long period by evaporative enrichment.

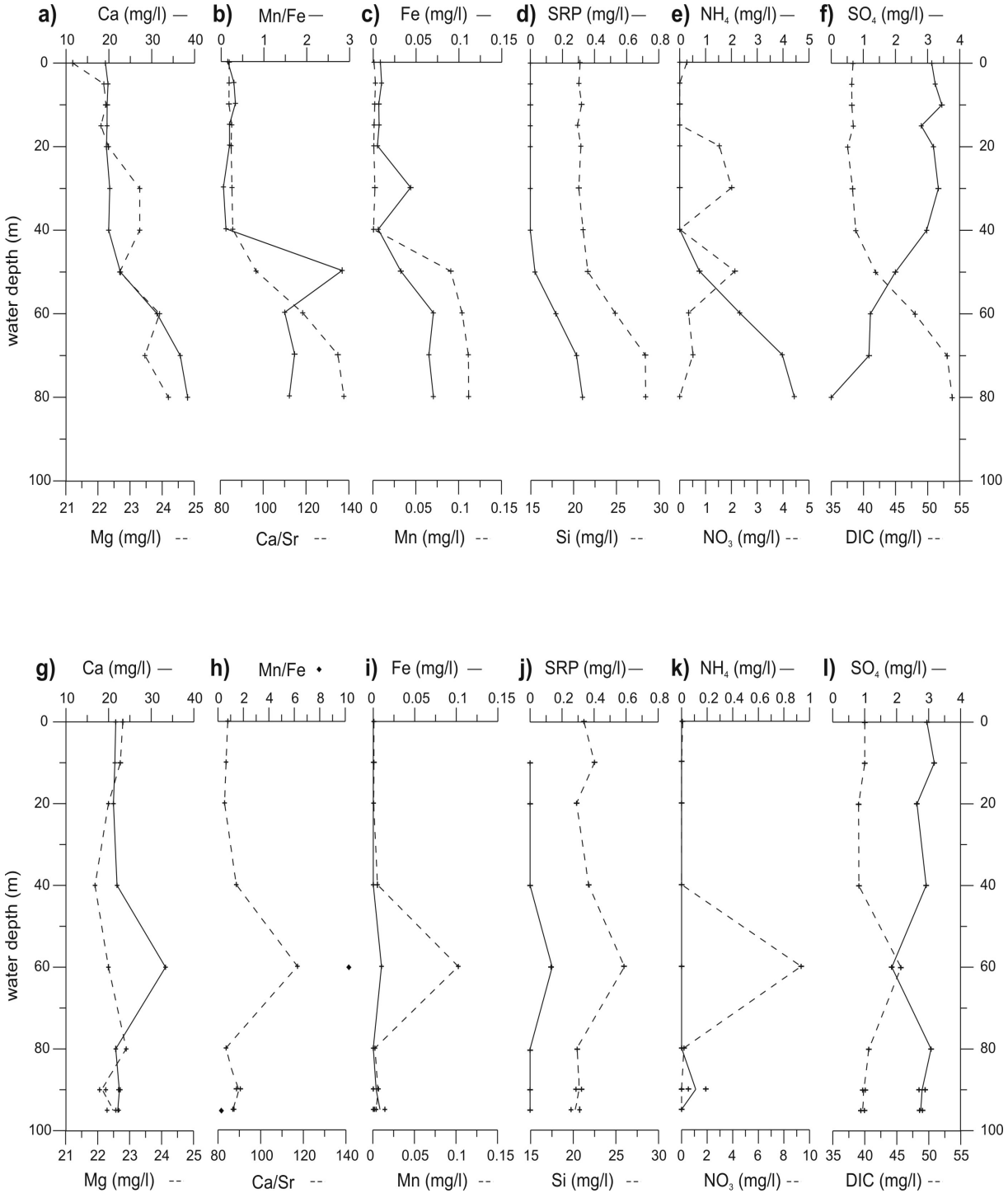

Fig. 2-3: Selected profiles of chemical lake water characteristics of Lake Challa: (a - f) were recovered on 23 August 2007 (6 pm), (g – l) were recovered on 28 November 2007 (12 pm), at 90 and 95 m water depth samples are duplicate. For the complete water chemistry data sets see Table A. 8-1.

Thermal and chemical stratification

Limnological surveys conducted between September 1999 and November 2007 in combination with meteorological monitoring data from Voi (Fig. 2-2) enable to establish a model of seasonal changes in the thermal and chemical stratification of Lake Challa. The seasonal formation of a well defined thermocline is related to warming during the southern hemisphere summer (October – May) and generally low wind stress during this season. The thermal stratification of the water column is not sustained due to cooling and intensified wind. Our monitoring data imply a minimum turnover of the upper 45 m water column (Fig. 2-5). Temperature differences between surface and bottom waters are reduced to approximately 1 °C during the southern hemisphere winter (Fig. 2-4; Fig. 2-5).

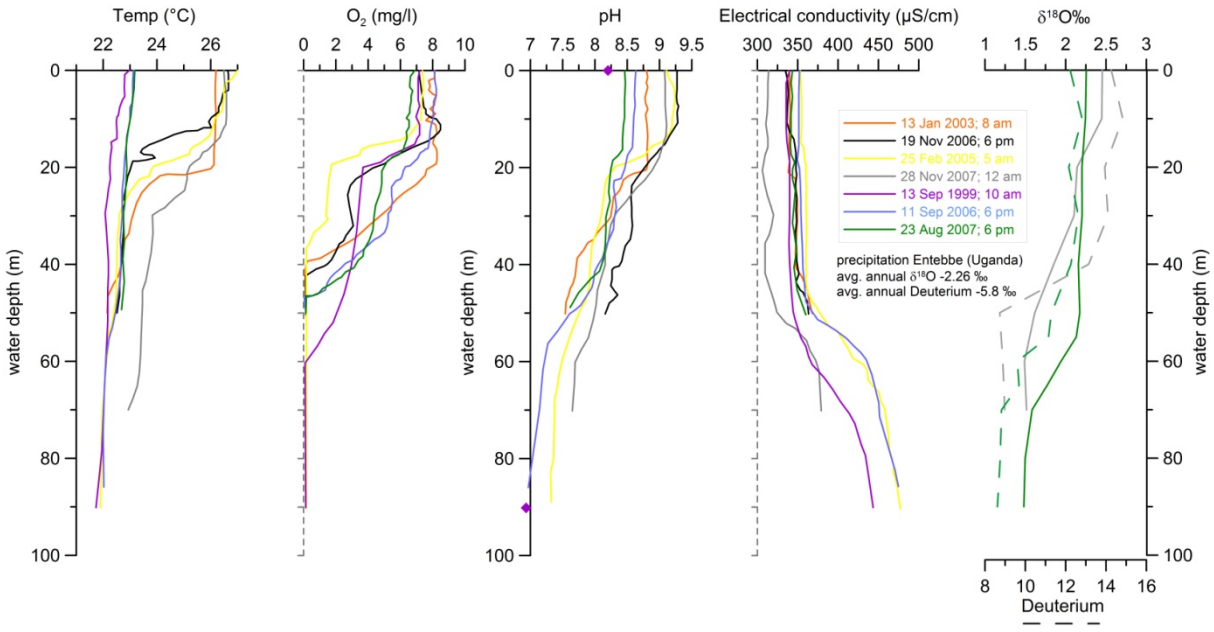

Fig. 2-4: Profiles of physical lake water characteristics of Lake Challa, measured between September 1999 and November 2007. Comparability of profiles from November 2007 and September 1999 (> 15 m) (dashed lines) with the rest of the profiles is ambiguous as those measurements were performed after bringing up the samples to the surface.

Profiles of temperature and oxygen document distinct inter-annual variations in the intensity of the seasonal mixing events in dependence on cooling and wind stress (Fig. 2-4; Fig. 2-5). There is, however, no simple correlation between water column mixing and the penetration depth of O_2 since the advective downward flux of O_2 is determined also by the diurnal production/consumption of O_2 by phytoplankton and O_2 consumption due to organic matter degradation by microbial mediated organic matter degradation. The increase in EC at ~45-50 m in all profiles (> 50 m) suggests a limit to seasonal mixing at around this depth (Fig. 2-4). Profiles of O_2 (Fig. 2-4) and the finely laminated nature of surface sediments Fig. 2-8; Fig. 2-7) both indicate that the lake bottom and the lower water column are anoxic throughout most of the year.

The O_2-profile in November 2006 exhibits maximum O_2 concentrations at ~10 – 15 m water depth, whereas in all other profiles O_2 concentrations are relatively constant (or decrease with depth) within the upper ~15 m (Fig. 2-4). Such maxima commonly develop in stratified lakes and reflect enhanced primary productivity in relation to nutrient availability (Wetzel, 1983). Transparency of surface waters in the stratified Lake Challa is high (Secchi depth of 5 to 7 m, (Damsté et al., 2009)), oxygen and turbidity are correlated with the abundance of phytoplankton and reach maxima close to the thermocline.

The seasonal mixing process is independently documented by the $\delta^{18}O$ water profiles from August and November 2007 (Fig. 2-4). Heavier isotope composition of the epilimnion in the November profile is related to the evaporative enrichment of ^{18}O during the seasonal stratification of the water body (cf. precipitation Entebbe (Uganda): average annual $\delta^{18}O$ -2.26 ‰; average annual Deuterium -5.8 ‰) (IAEA, 1992). The profile from August documents the mixing of the upper 50 m water column. Lake Challa $\delta^{18}O$ isotopes are strongly linked to precipitation and evaporation, whereas heavier values reflect increased evaporation. The pattern of the $\delta^{18}O$ profile from August showing a gradient between 55 and 70 m depth and about 1 ‰ lighter $\delta^{18}O$ values below 70 m implies that the overturn was restricted to the upper 55 m of the water column.

Potential components of the detrital allochthonous sediment fraction

The siliciclastic sediment fraction principally derives from local materials by surface run-off of a rather restricted area and aeolian influx of a wider source region. Table A. 8-2 compiles the bulk chemical composition of various representative materials from the close and wider vicinity of Lake Challa. Local soils and their basic precursor rocks distinctly differ in their chemical composition from acidic gneisses of the basement which outcrops in some distance from the lake, particularly, by much higher Ti, P, and Mg contents. Dust influx of remote provenance by dry- or wet deposition, if contributing in substantial amounts to the bulk siliciclastic influx, may be characterised by geochemical signatures similar to loess or mean Upper Continental Crust Composition (UCC). As the potential gneiss component, this component distinctly differs from local debris by lower Ti, Fe, Mg, and P concentrations.

Sediment trap samples

Microscopic observations (optical and electron microscopy) of sediment trap samples reveals that the collected materials comprise three major components: (i) autochthonous calcite, predominantly precipitated in the southern hemisphere summer, (Table A. 8-3) (ii) amorphous organic and fine-grained (clay-sized) siliciclastic matter settling during the long rainy season, and (iii) diatom frustules mainly deposited during the southern hemisphere winter period (Table A. 8-3).

The percentage of siliciclastic matter in the collected trap materials is estimated for the assumption of a constant Al_2O_3 concentration of the inorganic detrital influx (15.6 wt. %, mean continental crust composition after (Taylor, 1964)). On the basis of this assumption the siliciclastic matter in the traps ranged between 20.3 and 49.6 wt. % (average: 26.7 wt. %, SD 7.0). Values above 30 % are exclusively estimated for sediment trap materials collected between November and March during wet conditions.

The Al_2O_3/TiO_2 mass ratio of most samples is rather low (Table A. 8-3), ranging between 0.8 and 19.4 as expected for input of local rock particles of basaltic composition (Average basalt 11.0, (Taylor,

1964)**)**. However, six trap samples show distinctly higher Al_2O_3/TiO_2 (32.4 - 109.7) and Al/Fe (6.0 - 15.3) ratios. A second siliciclastic component, probably of remote provenance, obviously contributes to the detrital input of Lake Challa. The maximum Al_2O_3/TiO_2 ratio is obtained for the trap materials collected in August 2008 during the dry/windy season (Table A. 8-3). Al_2O_3/TiO_2 and La/Y show an inverse relationship. The La/Y roughly documents changes in the LREE/HREE element ratio (Light/Heavy Rare Earth Elements). The inverse correlation identifies the local siliciclastic endmember to be enriched in LREE against the remote component.

Lake Challa may receive substantial dissolved input of Fe and Mn input by groundwater inflow. Such contributions are identifiable in sediments with low detrital influx of Fe, Mn by normalization using conservative elements (e.g., Al, Ti, Sc). Trap samples with dominance of the basaltic endmember in the siliciclastic component show relatively low RSD values of 12.7 and 17.2 % for Fe/Ti and Fe/Sc, respectively. There is no significant lowering of Fe/Ti and Fe/Sc for trap materials collected during the dry/windy season. Mn/Ti, Mn/Sc and Mn/Fe, in contrast, show distinct coinciding maxima during the overturn events between June-August 2007, June 2008 and July - September 2009 (cf. Fig. 2-5). Hydrochemical groundwater composition (no data available) and pH/Eh conditions obviously favour specifically the ingrowth of enhanced dissolved Mn concentrations versus Fe in the anoxic deep water during lake stratification. The Mn is seasonally precipitated by deep water oxygenation (Fig. 2-5). The bulk Ca-concentration (component (i) of the trap materials show a high variation range (0.2 - 32.2 wt. %)). The latter reflects distinct seasonal variation in precipitation of autochthonous calcite (cf. microscopic component analyses, Table A. 8-3). Estimated $CaCO_3$ concentrations based on an constant Ca/Al mass ratio of 0.25 for the silicate fraction gives a calcite variation range between 0 and 78 wt.-%. Calcite concentrations above ~35 % are obtained between November and March in the 'short rain' season. A positive correlation between the balanced calcite content and Ca/Sr ($R^2 = 0.86$) indicates the authochthonous $CaCO_3$ as low-Sr component (cf. Ca/Sr water profile, Fig. 2-3). Total phosphor in the sediment trap samples comprises (i) organically-bound P of planktonic matter, (ii) dissolved PO_4 removed by chemical (co)-precipitation or sorption on settling inorganic particles, and (iii) P associated with the allochthonous detrital organic and inorganic input. The TOC/P mole ratio of the trap materials varying between 9.0 and 250.1 show major positive and negative deviations from Redfield composition (C : P = 106 : 1). TOC/P values distinctly below 106 indicate substantial P contributions from non-planktonic source. P and TOC positively correlate ($R^2 = 0.51$) with excess of P if samples with TOC/P < 60 are not considered (Fig. 2-6). The same selection of trap samples also shows a positive correlation with S_{total} ($R^2 = 0.78$). We conclude that sulphur dominantly occurs organically bound (TOC-S correlation, all samples $R^2 = 0.80$ (Fig. 2-6)). Calcium shows not at all positive correlation with P. Sorption of PO_4 onto settling calcite crystals can be rejected as a significant controlling factor for the abiotic removal of PO_4 from the water body. Diatoms were hardly detectable by microscopic inspection in the trap materials from November to March (Table A. 8-3). Biogenic silica concentrations as estimated by the (100-Silciclastic-CaCO3-TOC) difference are typically enhanced between June and September. In 2008, trap materials document an earlier begin of the increase in biogenic silica (La Niña year).

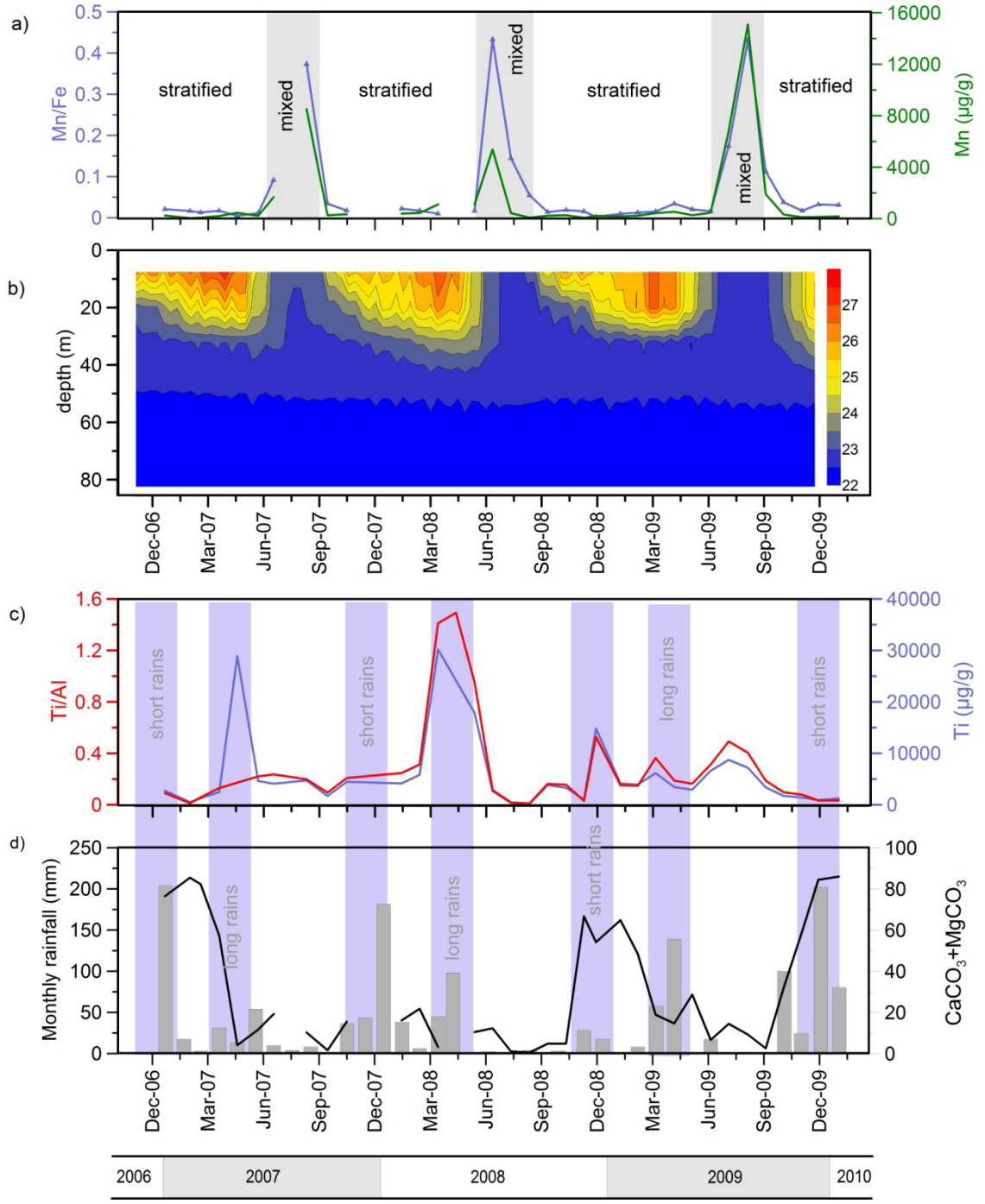

Fig. 2-5: Analysis of sediment trap samples in comparison (a) Mn/Fe ratio and Mn (b) thermistor data in various depth (c+d) dependency of elements with rainfall from Voi station, reflecting allochthonous input (c) and the trend autochthonous calcite

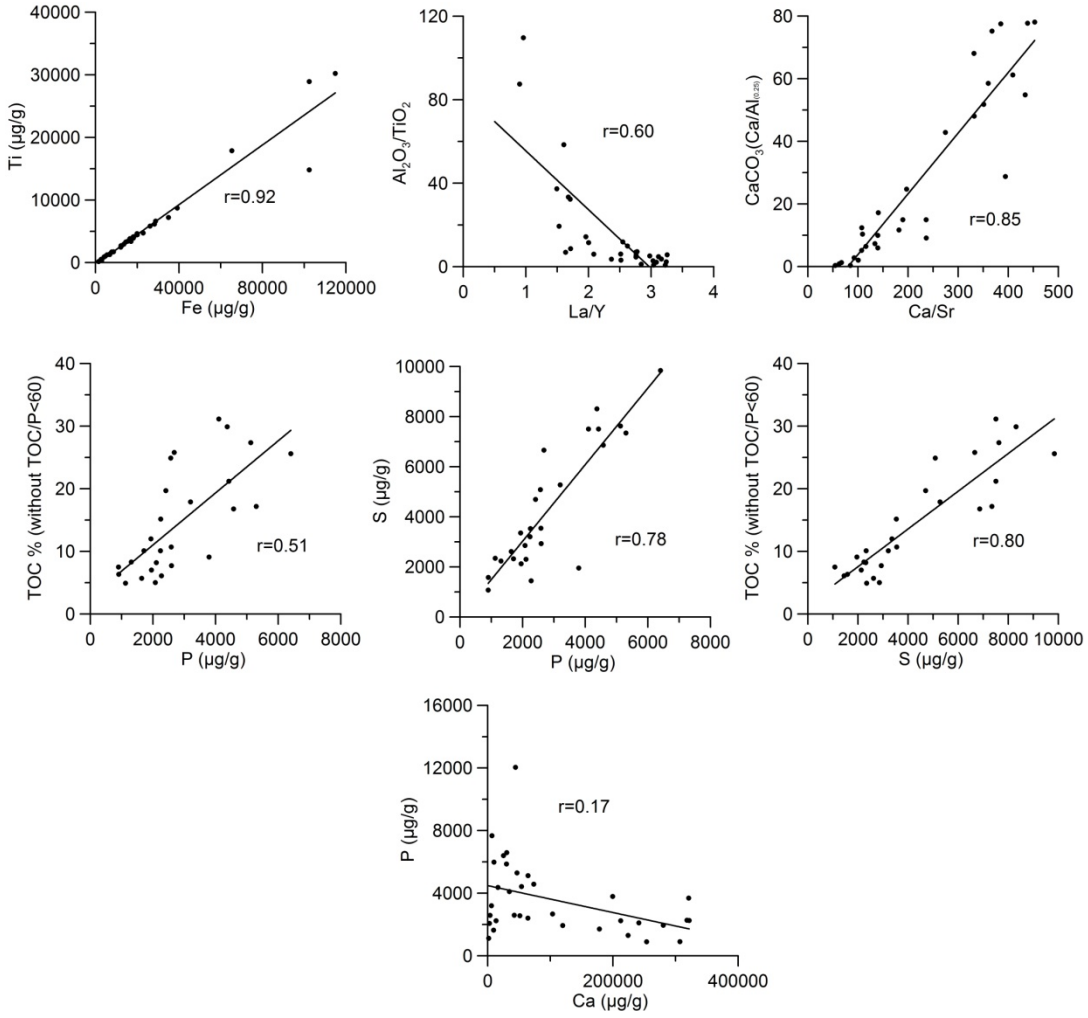

Fig. 2-6: Correlation between selected elements derived from sediment trap samples.

Sediments

In 2005 a 25 m long overlapping composite profile was recovered from the centre of Lake Challa (Verschuren et al., 2009). Most of the record consists of varves deposited at sedimentation rates between 0.08 and 7 mm yr^{-1}. The varves consist of light-dark couplets similar to those obtained in the short gravity cores that were analysed in this study and are described in the following. Based on microscopic inspection, the dark layers are mainly composed of amorphous organic matter and fine-grained siliciclastics. Single silt-sized calcite crystals are imbedded in this matrix. Diatom skeletons are the dominant constituent of the light layers (Fig. 2-8). Variation in varve thickness (annual sedimentation) mainly depends on the thickness of the seasonal light layer. Consistently, µXRF scans show Ti, Fe maxima and Si/Al minima for the dark laminae. Light diatom-rich layers show Si/Al maxima and Fe, Ti minima. (Fig. 2-7). Ca/Al maxima occurring within the dark sublayers document seasonal enhanced deposition of autochthonous calcite.

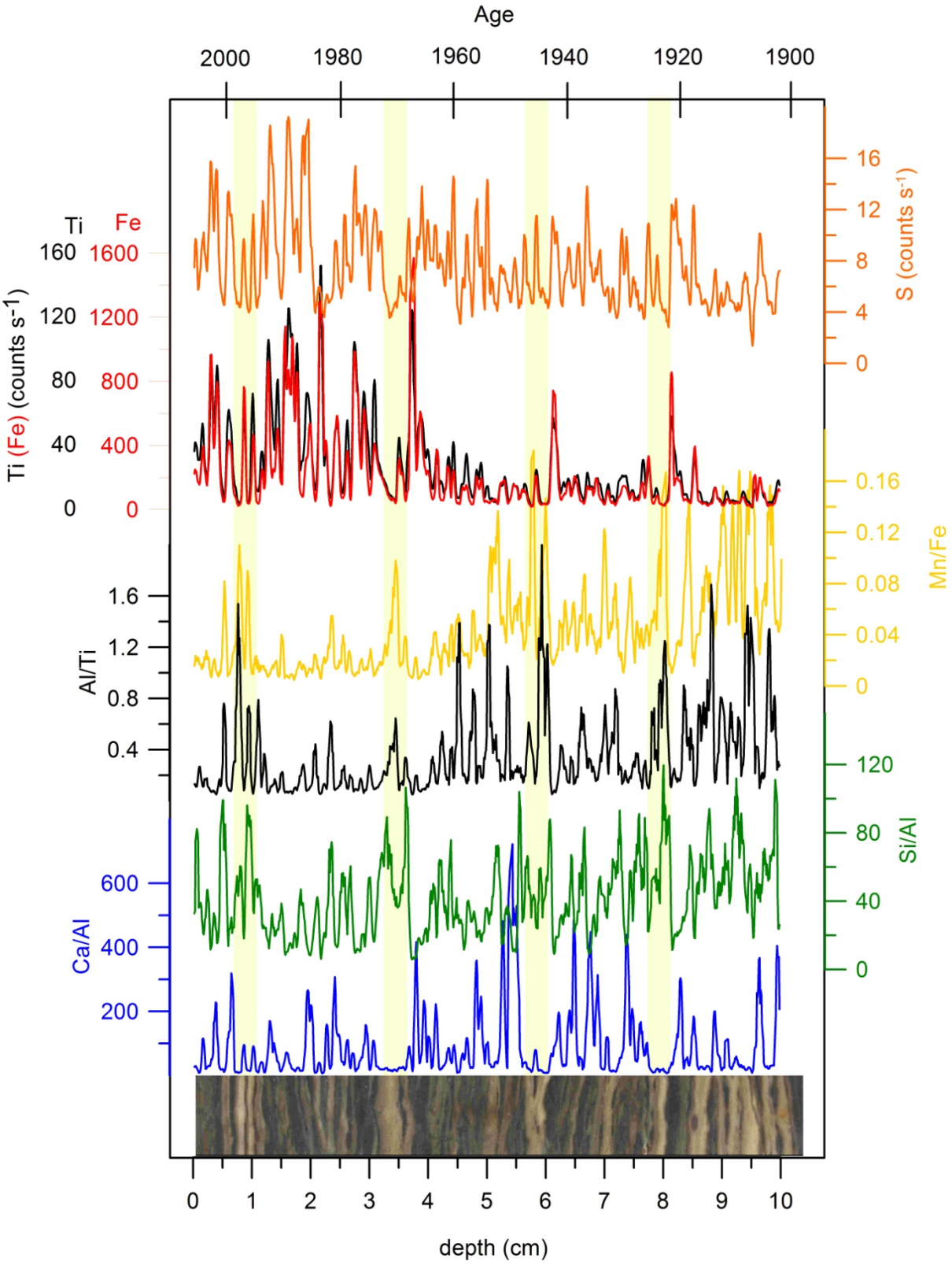

Fig. 2-7: Selected µXRF scanning profiles and converted intensity ratios of an exemplary thin section block from short core CH05-1G (0–10 cm depth). Curves represent 5-point running averages; yellow bars mark prominent diatom laminae, blue bars prominent darker laminae.

Furthermore, the µXRF scans document coincidence between diatom blooms (Si/Al-maxima) and enhanced chemical precipitation of Mn (Mn/Fe, Mn/Ti-maxima). Total sulphur is clearly enriched in the dark layers. Higher S intensities in the dark laminae (Fig. 2-7) are related to organically-bound S, and/or, Fe-sulphide. In the µXRF Scans, Al/Ti count ratios show distinct higher peaks in the light layer. Al/Ti maxima document influx of siliciclastic matter of remote provenance during the windy/dry season. Furthermore, the µXRF scans document distinct Mn/Fe peaks that are interpreted as indications for chemical precipitation of Mn during overturn events (Fig. 2-5). These peaks show some coincidence with Mn/Ti and Fe/Ti peaks that strictly occur inside of the light layers. The bulk composition of the silicates in the light layer, however, differs from those of the dark layers by relatively enhanced contributions of a remote component characterised by high Al/Ti ratios. Normalization using Ti, therefore overestimates the excess of Fe and Mn related to chemical precipitation. Mn/Al (not shown) shows coincidence with the maxima in the Mn/Ti plot, whereas Fe/Al partially shows inverse correlation with Fe/Ti. Based on monthly analytical data of the trap materials we inferred higher chemical precipitation rates for Mn than for Fe. The higher sensitivity of the Mn/Al intensity ratio in the sediments for the chemical precipitation in Lake Challa against Fe/Al corresponds with this finding.

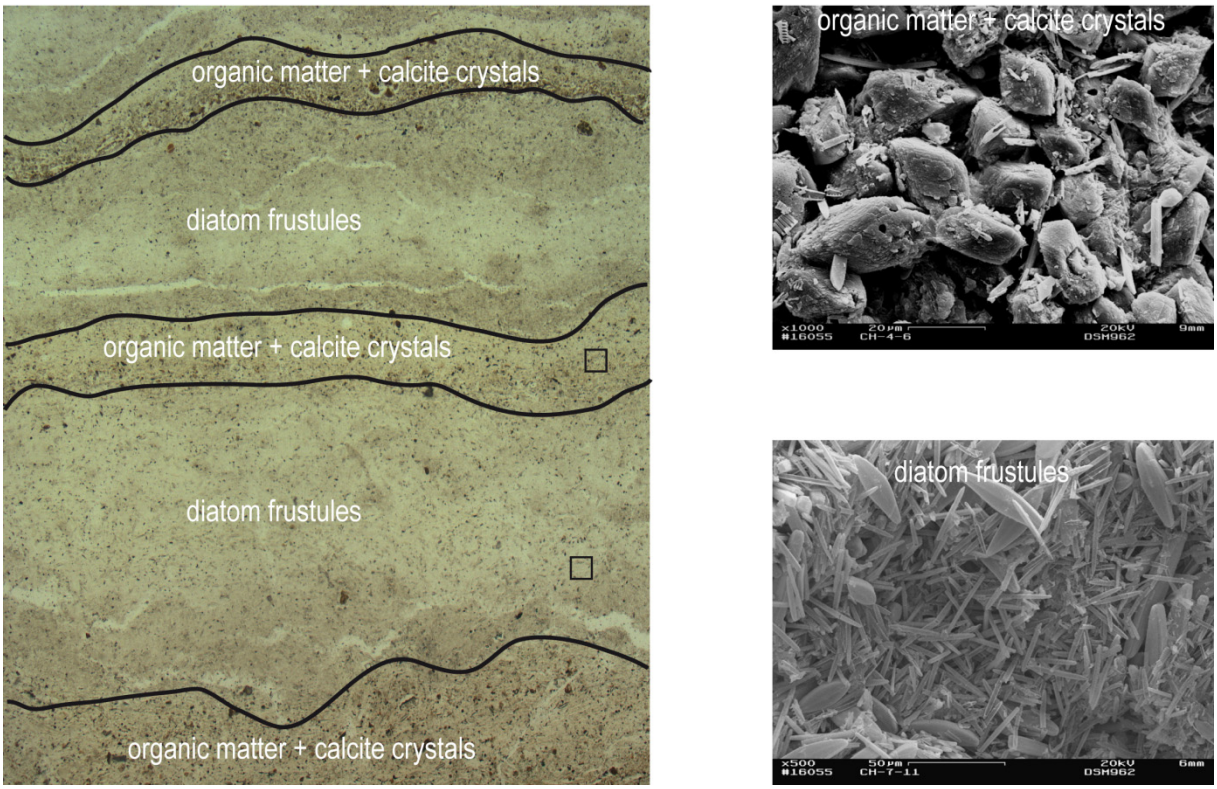

Fig. 2-8: Thin section photograph of laminated sediments of CH05-1G (1 cm depth) under normal white light, showing alternating lighter (diatom) and darker (detrital, calcite) laminae. Upper right close-up shows SEM photograph of calcite crystals from Lake Challa sediments (scale 20 µm). Lower right close-up shows light diatom layer (scale 50 µm).

Sedimentation model

The sedimentary deposits in Lake Challa, as documented by monthly trap data between 2006 and 2010, comprise ~20-50 wt. % siliciclastic matter, and inverse correlating contributions by autochothonous calcite and organic matter (including biogenic silica) each reaching maxima in a similar order of magnitude between 0-70wt. % ([100-(Siliclastics+$CaCO_3$+TOC]).

The influx of local siliciclastics is dominated by local debris of basaltic composition during the rainy season (November- April) which may be washed into the lake by surface runoff. Probably, the lake receives dissolved nutrient influx by surface run off. Nutrient influx by groundwater inflow depends on seepage of the rainfall and therefore may increase with some delay. Groundwater inflow, possibly, may also increase as result of lake level lowering in the the dry season. The influx of nitrogen and PO_4 is hardly detectable in lake water since it will be immediately consumed by phytoplankton. During the rainy season calcite reaches over-saturation in the upper 20 m water column. Seasonal biogenically induced precipitation of low-Sr calcite crystals is well documented by the water profiles of Ca, DIC, Ca/Sr, monthly trap data and the composition of calcareous organic-rich sub-layers in the sediment.

Diatom grow is strongly limited by SRP availability in the stratified lake. Partial overturn of the water column is related to increase of local wind stress and cooling during the dry season (May-October). Lake internal nutrient accumulation, particularly by the advective transport of SRP in the phototrophic zone supports seasonal diatom blooms. Hydrochemical data available for overturn event in August 2007 document under-saturation for calcite for the entire water column. In monthly trap materials from 2006-2009 calcite contents are distinctly decreased or even completely absent during the dry season. A 100-years sediment record of the lake documents regularly presence of distinct non-calcareous seasonal light diatom layers. The decline or even the absence of calcite precipitation is associated with a number of factors: (i) calcite precipitation in the previous season, (ii) temperature decrease, (iii) mixing with CO_2-rich deep water which puffers the pH increase associated with the CO_2 uptake by phytoplankton, (iv) and possible kinetic inhibition of crystal growth by PO_4 (Dittrich and Koschel, 2002).

The mixing of the water column shows inter-annual variability in terms of intensity, duration and beginning. During the seasonal water column stratification Fe^{2+} and Mn^{2+} get enriched in the anoxic deep water. Dissolved Mn and Fe precipitate by oxygenation of the deep during the overturn events. The net accumulation of chemical precipitated Mn in the sediment distinctly exceeds that of Fe due to the hydrochemical characteristics of the groundwater inflow and/or prevailing pH/Eh conditions. The chemical precipitation of Mn is sensitively recorded in μXRF scans of the sediments by Mn/Ti (Al), Mn/Fe maxima that coincide with distinct light diatom-rich laminae deposited during the overturn events in the dry season. Chemical characteristics of monthly trap materials demonstrate that the siliclastic influx comprises a local (basaltic) and a remote component characterized by high Al/Ti, and a La/Y mass ratio close to 1. The ratio of both end members in the depositional flux shows seasonal variability. Siliciclastic matter deposited during the dry/windy season occurring in light layer is clearly enriched in the high Al/Ti component and reflects aeolian input.

The climate archive Lake Challa

A pronounced feature of Lake Calla sediments are distinct season diatom layers. Photosynthetic production in the lake is strongly limited by SRP availability. Diatom blooms are associated with overturn events in the dry season. The extent of the diatom bloom, which is positively correlated with the lake-internal P-cycle during the overturn, is quantifiable by the thickness of the light diatom layers. The seasonal cycling of deep water SRP reservoir strongly depends on wind strength and temperature decrease during the dry season, therefore the net accumulation of biogenic opal can use as a proxy to reconstruct wind variations during the dry season. The deep water SRP pool, however, does not represent a constant parameter. Accumulation of SRP in the deep water depends on (i) external influx (mainly groundwater inflow), (ii) SRP removal during previous overturn events, (iii) SRP flux from the surface sediments across the sediment/water interface. The latter has to be considered for palaeoclimatic interpretations. Probably a more robust proxy is Al/Ti and La/Y. Increase of Al/Ti, decrease of La/Y potentially record enhanced aeolian influx of remote provenance related to changes in the wind regime and/or the dryness in the source region of the dust. Wind induced mixing lead to higher Mn/Fe (Mn/Ti) and Si/Al ratios. The similar trend to Al/Ti illustrate the link between the external signal via dust and the internal lake response via mixing. Both record combined produce an excellent proxy for wind strength, duration and intensity.

Conclusions

The limnological surveys conducted between September 1999 and November 2007 document seasonal variability in the hydrology of Lake Challa which is in agreement with meteorological observations in this region. During generally warmer southern hemisphere summer months (October – May), a stable water-column stratification develops and nutrient inflow during these rainy months supports peak photosynthetic activity in the deeper epilimnion of the lake. During southern hemisphere winter months (June – September), the temperature gradient within the water column is strongly reduced and south-easterly trade winds cause a pronounced thickening of the mixed layer. Deep and/or continuous mixing permits blooming of diatoms. Based on lake water analyses, preliminary results from sediment-trap studies and geochemical investigations on laminated sediments from a short core, we develop a model for the formation of laminated sediments in Lake Challa which is in good agreement with the observed seasonal changes in limnology and regional meteorological conditions. We showed that diatom blooms are related to deeper mixing in the lake, which is documented by relatively high Mn/Fe ratios within these light sediment laminae and in the sediment trap samples. Dark laminae are characterised by higher detrital influx and therefore high Fe, Ti and S intensities. Low Mn/Fe ratios and observations of Fe-sulphides within dark laminae suggest reducing conditions at the lake bottom during times of a well-stratified water column. Simultaneously high Al/Ti ratios document enhanced aeolian influx of remote provenance. The hydrological investigations presented in this study document distinct seasonality in the Lake Challa system. Sedimentological and geochemical investigations of recent sediments show that this signal is preserved in the sedimentary record, and results from ongoing lake monitoring will probably allow even finer differentiation of seasonal signals. The results from the Lake Challa sediment archive presented here constitute the site as highly valuable target for high-resolution palaeoclimate studies in East Africa.

Acknowledgement

This work has received funding from the ESF-EUROCORES program EuroCLIMATE (CHALLACEA) and through the Graduate School GRK 1364 Shaping Earth's Surface in a Variable Environment funded by the Deutsche Forschungsgemeinschaft (DFG) as well as C.W. is grateful for grant from Leibniz Center for Earth Surface Process and Climate Studies. Fieldwork was conducted with research permission of the Kenyan Ministry of Education and Science to Dirk Verschuren (MOEST 13/001/11C). We further acknowledge Jasper Moernaut (Ghent University, Belgium) for the bathymetric map, and Ursula Kegel (GFZ) for laboratory support. Caxton Mukhwana Oluseno is especially thanked for unfailing work in lake monitoring and finally all the Kenya crew members without whose assistance in transport, surveillance and accommodation this project could not be handled.

3 Reduced interannual rainfall variability in East Africa during the last ice age

Accepted for publication in: Science

Christian Wolff[1,2,3], Gerald H. Haug[3,4*], Axel Timmermann[5], Jaap S. Sinninghe Damsté[6,7], Achim Brauer[1], Daniel M. Sigman[8], Mark A. Cane[9], Dirk Verschuren[10]

[1]Helmholtz Centre Potsdam GFZ German Research Centre for Geosciences, Section 5.2 – Climate Dynamics and Landscape Development, Telegrafenberg, D-14473 Potsdam, Germany

[2]DFG Graduate School 1364, University of Potsdam, Institute of Geosciences, Karl-Liebknecht Strasse 24, Haus 27, D-14476 Potsdam, Germany

[3]DFG Leibniz Center for Earth Surface Process and Climate Studies, University of Potsdam, D-14476 Potsdam, Germany

[4]Geological Institute, Department of Earth Sciences, ETH Zürich, CH-8092 Zurich, Switzerland

[5]IPRC, SOEST, University of Hawai'i, 2525 Correa Road, HI 96822, United States

[6]Faculty of Geosciences, Utrecht University, PO Box 80021, 3508 TA Utrecht, The Netherlands

[7]Department of Marine Organic Biogeochemistry, NIOZ Royal Netherlands Institute for Sea Research, PO Box 59, 1790 AB Den Burg, The Netherlands

[8]Department of Geosciences, Princeton University, Princeton, New Jersey 08544, United States

[9]Lamont-Doherty Earth Observatory of Columbia University, Palisades, NY 10964-8000, United States

[10]Limnology Unit, Department of Biology, Ghent University, Ledeganckstraat 35, 9000 Gent, Belgium

Abstract

Interannual rainfall variations in equatorial East Africa are tightly linked to the El Niño Southern Oscillation (ENSO), with more rain and flooding during El Niño and droughts in La Niña years, both having severe impacts on human habitation and food security. Here we report evidence from an annually laminated lake sediment record from southeastern Kenya for interannual to centennial-scale changes in ENSO-related rainfall variability during the last three millennia and reductions in both the mean rate and the variability of rainfall in East Africa during the Last Glacial period. Climate model simulations support forward extrapolation from these lake sediment data that future warming will intensify the interannual variability of East Africa's rainfall.

Introduction

In the tropics, changes in rainfall patterns have severe consequences for millions of people. East Africa, in particular, has in recent years experienced both extreme flooding and severe droughts, with serious impacts on developing economies and wildlife throughout the region (Parry and Intergovernmental Panel on Climate Change. Working Group II., 2007). Seasonality in East African climate is controlled primarily by the biannual migration of the Intertropical Convergence Zone (ITCZ) across the region (Nicholson, 1996) (Fig. 1-1). As a result, equatorial East Africa experiences two climatological rainy seasons (Nicholson, 2000). Dry seasons are windy, due to the trade winds that straddle the ITCZ. Interannual variations in the seasonal migration of the East African ITCZ are driven to a large extent by the El Niño Southern Oscillation (ENSO) (Ropelewski and Halpert, 1987) and its related western Indian Ocean sea surface temperature (SST) anomalies (Goddard and Graham, 1999; Latif et al., 1999). El Niño events alter the atmospheric circulation, typically generating an equatorial Indian Ocean SST pattern that is warmer in the west and cooler in the east, a configuration sometimes referred to as the positive phase of the Indian Ocean Dipole Mode (Saji et al., 1999). Surface ocean warming in the western Indian Ocean leads to intensification and shifts of the ITCZ, bringing more precipitation to East Africa and weakening the local surface winds (Black et al., 2003; Hastenrath and Polzin, 2004) (Fig. 3-1a). El Niño thus tends to enhance East African rainfall indirectly by causing a warming in the western Indian Ocean, even though the direct teleconnection through the atmosphere tends to reduce rainfall (Goddard and Graham, 1999).

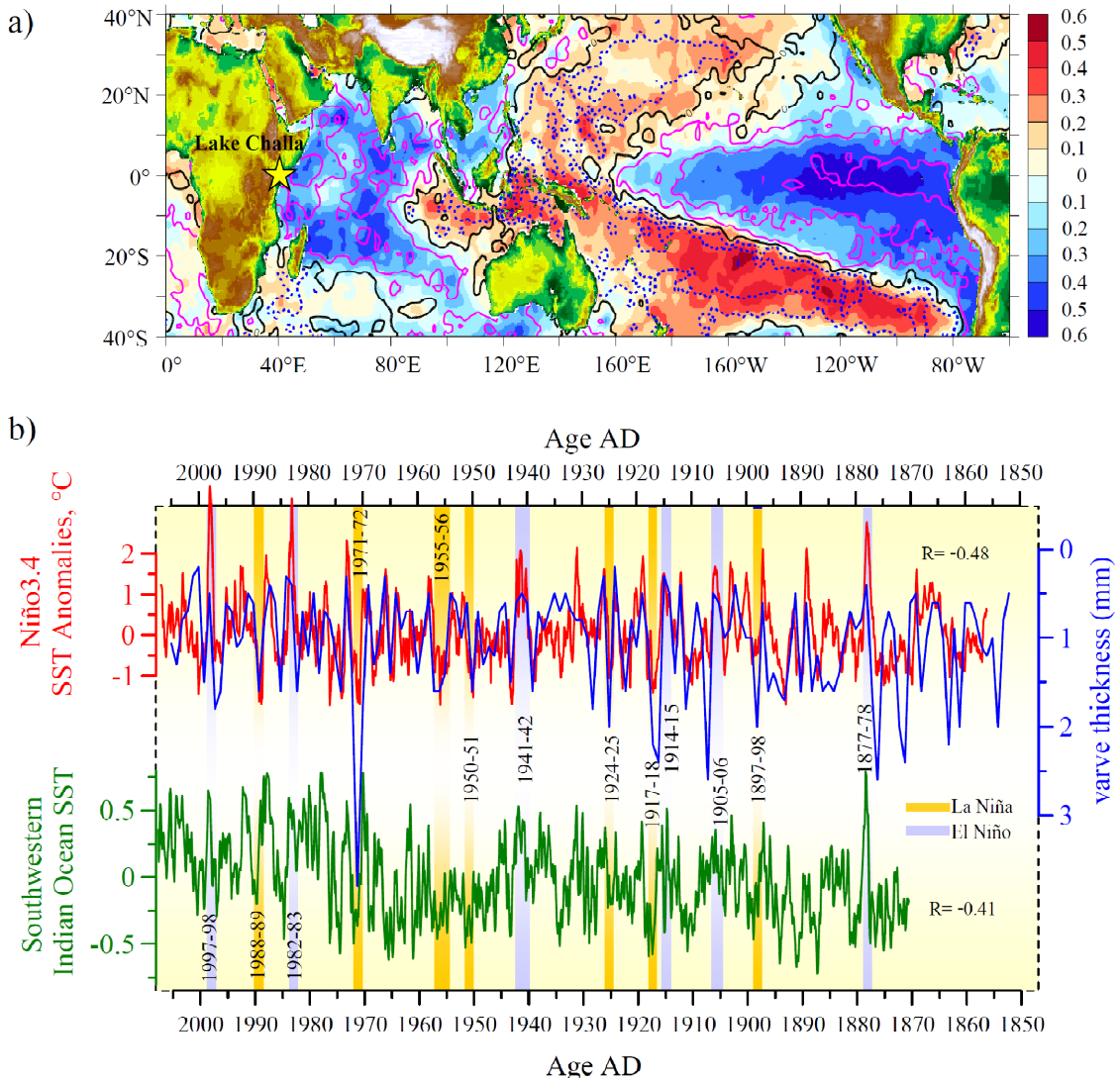

Fig. 3-1: The effect of tropical sea surface temperature anomalies on interannual climate variations in East Africa and varve thickness variations in Lake Challa. (a) Shading: Correlation between November 10 m wind speed anomalies near Lake Challa (yellow star) (3.5S-3S, 37-38E), obtained from the NCEP-NCAR reanalysis (Kalnay et al., 1996) and the November HadISST1 sea surface temperature anomalies (Rayner et al., 2003) at every grid point in the tropical Indo-Pacific from 1948-2011. Contours: Correlation between November precipitation anomalies at the WMO station 63816 in Same, Tanzania (4°05'S, 37°43'E, 872.0 m elevation), near Lake Challa and the November HadISST sea surface temperature anomalies (Rayner et al., 2003) at every grid point from 1950-1989, contour interval is 0.2 and the cyan (blue dashed) contours indicate positive (negative) correlations. The solid black line is the zero correlation contour. In November positive wind speed anomalies and negative precipitation anomalies near Lake Challa are significantly correlated with La Niña and positive Indian Ocean Dipole conditions at the 95% level (b) Time series of HadISST anomalies averaged over the western Indian Ocean from 48°E-72°E and 24°S-12°S (green line; 3-point running mean) (Rayner et al., 2003) and the Niño3.4 index (red line) (Kaplan et al., 1998) show a high degree of correlation with varve thickness in Lake Challa (blue line). Thin varves correspond to El Niño events (positive Niño3.4 values) and thick varves to La Niña events (negative Niño3.4 values).

Here we provide information on interannual climate variability in East Africa going back to the last ice age, using the annual varve-thickness record of sedimentation in Lake Challa (3°19'S, 37°42'E; 880 m above sea level), a freshwater crater lake on the lower east slope of Mt. Kilimanjaro (Kenya/Tanzania) (Fig. 3-2).

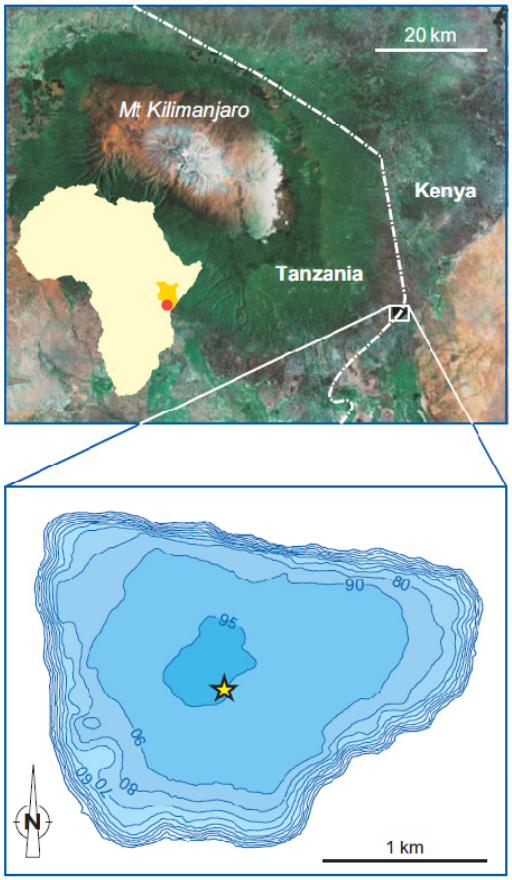

Fig. 3-2: Position of Lake Challa (3°19'S, 37°42'E; 880 m asl.) and its catchment area on the lower east slope of Mt. Kilimanjaro on the border between Kenya and Tanzania. The yellow star indicates the 2005 core site. Depth contours (Moernaut et al., 2010) are drawn at 10 m intervals to 90 m depth, and at 95 m depth.

Methods

Two time slices of climatic interest were chosen from the existing 20.82 m composite profile (Verschuren et al., 2009): the uppermost 2.80 m represents the last 3056 varve years and a 3.07 m long interval between 14.38 and 17.45 m depth spans a floating chronology of 2554 varve years; both are linked to and consistent with the absolute calendar time scale using the existing age model based on ^{14}C dating (Verschuren et al., 2009) (Fig. 1-4). Microscopic varve counting was carried out on two continuous series of overlapping thin sections (size 120 x 35 mm with a 2 cm overlap) resulting in construction of a varve chronology. The thin sections were prepared from slabs of fresh sediment by shock-freezing in liquid nitrogen followed by freeze-drying for 48 h and impregnation with Araldite

resin. A special microscope stage equipped with a micrometer drive allowed precise movement of thin sections for varve thickness measurements. Spectral analyses of varve thickness were undertaken using a Fast Fourier Transform routine in AnalySeries (Paillard et al., 1996). Wavelet power spectra were generated using the method of (Torrence and Compo, 1998). All data time series were normalized and detrended prior to analysis. Correlation coefficients were calculated by using a moving cross-correlation routine (Nowaczyk et al., 2002) in Moving Cross Correlation 2 (© N. R. Nowaczyk; GFZ Potsdam).

Results and Discussion

The Lake Challa sediment profile is dominated by thick sequences of fine laminations. These laminated sequences, deposited under anoxic conditions, consist of light-dark couplets that accumulated in the lake over the last 25,000 years (Verschuren et al., 2009) at a sedimentation rate varying between 0.08 and 7 mm yr-1 (Fig. 1-4). The darker layers consist largely of amorphous organic matter derived from phytoplankton and calcite crystals precipitated from the water column, while diatom frustules are the dominant constituent of the light layers. In order to refine our interpretation of seasonal layer deposition in Lake Challa, a sediment trap program was initiated in 2006 at an offshore location in the lake. Analysis of the monthly collected sediment trap material confirmed the annual origin of the dark/light couplets, with the light layer deposited during the long dry season (June-October, i.e. centered on the austral winter season) and the dark layer representing the two rainy seasons (November-December and March-May) and the brief intervening dry season (January-February) (Fig. 3-3). Comparison of the thickness of the light and dark layer within a year's couplet indicates that the total varve thickness is controlled by the thickness of the light layer (Fig. 3-4). Thus, varve thickness mainly reflects the quantity of diatom frustules deposited during the dry season and in particular during April to September.

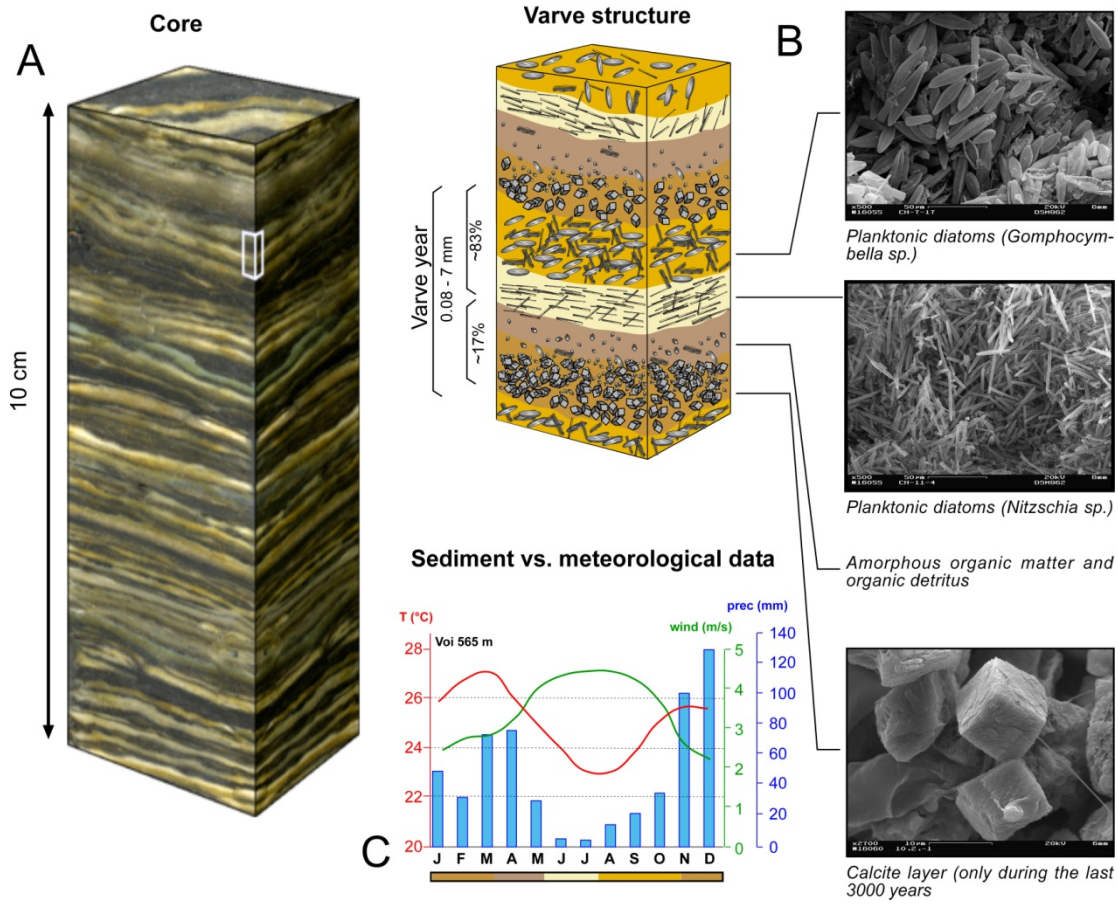

*Fig. 3-3: Structure of finely laminated Lake Challa sediments. (**A**) Lake Challa sediment column showing the succession of light and dark layers. (**B**) Microfacies analyses reveal that the dark layers predominantly consist of amorphous organic matter and crystals of endogenic calcite. Diatom frustules are the overall dominant constituents of the light layer. Light layers are usually the most prominent, ranging from 20% to 99.7% (mean 83%) of total varve thickness in the two studied sections, whereas the dark layers range from 0.3% to 80% (mean 17%). (**C**) Comparison of the respective light and dark layer components collected in monthly sediment-trap samples (coloured bar) with meteorological data from Voi (80 km east of Lake Challa, Kenya) allows us to connect the dark layer to the warm and wet southern hemisphere summer and the light diatom layer to the cool, dry and windy southern hemisphere winter. We therefore interpret each light/dark couplet as a varve, representing one full year of lacustrine sedimentation.*

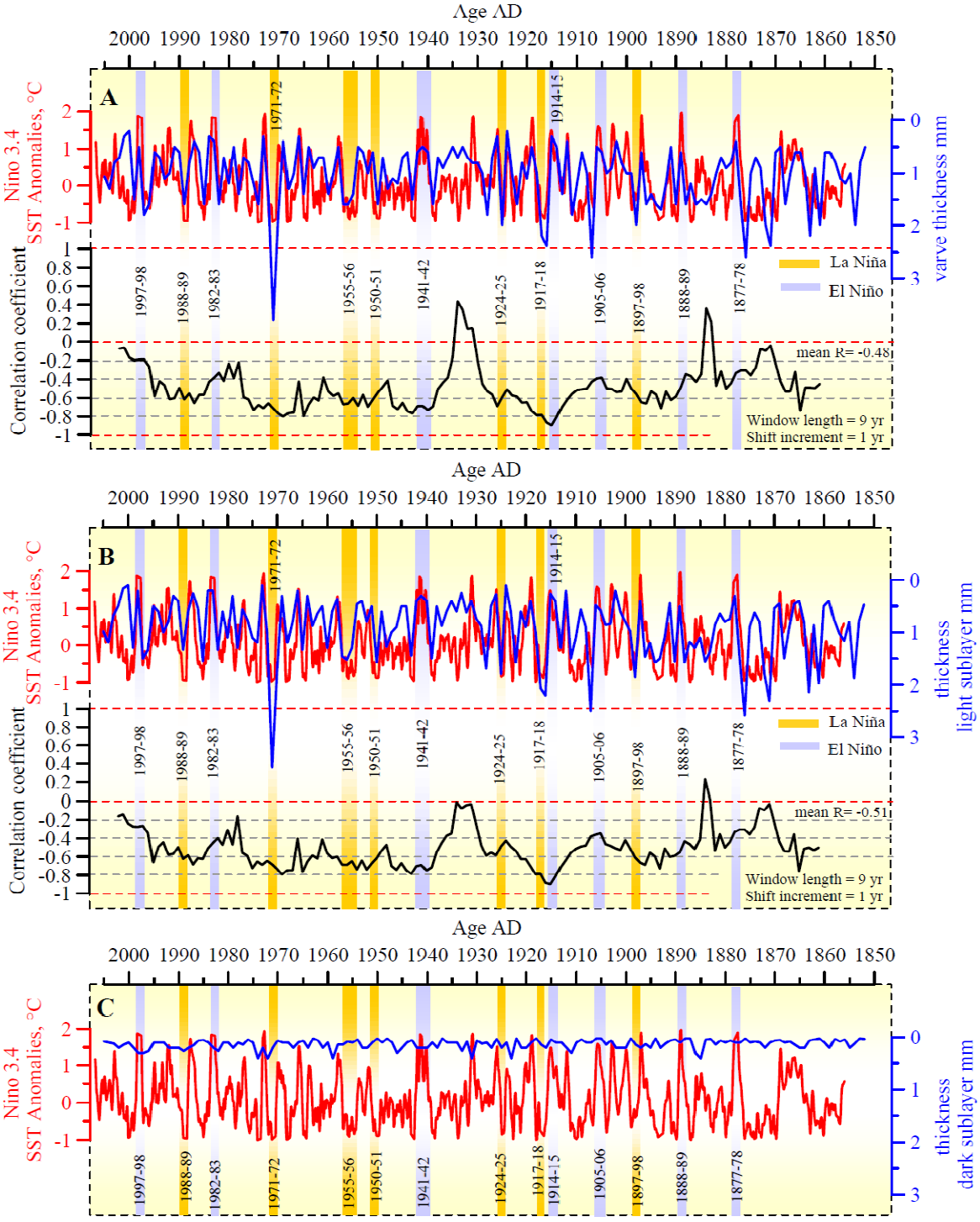

Fig. 3-4: Variability in Lake Challa varve thickness over the last 155 years. Comparison of total varve thickness (A), light (diatom) layer thickness (B) and dark layer thickness (C) shows that total varve thickness is controlled by variability in light layer thickness. The black line at the bottom of panels A and B show the nearly identical trends of the moving correlation coefficient between either total varve thickness (A) or light-layer thickness (B) with the Nino3.4 index (Kaplan et al., 1998).

In southeastern Kenya, the windy season begins in April/May, when the ITCZ moves north across the equator and southerly winds become dominant. These winds, which in the modern climate normally last until late October, combine with seasonally lower insolation to cool the lake surface and deepen the mixed layer of the lake from late June to September. During episodes of high wind stress, deeper convection extends to below 35 m depth (as deep as 40-45 m in some years; Fig. 3-5), making the dissolved nutrients which accumulate over time in the lake lower water column again available for phytoplankton growth at the lake surface. Enhanced nutrient availability coinciding with a more turbulent water column promotes diatom blooms (Pilskaln and Johnson, 1991), which are preserved as the light layer in the varves.

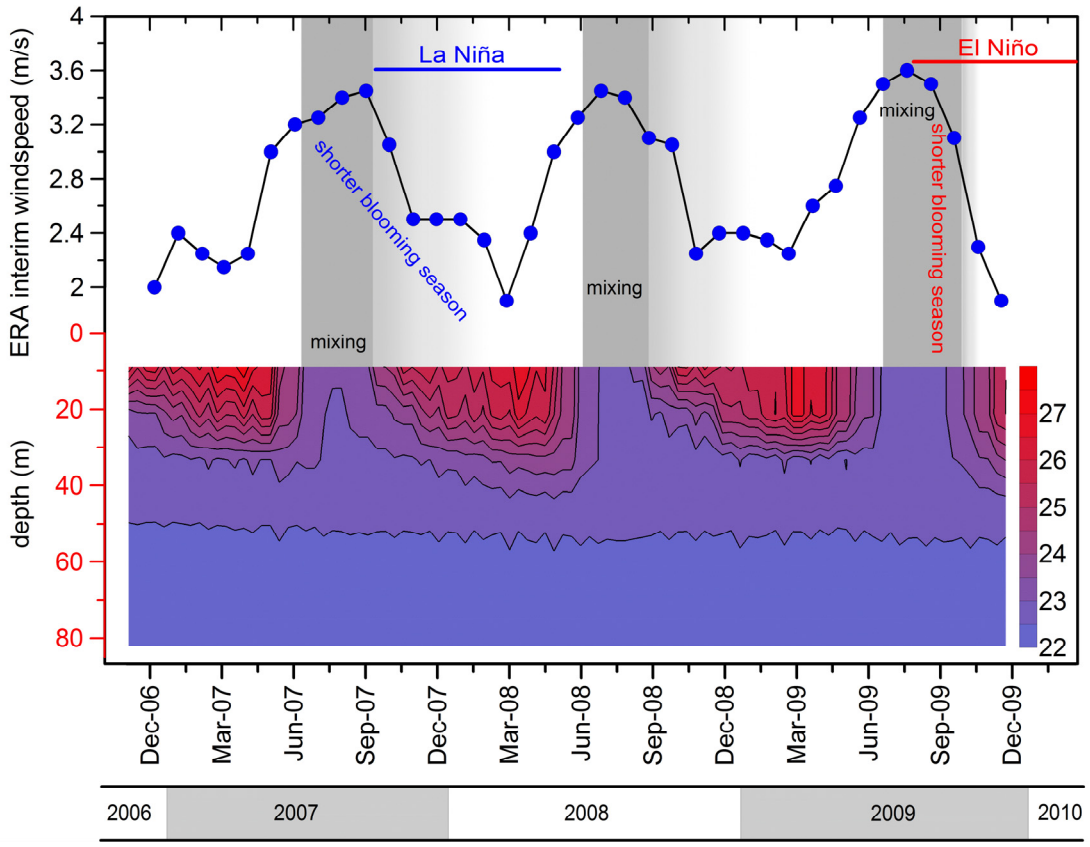

Fig. 3-5: Schematic illustration of the processes governing varve formation in Lake Challa: Mean monthly wind-speed (in m/s) obtained from the ERA interim dataset (Simmons et al., 2007) and in-situ measurements of temperature variation with depth in the water column of Lake Challa (>10 m water depth), measured between December 2006 and January 2010. La Niña and El Niño events have their largest impact on East African windspeeds in October and November (Fig. 3-1a). During La Niña events, such as 2007/2008 the climatological windy season in East Africa is prolonged, which leads to fairly gradual development of a warm upper water layer, a longer period of diatom growth and hence thicker varves. El Niño events such as the 2009/2010 terminate the windy-season in November, which results in more rapid development of a thick and warm upper water layer interruption of diatom growth and reduced thickness of the varves.

Therefore, we interpret thick varves to indicate years of longer windy conditions. Conversely, thin varves reflect reduced diatom productivity due to weaker winds, characteristic of years when the ITCZ remains overhead or nearby for a greater fraction of the year. Given the modern control of seasonal ITCZ location on wind and rain in this region (Nicholson, 1996; Nicholson, 2000; Ropelewski and

Halpert, 1987) and the broad inverse relationship between rainfall and windiness at the interannual time scale (Fig. 3-6), thick varves represent windier and thus drier years.

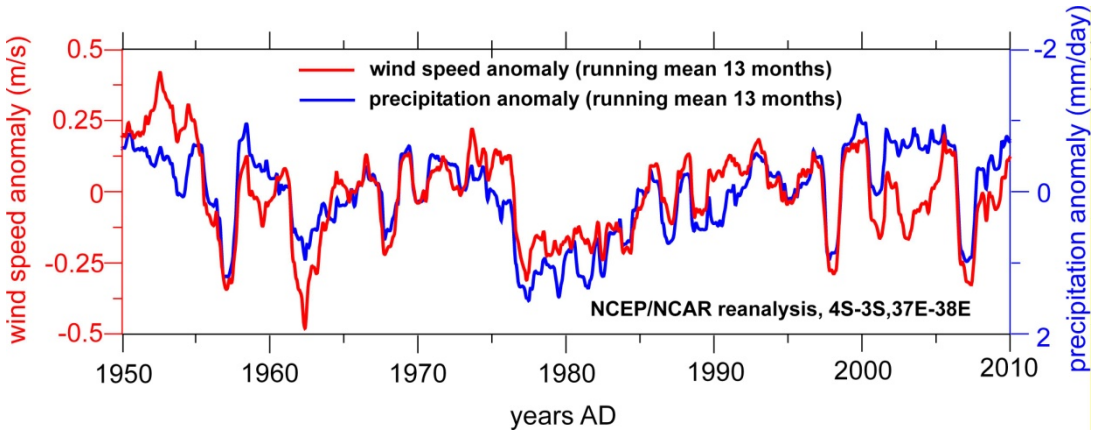

Fig. 3-6: Comparison between wind speed (13-months running mean) and negative precipitation anomalies (13-months running mean) near Lake Challa illustrates the inverse relationship between rainfall and wind speed on interannual timescales in the region of Lake Challa. Anomalies at Lake Challa were obtained from the NCEP-NCAR reanalysis (Kalnay et al., 1996) dataset.

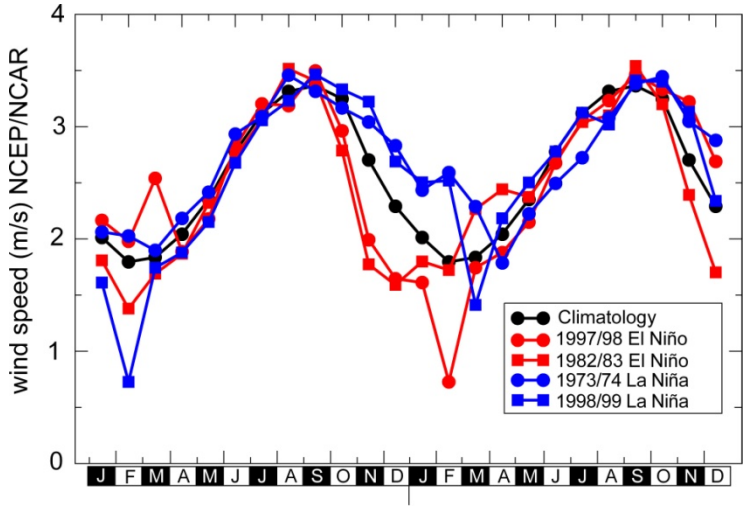

Fig. 3-7: Monthly wind speed (m/s) near Lake Challa based on NCEP/NCAR Reanalysis data (Kalnay et al., 1996) for the El Niño events 1997/1998 and 1982/1983 (red lines) and La Niña events 1973/1974 and 1998/1999 (blue lines), in relation to the long-term means (black line, 1971-2000). La Niña events prolong the windy season through the short rain season, whereas El Niño events terminate it in November. Note that wind speeds during May-September change very little in response to ENSO.

El Niño (La Niña) events are associated with wetter (drier) conditions in East Africa and decreased (increased) surface wind speeds (Fig. 3-1a, Fig. 3-7). We verified the regional significance of our varve-thickness record as an ENSO/ITCZ-sensitive record by comparing the varve thickness data of the last 150 years with an ENSO index and a western Indian Ocean SST index (Kaplan et al., 1998; Rayner et al., 2003) (Fig. 3-1b). To a remarkable degree, thick varves coincide with La Niña years, while thin varves correspond to El Niño years (Fig. 3-8), supporting our expectations based on the annual cycle. It should be noted here that the varve thickness record is particularly sensitive to La Niña

conditions and shows some evidence for saturation during El Niño years. The results confirm that varve thickness in Lake Challa is a robust indicator of regional climate and its broader sensitivities.

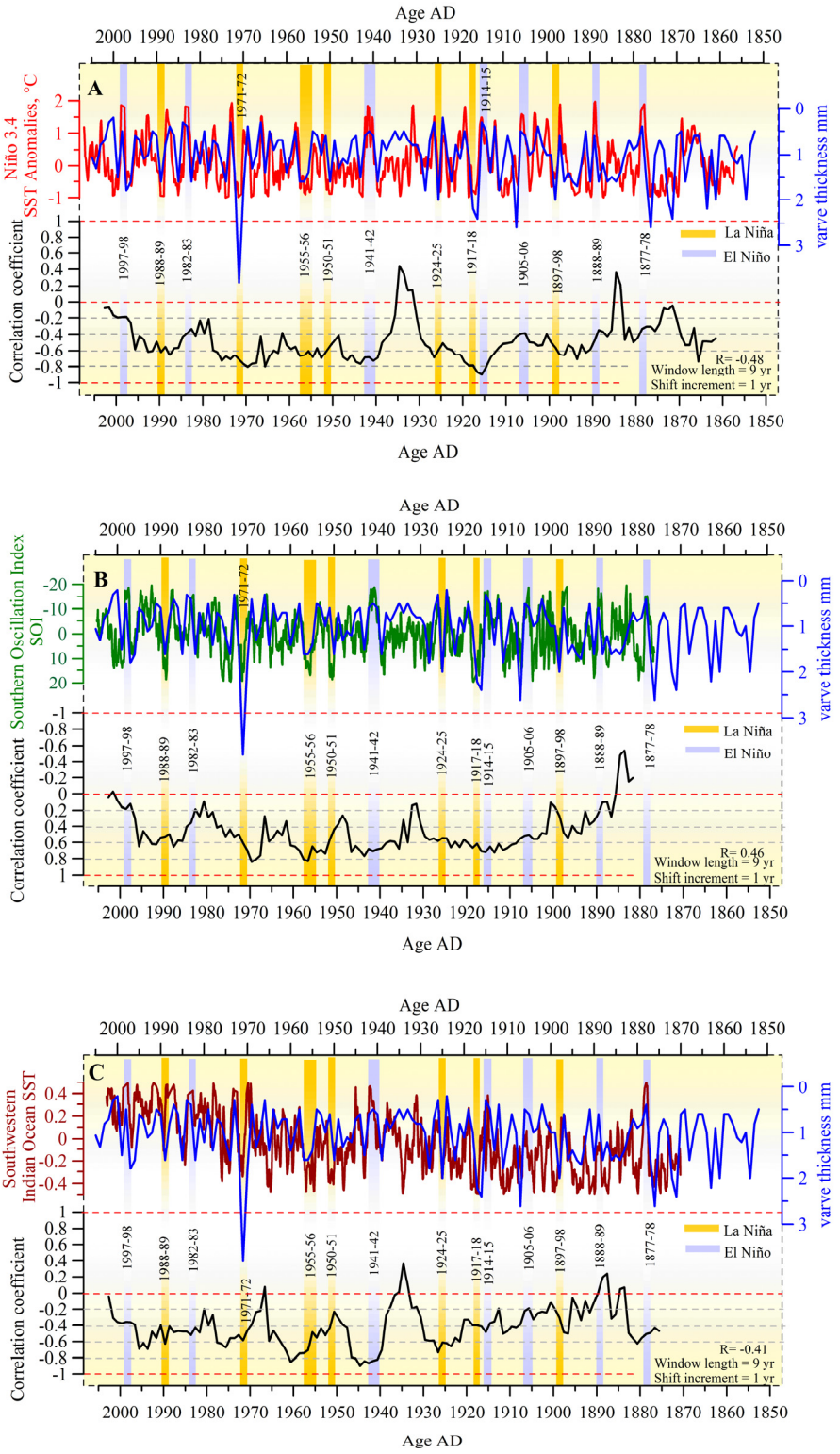

Fig. 3-8: Comparison between variation in Challa varve thickness over the last 155 years and the time series of Niño 3.4 anomalies (Kaplan et al., 1998) (A; as in Fig. 3-4), Southern Oscillation Index (Ropelewski and Jones, 1987) (B) and HadISST1 anomalies over the western Indian Ocean from 48°E-72°E and 24°S-12°S (Rayner et al., 2003) (C). The black lines show the moving correlation coefficients.

The correspondence between Lake Challa varve thickness and regional rainfall can also be evaluated in the more distant past by comparison to other proxies. Combined 25,000-year records of an organic biomarker (BIT-index) rainfall proxy from Lake Challa as well as lake level inferred from seismic stratigraphy (Moernaut et al., 2010; Verschuren et al., 2009) show that climate in easternmost equatorial Africa was generally much drier than today between 20.5-16.5 ka BP. The average varve thickness in Lake Challa is greater between ~18,500 and 21,000 years BP (14.38-17.45 m core depth), which includes the later part of the Last Glacial Maximum (LGM, recently defined as the period 26.5-19 ka BP, (Clark et al., 2009)), than in the last 3,000 years (0-2.80 m core depth) (Fig. 3-9). Further, during the Maunder and Spörer sunspot minima within the Little Ice Age (AD 1270-1750), below-average varve thickness at Lake Challa coincided with high lake level in nearby Lake Naivasha (Verschuren et al., 2000). These correspondences (Fig. 3-9) provide evidence for a broad negative relationship between the length of the windy season and rainfall, also on time scales of centuries and millennia. Lake Challa varves primarily capture the rainfall variability that is inherently anti-correlated to local windiness (Fig. 3-6). This type of variability dominates the interannual to decadal variability evident in instrumental data (Fig. 3-1a), and, in general, it is associated with the regionality of atmospheric convergence (e.g., the ITCZ and its migration). The correspondences noted above between the varve thickness record and lake level and BIT index data suggest that, even on centennial to millennial timescales, a substantial part of variability in East African rainfall is driven by changes in the global and/or regional geometry of convection. In the same vein, a record from the Cariaco Basin (Haug et al., 2001) identifies the Little Ice Age as mostly a dry, rather than wet interval. This anti-correlation between equatorial East Africa and northern South America is consistent with ENSO's global impacts on the locations of convection (Kiladis and Diaz, 1989; Ropelewski and Halpert, 1987).

As reconstructed from the Lake Challa varve-thickness record, ENSO-related interannual rainfall variability has undergone changes and transitions during the last 3,000 years (Fig. 3-10). Our reconstruction indicates that this variability was strongly muted during the period between 300 BC and 300 AD, in agreement with ENSO proxy data from Ecuador (Moy et al., 2002). An increase in variability is observed for the period 400 AD-750 AD. The gradual decline in variability during the Medieval Climate Anomaly terminated abruptly around 1300 AD. A second, less prominent phase of variance reduction occurred during the Little Ice Age (1400 AD-1750 AD). The drivers for these prominent century-scale variations are unknown. More detailed comparisons with other ENSO-sensitive paleo-proxies may shed light on the exact role of Pacific versus Indian Ocean SST control in rainfall variability over tropical East Africa during these periods (Goddard and Graham, 1999).

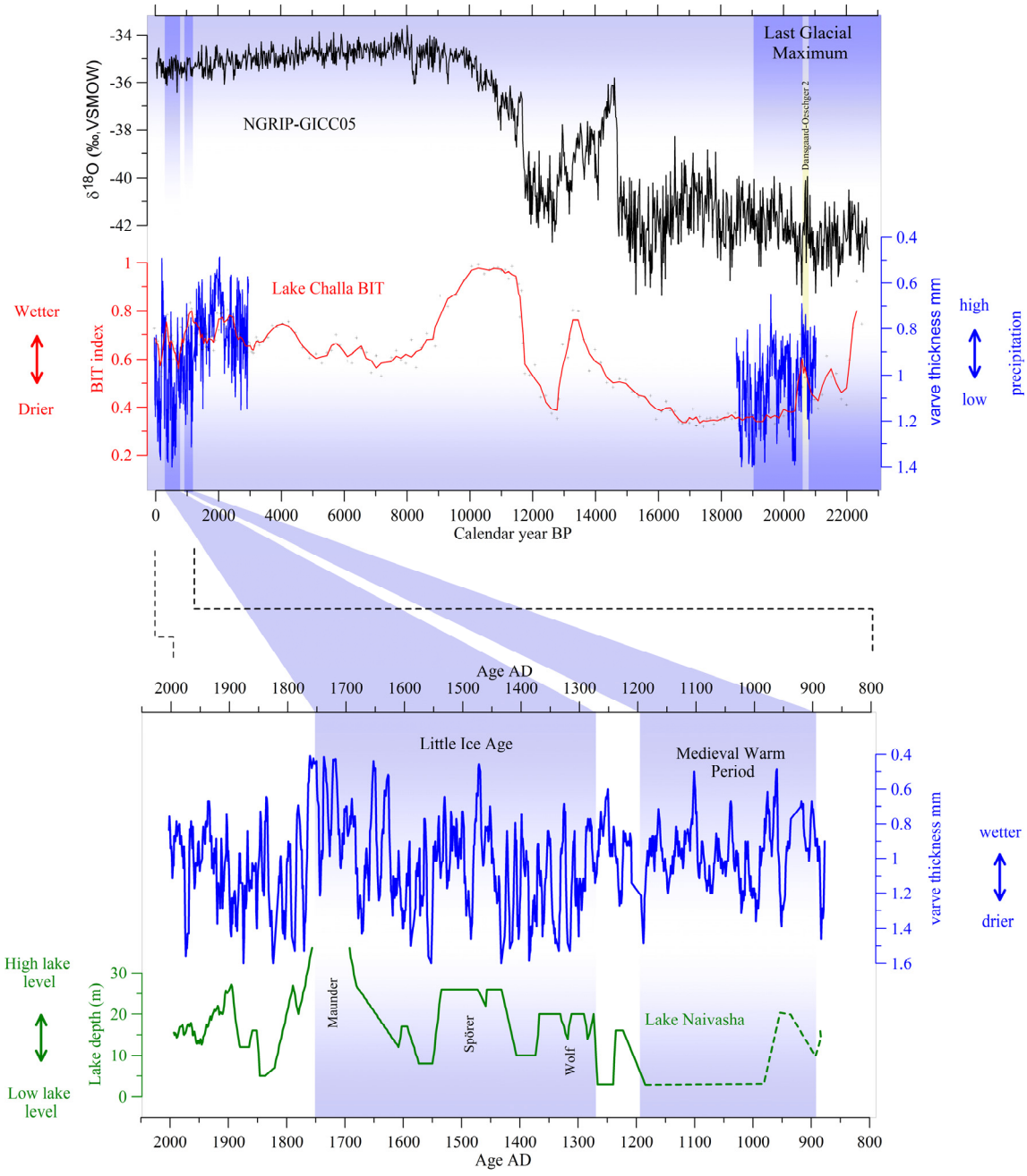

Fig. 3-9: Varve thickness data with selected other climate records spanning the last 22,500 years (top) and the past 1100 years (bottom). (Top) The mean varve thickness data (blue line, 21-point running mean) in comparison with the Greenland $\delta^{18}O$ ice core record on the GICC05 timescale (NGRIP-GICC05, (black line) (Rasmussen et al., 2006); and the Lake Challa BIT-index rainfall reconstruction (red line; 3-point running mean) (Verschuren et al., 2009). The BIT index is based on the contribution of soil-derived bacterial membrane lipids relative to aquatically produced crenarchaeotal membrane lipids (Hopmans et al., 2004). (Bottom) Varve thickness data (blue line, 7-point running mean) during the past 1100 years compared with the lake-level record from Lake Naivasha in central Kenya (Verschuren et al., 2000) (green line).

During the last ice age, climate in tropical Africa differed greatly from modern climate (Gasse et al., 2008). The greater mean varve thickness in Lake Challa suggests on average stronger winds during the peak glacial climate, reminiscent of colder conditions in the western Indian Ocean (Sonzogni et al., 1998). On interannual timescales, the SST anomalies in the western Indian Ocean are strongly controlled by ENSO; however, on glacial-interglacial time scales, the role of external forcings such as reduced greenhouse gas concentrations, orbital forcing, and remote effects of the expanded ice sheets (Justino and Peltier, 2008) must also be considered.

Instrumental data show that winds and rainfall are highly anti-correlated on interannual to decadal time scales (Fig. 3-1, Fig. 3-6). Thus, the use of Lake Challa varves to reconstruct rainfall variability is better justified when applied to these time scales. In this context, the interannual variability of the Lake Challa varves suggests an important difference between LGM and late Holocene conditions. The variability in varve thickness might be expected to be intrinsically related to mean varve thickness. However, while mean varve thickness in the 2554-year long glacial section of our core is greater than in the 3056-year long Late Holocene section, its interannual variability is markedly less (Fig. 3-10, Fig. 6-1). This result – less variability when varves are thicker – indicates reduced variability in East African winds and rainfall at ENSO time scales under cold LGM conditions. It is notable that the late Holocene sediments, characterized by thinner varves on average, nevertheless have the thickest individual varves (Fig. 3-10). Thus, while the interglacial is generally characterized by wetter, less windy conditions, it has experienced years that were windier (and thus very likely also drier) than prevailed during the last ice age (McGee et al., 2010).

These findings of a more interannually stable climate in East Africa during colder periods support the notion of strong sensitivity of the winds and the hydrological cycle to the larger scale climate. Warmer climate states appear to produce greater climate variability. This inference fits the growing consensus that current global warming will intensify the hydrological cycle, with wet regions and periods becoming wetter and dry regions and periods becoming drier (Held and Soden, 2006). As an example of this tendency from models, experiments with the NCAR CCSM3 coupled general circulation model for Last Glacial Maximum, pre-industrial and modern conditions, and a doubling of pre-industrial CO_2 levels (Otto-Bliesner et al., 2006; Yeager et al., 2006) show the same trends in mean rainfall and rainfall variability in eastern equatorial Africa in relation to mean temperatures as indicated by our lake varve data (Fig. 3-10): under warmer climates, both mean rainfall and interannual rainfall variability are greater (Fig. 3-10). A future increase in the interannual variability of rainfall in equatorial eastern Africa, which is projected by the model and supported by our varve thickness data, may bring further environmental stress to a region with reduced capacity to adapt to the mounting adverse effects of global climate change.

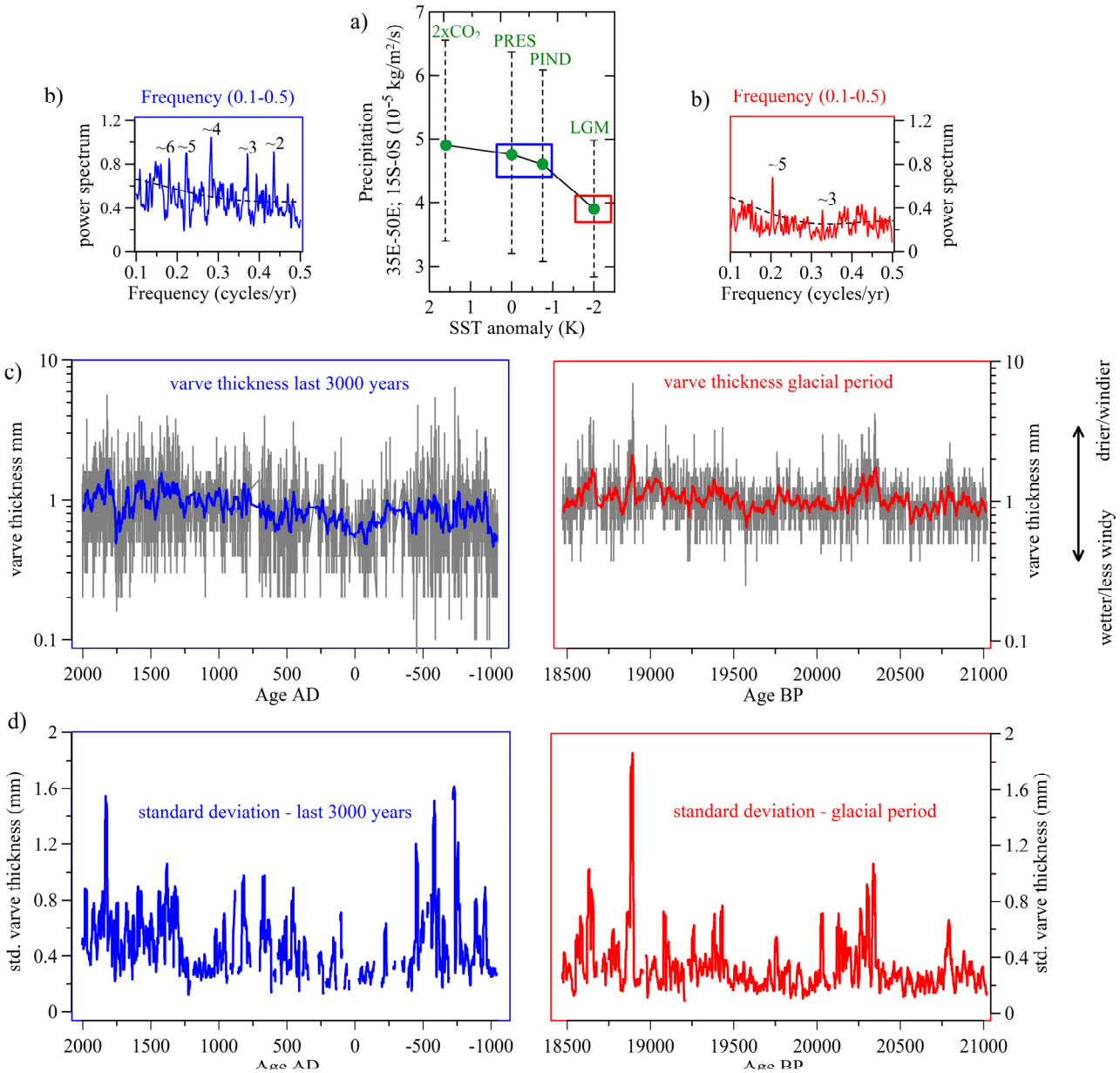

Fig. 3-10: (a) Simulated East African rainfall (average from 15°S-0°S and 35°E-50°E) and Indian Ocean surface temperature changes (average from 24°S-12°N and 48°E-72°E) for a series of Coupled General Circulation Model Simulations conducted with the CCSM3 climate model. The labels LGM, PIND, PRES, and 2xCO2 refer to the Last Glacial Maximum experiments, the pre-industrial control run, the present-day control run, and a CO2-doubling experiment, respectively. The green dots represent the mean of simulated East African precipitation as a function of western Indian Ocean SST change relative to the PRES run. The vertical bars feature the standard deviation of the simulated annual and interannual rainfall variability. Indian Ocean warming leads to an intensification of the ITCZ and increased variability. (b) Power spectrum on varve thickness for the last 3,000 years (blue line) and between 18,500-21,000 years BP (red line); the dashed lines represent the 95% significance level for a red noise spectrum. (c) Varve thickness time series (c) for the last 3,000 years and between 18,500-21,000 years BP (grey line shows raw varve thickness data, while thick blue and red lines show a 21-point running mean). (d) Corresponding running standard deviation for the last 3,000 years and between 18,500-21,000 years BP per 15-year.

Acknowledgement

This work received funding from the ESF-EUROCORES program EuroCLIMATE (FP28 CHALLACEA) and through the Graduate School GRK 1364 Shaping Earth's Surface in a Variable Environment funded by the Deutsche Forschungsgemeinschaft (DFG). C.W. is grateful for grant from Leibniz Center for Earth Surface Process and Climate Studies. A.T. received support from NSF grant No. AGS-1010869 and the Japan Agency for Marine-Earth Science and Technology (JAMSTEC). Fieldwork was conducted with research permission of the Kenyan Ministry of Education and Science to D.V. (MOEST 13/001/11C). We gratefully acknowledge C. M. Oluseno, I. Kristen, U. Frank and A. Hoechner for comments and assistance and the CHALLACEA team for stimulating discussions.

4 Seasonality in precipitation and evaporation for the last 25,000 years revealed by oxygen isotope records from Mount Kilimanjaro

Accepted for publication in: Geology

Philip A. Barker[1], Elizabeth R. Hurrell[1], Melanie J. Leng[2], Christian Wolff[3], Christine Cocquyt[4], Hilary J. Sloane[2], and Dirk Verschuren[5]

[1]*Lancaster Environment Centre, Lancaster University, Lancaster, LA1 4YQ, UK*

[2]*NERC Isotope Geosciences Laboratory, British Geological Survey, Keyworth, Nottingham, NG12 5GG, UK*

[3]*Helmholtz-Centre Potsdam, GFZ German Research Centre for Geosciences Section 5.2 Climate Dynamics and Landscape Development Telegrafenberg, C 320, D-14473 Potsdam Germany*

[4]*National Botanic Garden of Belgium, Domein van Bouchout, 1860 Meise, Belgium*

[5]*Limnology Unit, Department of Biology, Ghent University, Ledeganckstraat 35, 9000 Ghent, Belgium*

Abstract

Multi-proxy analysis of a well-dated 25,000-year (25 ka) lake-sediment sequence from Lake Challa, on the eastern flank of Mt Kilimanjaro, reveal the climatic controls governing the lake's palaeohydrology and the climate-proxy record contained in the mountain's receding ice cap. The oxygen-isotope record extracted from diatom silica ($\delta^{18}O_{diatom}$) in Lake Challa sediments captured dry conditions during the last glacial period and a wet late-glacial transition to the Holocene interrupted by Younger Dryas drought, and it faithfully traced gradual weakening of the southeastern monsoon during the Holocene. Overall, $\delta^{18}O_{diatom}$ matches the branched isoprenoid tetraether (BIT) index of rainfall-induced soil run-off, except during 25–22 ka BP and the last 5 ka when precessional insolation forcing enhanced the northeastern monsoon. This pattern arises because during these two periods, a weakened southeastern monsoon reduced the amount of rainfall during the long rain season and enhanced the opposing effect of evaporation intensity and/or length of the austral winter dry season. Importantly, our lake-based reconstruction of moisture-balance seasonality in equatorial East Africa also helps understand the oxygen-isotope record contained in Mt. Kilimanjaro ice. Negative correlation between ice-core $\delta^{18}O$ and Lake Challa $\delta^{18}O_{diatom}$ implies that temperature, not moisture balance, is the primary climate control on the long-term trend in ice-core $\delta^{18}O$.

Introduction

Low-latitude Quaternary climates are characterized by shifts between exceptionally wet and profoundly arid conditions lasting centuries to millennia (Gasse, 2000). These contrasting climate regimes are especially marked in East Africa where many lakes desiccated completely during the last glacial maximum (LGM) or shortly afterward, yet rose to far above their present levels during the Early Holocene (Gasse, 2000; Trauth et al., 2010). Shifts in the ratio between precipitation and evaporation (P/E) due to variation in orbital insolation influencing monsoonal circulation and the mean annual position of the Intertropical Convergence Zone (ITCZ) are thought to provide the main mechanism behind these contrasting states (Kutzbach and Street-Perrott, 1985). The direct impact of temperature variation on these lake-level fluctuations is considered minor in comparison, even though the moisture-balance variations partly track the main trends in reconstructed lake temperature (Tierney et al., 2008). Resolving the relative contributions of precipitation and temperature on the oxygen isotope ratio of glacier ice ($\delta^{18}O_{ice}$) on Mt. Kilimanjaro (Thompson et al., 2002) remains highly controversial (Gasse, 2002; Kaser, 2004; Thompson, 2003, 2006) yet it is vital if tropical ice cores are to achieve the palaeoclimatic importance of their polar counterparts. (Thompson et al., 2002) interpreted variation in the $\delta^{18}O_{ice}$ on Mt. Kilimanjaro within the last 11.7 ka in terms of temperature change, with higher (i.e., less negative) values representing a higher condensation temperature. These authors inferred relatively warm conditions in equatorial East Africa during the early Holocene (11–6 ka) and cooler conditions during the Late Holocene (3.5–0 ka) separated by considerable variability during the middle Holocene (6–5 ka and 5–3.5ka). This temperature-based interpretation of the ice-core $\delta^{18}O$ was criticized because the amount effect (Rozanski et al., 1992), regional circulation systems determining air mass source and condensation history can have a critical impact on $\delta^{18}O_{precip}$ (Gasse, 2002; Vuille et al., 2005). Moreover, a paucity of independent dating led to suspicion that the Mt. Kilimanjaro ice core record may not be continuous; indeed it has recently been suggested that gaps are likely present, as a result of episodes of relative aridity halting accumulation and enabling sublimation of the ice (Kaser et al., 2010). Nevertheless, good correlation of Ca and Mg signatures of windblown dust in the ice with the timing of East African lake lowstands (Gasse, 2000), suggest that any temporal gaps do not completely compromise $\delta^{18}O_{ice}$. Despite its issues of interpretation and limited chronological constraints, the Holocene ice core record from Mt. Kilimanjaro is unique in

Africa (Thompson et al., 2002) and demands further investigation. An opportunity to examine the validity of the temperature-based interpretation of Mt. Kilimanjaro $\delta^{18}O_{ice}$ and extend its ~11.7 ka oxygen-isotope record further back in time is provided by a 25-ka continuous sediment record from Lake Challa, a 97-m deep crater lake situated at an altitude of 880 m asl on the eastern flank of Mt. Kilimanjaro (Verschuren et al., 2009) (Fig. 4-1).

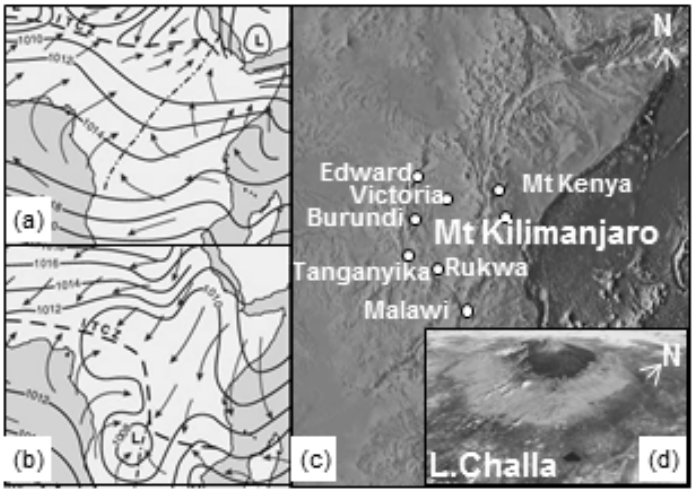

Fig. 4-1: Location and climatology (a) January airflows with ITCZ (dashed line) to the north adapted from (Gasse, 2000); (b) July airflow and southern-most ITCZ position; (c) Location of African sites mentioned in text, base map adapted from NGDC, Boulder; (d) Mt. Kilimanjaro and Lake Challa.

The hydrological budget of Lake Challa depends on local precipitation, groundwater inflow and outflow, and strong evaporation from the lake as demonstrated by surface-water oxygen isotope values ($\delta^{18}O_{lake}$) of between +1.5 and+2.5‰ whereas the mean weighted $\delta^{18}O$ of local rainfall and springs is around –4‰, (Payne, 1970). P/E increases during the relatively warm main wet season (March to May), reducing $\delta^{18}O_{lake}$, and P/E falls during the cooler, windier, dry season (June to September) when evaporation causes $\delta^{18}O_{lake}$ to rise (Fig. 4-2). $\delta^{18}O_{lake}$ was strongly impacted by the exceptional rains of December 2006 and January 2007 (Fig. 4-2), with a lag of only a few months. Therefore, at multi-annual scales, $\delta^{18}O_{lake}$ reflects the aggregated balance between the amount of precipitation and the intensity and duration of dry-season evaporation. We propose that if our lake-based oxygen-isotope record is driven by hydrological changes while Mt. Kilimanjaro $\delta^{18}O_{ice}$ is mainly a temperature proxy, then long-term patterns in these data should be negatively related, such that relatively wet conditions (low $\delta^{18}O_{lake}$) correlate with warmer inferred air temperatures (high $\delta^{18}O_{ice}$) and vice versa.

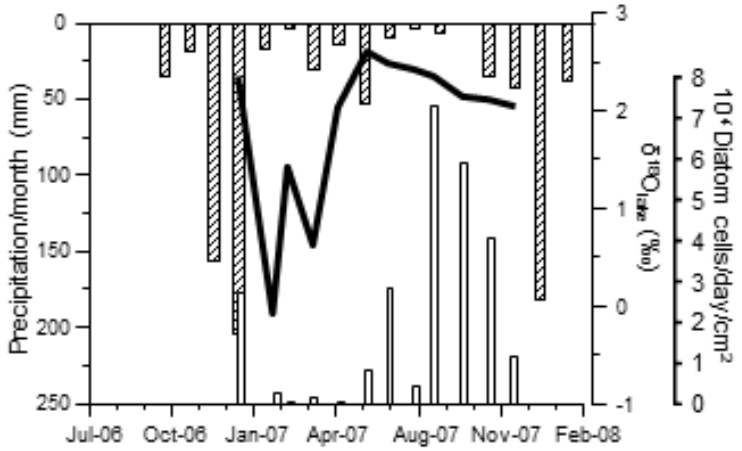

Fig. 4-2: Monthly precipitation (hatched histogram bars), lake $\delta^{18}O$ (solid line) and diatom abundance data (open bars) from Lake Challa. Monthly precipitation is from Voi meteorological station (http://www7.ncdc.noaa.gov/CDO/cdo).

Here we test this hypothesis using the record of oxygen isotope variation in diatom silica ($\delta^{18}O_{diatom}$) from Lake Challa sediments. $\delta^{18}O_{diatom}$ is a function of $\delta^{18}O_{lake}$ moderated by a temperature fractionation –0.2‰ per °C (Leng and Barker, 2006) skewed toward the period of greatest diatom productivity, which is the dry season in Lake Challa (Fig. 4-2). The most important diatom genera during 2006–2007, and also in the sediments, are *Gomphocymbella* and *Nitzschia*, with the former making by far the greatest contribution in terms of dry mass of biogenic silica. We compare this oxygen-isotope proxy with a reconstruction of rainfall-induced surface run-off in Lake Challa (Verschuren et al., 2009) using the branched isoprenoid tetraether (BIT) index, an organic biomarker for the ratio of soil bacteria versus aquatic crenarchaeota (Hopmans et al., 2004). High BIT-index values reflect enhanced soil inwash and hence wet conditions, or at least a relatively high frequency of intense rainfall. This hydroclimatic interpretation of the BIT index is supported by monthly sediment-trap data from Lake Challa (Damsté et al., 2009) as well as its concordance with Challa's lake-level fluctuations revealed by seismic stratigraphy (Moernaut et al., 2010). We therefore have the opportunity to assess the relative roles of precipitation versus the intensity and duration of dry-season evaporation on the palaeohydrology of this equatorial lake.

Methods

In 2003 and 2005 lake-sediment cores were retrieved from a central location in Lake Challa (Verschuren et al., 2009). Cross-correlation of the overlapping core units produced a 20.82 m long composite core. Chronology was established through high-resolution ^{14}C dating of bulk organic matter, corrected for an evolving old-carbon age-offset ('reservoir effect') by comparing overlapping ^{210}Pb and ^{14}C dates, paired ^{14}C dates on bulk organic matter and terrestrial plant macrofossils, and wiggle-matching well-dated core sections with ^{14}C anomalies in the INTCAL04 curve (Verschuren et al., 2009).

A total of 123 core samples were analyzed for $\delta^{18}O_{diatom}$. Samples were treated in hot 10% HCl, 30% H_2O_2 and 63% HNO_3 to remove carbonate and oxidize organic material and sieved to remove sponge spicules and mineral particles. Optical microscopy and SEM imaging was used to verify sample purity. Oxygen isotope analysis was undertaken at the NERC Isotope Geosciences Laboratory, using the stepped-wise fluorination technique (Leng and Sloane, 2008). Twelve monthly surface-water samples were collected over a one-year period from December 2006 to December 2007, and stored in sealed airtight polypropylene bottles. Aliquots were analyzed for $\delta^{18}O$ referenced to VSMOW at the Alfred Wegener Institute for Marine and Polar Research (Meyer et al., 2000). Twelve monthly sediment samples were collected in a double-funnelled sediment trap suspended at 35 m depth, and stored frozen until analysis. Diatom assemblages in these sediment-trap samples were studied as part of total phytoplankton counts.

Results

Gomphocymbella and *Nitzschia* spp. together comprise > 90 % of the fossil diatoms present in Lake Challa core samples. Although *Nitzschia* spp. are more abundant during the Holocene (Milne, 2007), *Gomphocymbella* are the most important in terms of biovolume throughout the 25-ka sequence. The $\delta^{18}O_{diatom}$ values fall within a narrow range of 5‰ (Fig. 4-3: +36.7 to +42 ‰), consistent with the unusual visual purity of these samples. Their long-term variation approximates a quasi-sinusoidal curve, with values rising from a mean of +39 ‰ at 25 – 23 ka to +40 ‰ during the LGM (23 - 19 ka) and until ~14.5ka BP. After 14.5ka, $\delta^{18}O_{diatom}$ values fall to a minimum of +37.4‰ at 13.3 ka. Higher (+39 ‰) values occur during the Younger Dryas (YD) period (12.9 - 11.7 ka), after which they decline again below 38‰, to a minimum value of 36.7 ‰ at 9.0 ka BP. From this point an irregular but sustained increase in $\delta^{18}O_{diatom}$ leads to a maximum of +41.6 ‰ at 2.5 ka BP. After 2.5 ka BP $\delta^{18}O_{diatom}$ values again decrease, first gradually and then more sharply during the last millennium.

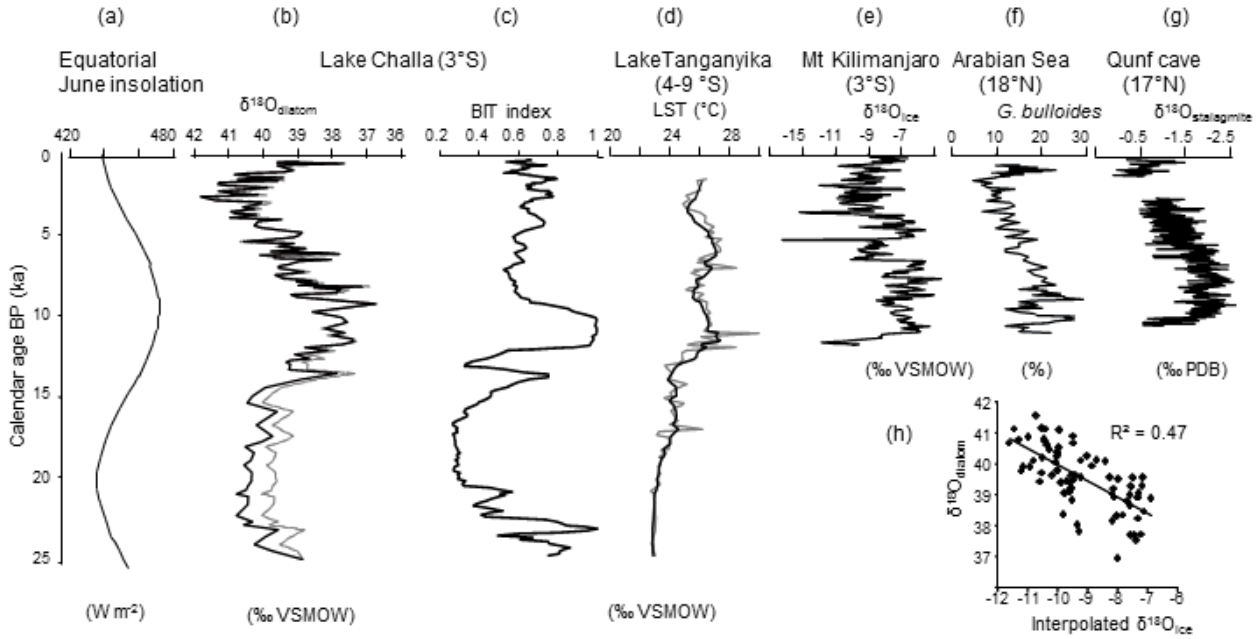

Fig. 4-3: (a) Equatorial insolation for June (Berger and Loutre, 1991). (b) Lake Challa diatom based oxygen isotope values (gray dashed) and with a temperature adjustment (solid). Calibrated against Vienna Standard Mean Ocean Water (VSMOW), scale reversed. (c) Lake Challa branched isoprenoid tetraether (BIT) index (3pt running mean (Verschuren et al., 2009). (d) Lake Tanganyika TEX_{86} lake surface temperatures (LST) (Tierney et al., 2008). (e) Mount Kilimanjaro ice core $\delta^{18}O$ (Thompson et al., 2002). (f) Arabian Sea foraminifera record (% G. bulloides)(Gupta et al., 2003). (g) Qunf cave speleothem $\delta^{18}O$ values (Fleitmann et al., 2003) calibrated against the Pee Dee Belemnite standard (PDB). (h) Correlation between Lake Challa $\delta^{18}O_{diatom}$ and Kilimanjaro ice core $\delta^{18}O_{ice}$. The ice core data were smoothed with a 3pt running mean and interpolated.

Discussion

The $\delta^{18}O_{diatom}$ data reveal millennial-scale trends in hydrological balance (P/E), with relatively humid conditions before 23 ka BP, a long dry period spanning the LGM until ~14.5 ka BP, and wet conditions dominating the late-glacial period and early Holocene until around 8 ka BP. Peak late-Holocene $\delta^{18}O_{diatom}$ values seem to suggest that the period between 4 and 1.5 ka BP was drier than the LGM. However, glacial-age $\delta^{18}O_{diatom}$ values may be less enriched compared to Holocene values because of the fractionation effect of lower temperatures. Lacking data on the magnitude of LGM lake-cooling in Lake Challa, we used the best-available temperature record for East Africa, a TEX_{86}-based reconstruction from Lake Tanganyika (Tierney et al., 2008), to test this assertion and to re-calculate Challa $\delta^{18}O_{diatom}$ values. An adjustment of -0.2 ‰ per °C increases $\delta^{18}O_{diatom}$ by 1‰ from 25 ka to 16 ka and by 0.5‰ during the late-glacial period and Younger Dryas; values still less than that during the Late Holocene (Fig. 4-3). This pattern cannot be attributed to a change in source water $\delta^{18}O$, since Indian Ocean surface water was actually enriched (by 1.5 ‰) during the LGM (Levi et al., 2007).

The main long-term trend in Lake Challa $\delta^{18}O_{diatom}$ values compares favorably with variation in June equatorial insolation (Berger and Loutre, 1991) (Fig. 4-3), consistent with the dominant influence of the precession cycle on tropical monsoon intensity (Kutzbach and Street-Perrott, 1985). Other high-resolution proxy records from throughout the Indian Ocean monsoon domain (Fleitmann et al., 2003;

Gupta, 2003) showed that the Northern Hemisphere summer monsoon weakened gradually in the Holocene, in line with similar evidence from the tropical Pacific (e.g., (Mckenzie et al., 2010) and Atlantic (Haug et al., 2001). Palaeohydrological reconstructions from tropical Africa based on lake proxies rarely reveal this smooth precession-driven evolution of the monsoon, and instead are punctuated by abrupt hydrological events, and/or step-like transitions (Gasse, 2000). To what extent these proxy signatures actually reflect abrupt change in monsoon rainfall (Tierney et al., 2008), or are the expression of proxy- or archive-specific thresholds (Shanahan et al., 2009) is often debated. In contrast with many other lake-based proxies, Lake Challa $\delta^{18}O_{diatom}$ is largely independent of landscape processes, because most water input occurs via shallow groundwater. Also, since lake surface area in this steep-sided crater basin has remained virtually constant throughout the range of lake-level fluctuation over the last 25ka (Moernaut et al., 2010), isotopic enrichment due to evaporation is more directly linked to local insolation and relative humidity than to lake-volume changes. Therefore, the Challa $\delta^{18}O_{diatom}$ record is tuned to the underlying processes of local precipitation and, especially, seasonal evaporative losses from the lake surface, only modified by small temperature effects. As a result, these $\delta^{18}O_{diatom}$ data primarily reveal gradual insolation forcing of the lake's isotope hydrology.

Comparison of Challa $\delta^{18}O_{diatom}$ with the Challa BIT index (Fig. 4-3) allows us to assess the relative importance of variation in P and E. These records are broadly similar for the period 20.5–8.5 ka, suggesting that run-off and P/E are closely related during the LGM and the deglaciation period including the early Holocene. The BIT index identifies strong aridity during the YD whereas a more muted change occurs in $\delta^{18}O_{diatom}$. Thus if P was significantly lower during the YD as suggested by the BIT index, then E must have been similarly lower at that time, most likely due to significantly reduced. The two hydrological proxies diverge most strongly during the Late Holocene, when $\delta^{18}O_{diatom}$ indicates greatest aridity (lowest P/E) around 2.5ka while the BIT index indicates surface run-off to have increased relative to the mid-Holocene. Considering the somewhat cooler late-Holocene climate suggested by the Tanganyika TEX_{86} record, the most direct explanation is that E was greatly enhanced because a weak SE monsoon resulted in a reduced long rainy season and protracted main dry season.

The shifting balance between P and E in equatorial East Africa during the Holocene revealed by the Lake Challa $\delta^{18}O_{diatom}$ record is supported by other regional records. In Lake Edward dissolved solute concentration peaked from 5.4 ka to 2.0 ka (Russell and Johnson, 2005), and in Lake Victoria diatom-inferred lake level reached a minimum at 2.7 - 2.4 ka (Stager and Mayewski, 1997). Lake Naivasha stood dry ~3 ka BP (Richardson and Dussinger, 1986), while Simba and Small Hall Tarns on Mt. Kenya recorded lowest P/E ratios in the period 5.5 - 3 ka (Barker, 2001). We propose that a protracted northern hemisphere summer dry season (currently lasting from June to September), due to partial failure of the long rains associated with a weakened southeastern monsoon, was a major contributor to the late-Holocene fall in P/E in this region. We further note that similar orbital forcing and distribution of seasonal insolation, occurred in the period 25 - 22 ka BP, a period also characterized by a combination of relatively low P/E (seasonally dry conditions) inferred from $\delta^{18}O_{diatom}$ versus high annual rainfall inferred from BIT (Fig. 4-3).

Finally, comparison of the Holocene section of the Lake Challa $\delta^{18}O_{diatom}$ record with the Mt. Kilimanjaro $\delta^{18}O_{ice}$ record reveals a negative relationship (Fig. 4-3). Given that these two $\delta^{18}O$ records derive from the same precipitation source, this divergence must be attributed to differences in isotope fractionation processes caused by contrasting climate controls. Since P/E is the major variable driving $\delta^{18}O_{lake}$ (as represented by $\delta^{18}O_{diatom}$), the largely opposing trajectory of $\delta^{18}O_{ice}$ suggests that moisture balance cannot be its major control. By elimination, our data support the primary climatic

interpretation of the Mt. Kilimanjaro $\delta^{18}O_{ice}$ record in terms of temperature rather than precipitation (Thompson et al., 2002), and its main inference of a relatively warm early Holocene followed by a cooler Late Holocene. Given the above-mentioned issues about the chronological integrity of the Kilimanjaro ice core shorter-term changes in the ice-core oxygen isotope data should be viewed with caution.

Paired palaeohydrological proxies extracted from the sediment record of Lake Challa support the fundamental control of low-latitude orbital insolation on equatorial East Africa, at least at times when the region was not overly impacted by the influence of northern hemisphere glaciation. Sea surface temperature of the western Indian Ocean is likely the dominant variable on moisture advection and along with relative continental temperatures, regulate the strength of monsoon airflows. Strong similarity of the Holocene section of the Challa $\delta^{18}O_{diatom}$ record with the Holocene record of Arabian Sea upwelling inferred from foraminiferal assemblages (Gupta et al., 2003) and with stalagmite-based records of summer monsoon rainfall on the Arabian peninsula (Fleitmann et al., 2003) indicate coherent forcing by the Indian monsoon (Fig. 4-3). Our investigation of Lake Challa sediments has produced new insights on the role of seasonality in moisture-balance trends at the millennial time scale, and on the climate controls on oxygen isotope records from an iconic tropical mountain.

5 Lake Challa sediments - Variations of East African wind and rainfall intensities over the past 25,000 years

To be submitted to: Palaeogeography, Palaeoclimatology, Palaeoecology

Iris Kristen[1], Christian Wolff[1,2,3], Birgit Plessen[1], Daniel Conley[4], Maureen Fagot[5], Norbert Nowaczyk[1], Ursula Röhl[6], Gerald H. Haug[3,7], Dirk Verschuren[5]

[1] *Helmholtz Centre Potsdam GFZ German Research Centre for Geosciences, Section 5.2 – Climate Dynamics and Landscape Development, Telegrafenberg, D-14473 Potsdam, Germany*

[2] *DFG Graduate School 1364, University of Potsdam, Institute of Earth and Environmental Science Karl-Liebknecht Strasse 24, Haus 27, D-14476, Germany*

[3] *DFG Leibniz Center for Earth Surface Process and Climate Studies, University of Potsdam, D-14476 Potsdam, Germany*

[4] *GeoBiosphere Centre, Department of Geology, Lund University, SE-223 62 Lund, Sweden*

[5] *Limnology Unit, Department of Biology, Ghent University, Ledeganckstraat 35, 9000 Gent, Belgium*

[6] *Marum – Center for Marine Environmental Research, University of Bremen, Germany*

[7] *Geological Institute, Department of Earth Sciences, ETH Zürich, CH-8092 Zürich, Switzerland*

Study site and modern day climate

Lake Challa (3°19'S, 37°42'E) is an app. 95 m deep freshwater crater lake situated at an altitude of 800 m asl on the eastern flank of Mt. Kilimanjaro. The surrounding steep crater walls reach up to 170 m height and confine the lake's catchment area to 4.2 km².

Lake Challa fills a volcanic crater within igneous rocks (predominantly trachy-basalts) of the tertiary Kilimanjaro complex (Bear, 1955). These basalts are covered by "calcareous tuffaceous grits", a calcite-cemented tuff that is probably related to the formation of the Challa crater (Downie and Wilkinson, 1972). Investigation of the sedimentary infill using seismic signals, estimates a thickness of lacustrine sediments to ~210 m and cover the last ~250,000 years (Moernaut et al., 2010).

Local precipitation is about 600 mm/yr (Payne, 1970). The hydrological budget is mainly based on overland run-off from the crater walls and the groundwater inflow (Payne, 1970). Groundwater inflow derives most probably from percolation of precipitation falling in and above the forest zone on the upper slopes of Mt. Kilimanjaro. In contrast, the annual sub-surface outflow is estimated to an amount of ~2.5% of the lake volume (Payne, 1970). In comparison, annual precipitation and annual evaporation of app. 1700 mm indicates a negative water balance for Lake Challa (Payne, 1970).

The climate of tropical Eastern Africa is controlled by the seasonal passage of the Inter-Tropical Convergence Zone (ITCZ; Fig. 5-1). Following its crossing over the equator during the equinoxes, rainfall occurs predominantly from October to December and March to May (Fig. 5-1). These two rain seasons are referred to as the 'long rains' (Mar–May), which normally are associated with the major amount of the annual rainfall, whereas the 'short rains' (Oct-Dec) are reported to show stronger interannual variability and presumably respond to changes in Indian Ocean surface temperature and related atmospheric circulation (Goddard and Graham, 1999; Latif et al., 1999).

Temperatures during the year in this region are lowest during southern hemisphere winter and highest during southern hemisphere summer (Fig. 5-1). Wind speeds show the inverse pattern. They are generally weaker from November to April and stronger between May and October. This pattern is the prevalent to south-easterly trade winds during the period of a northward displaced ITCZ during northern hemisphere summer (Fig. 5-1), whereas the north-easterly trade winds are less eminent during a southern displaced ITCZ around January and February.

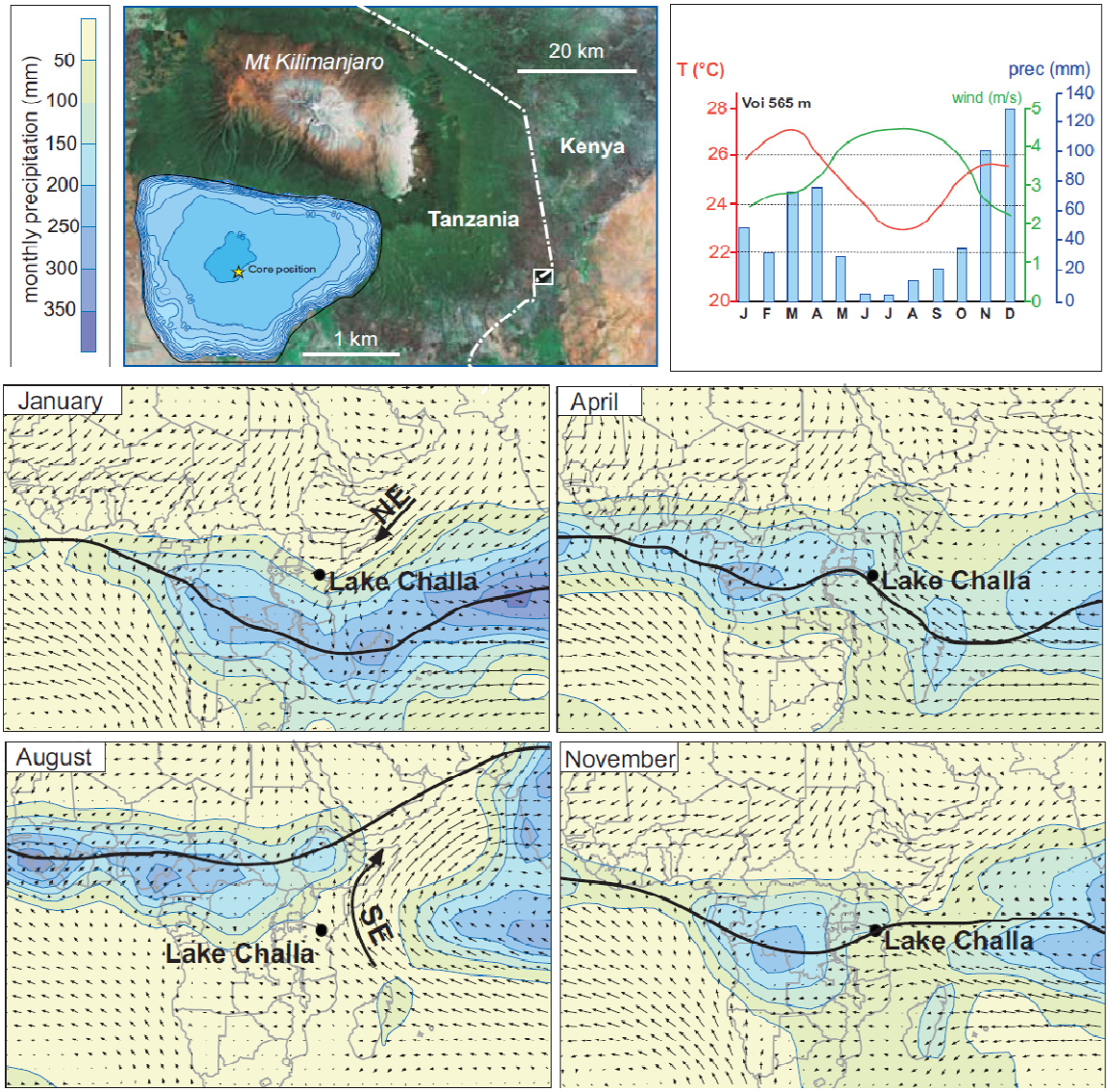

Fig. 5-1: Above: Geographical position of Lake Challa (3°19'S, 37°42'E, at 880 m above sea level) on the eastern slope of Mt. Kilimanjaro and bathymetry of the lake drawn at 10 m intervals to 90 m depth, and at 95 m depth (Moernaut et al., 2010). Yellow star indicate core site. Bottom: Seasonal migration of the ITCZ over East Africa in combination with monthly precipitation (shading, mm/month; contours drawn at 50-mm intervals) and wind components (wind vectors for the 925 hPa pressure level indicate wind direction with wind speed proportional to the length of the vector); from http://iridl.ldeo.columbia.edu

Composite profile, core chronology, methods and sediment characteristics

We focus on a 20.82 m long sediment composite profile, derived from several coring campaigns in 2003 (Kullenberg CH03-2K) and 2005 (CH05-1G, 2P, 3P; 4P). The composite profile was obtained by visual alignment of characteristic laminae and synchronisation of magnetic susceptibility. Furthermore, from the original core sequences, five horizons were identified as turbidites and were excluded.

The chronology of this sediment profile is based on 188 AMS ^{14}C dates and corrected for its evolving old-carbon age-offset ('reservoir effect'). Therefore, a combination of procedures have been applied: overlapping ^{210}Pb and ^{14}C dates, paired ^{14}C dates on bulk organic matter and terrestrial plant macrofossils, and wiggle-matching well-dated core sections with ^{14}C anomalies in the INTCAL04 curve (Verschuren et al., 2009).

Sampling of the composite profile for analysis of total carbon (TC), total organic carbon (TOC), total inorganic carbon (TIC), total nitrogen (TN) and biogenic silica (bSi) was conducted continuously at 2 cm resolution. After freeze-drying and grinding, samples for TOC analysis were decalcified with 20 % HCl and heated for 3 hours at 75 °C. About 20 mg of sediment were loaded in tin capsules (for TC, TN) and app. 3 mg of sediment were packed into silver capsules (for TOC), respectively, and combusted under oxygen flow at > 1000 °C. After combustion, CO_2 and N_2 were separated using a GC column and detected using thermal conductivity. The analyses were performed using an elemental analyser (NC25000 Carlo Erba) at the GeoForschungsZentrum Potsdam.

The results were referenced against lab-internal soil standards and a reference sample (Urea). The reproducibility for replicate analyses is better than 0.2 % for all analyses. TIC was determined as the difference between TC and TOC, and carbonate content is stoichiometrically calculated from TIC (factor 8.33). The amount of organic matter (OM) was estimated to be 1.0077*TOC+7.198 which is the regression between TOC and the percentage of loss-on-ignition (LOI) from core 03-2K. Water content and LOI are determined from the weight loss after drying 1 ml of a 1- or 2-cm interval sediment overnight at 105 °C and burning 4 hours at 550 °C, respectively (Dean, 1974).

Biogenic silica was extracted with 1 % $NaCO_3$ at 85 °C. A small percentage (5 %) of samples were extracted using the traditional 5 hour extraction with sub-samples removed at 3, 4 and 5 hours and analyzed for extracted bSi (Conley and Schelske, 2002), however, no significant increases in slope were observed. Therefore, all the samples were extracted in duplicate using a 3 hour extraction to determine the biogenic silica concentrations.

Changes in the element composition of the sediment profile were studied by means of X-ray fluorescence (XRF) scanning. This is a semi-quantitative, non-destructive logging method that provides records of changing element intensities for major and minor elements. XRF scanning of split sediment cores in 1 cm resolution was done as described in (Röhl and Abrams, 2000). The measurements were performed using the X-ray fluorescence Core Scanner II at MARUM, University of Bremen (Germany).

Results and discussion

General sediment characteristics

The finely laminated 25 m long composite profile represents sedimentation over the last 25,000 years (Verschuren et al., 2009). Results from a monthly cleared sediment trap indicate, that the laminated sequences consist of light-dark couplets. The dark layers are mainly composed of amorphous organic matter and fine-grained siliclastics. Calcite crystals are imbedded in this matrix (<5.3 m). Diatom skeletons are the dominant constituent of the light layers (Wolff, chapter 2; chapter 3). Over the entire profile total organic carbon contents (TOC) vary between ~1 and 16 %, and reach maximum values between 7.5 and 8.5 m (9,000 to 11,000 BP) sediment depth. Carbonates are virtually absent below 5.3 m (6,300 BP) and show maximum values up to 30 % in the top 1.5 m (Fig. 5-2). Biogenic silica contents range from 10 to 75 % with average values around 37 %. A nearly identically trend can be observed by Mn/Fe and Al/Ti ratios with highest values during the last 4,000 years and between 18,000 to 25,000 BP. Between both periods ratios reach values around 0.15 for Al/Ti and 0.04 for Mn/Fe (Fig. 5-2). In contrast, the opposite trend can be observed by TOC/TN during the Al/Ti and Mn/Fe minima.

Sources and Processes of sediment input

Microscopic- and geochemical analysis of a monthly cleared sediment trap from the centre of Lake Challa indicate, that the annual accumulated material can link to three major components: a) autochthonous calcite b) amorphous organic- and siliclastic matter as well as c) diatoms.

In the region of Lake Challa, the windy season begins in May, when the ITCZ moves northwards and southerly winds become dominant. These winds, combined with cool and dry air, cool down the lake surface and deepen the mixed layer of the lake from June to September. Less windy conditions in the following months construct a new stratified water body which supports calcite precipitation afterwards. The onset of the long rain season around March prevent the calcite precipitation and induce an organic matter input which is limited to May when the windy season starts and the annual sedimentation cycle begins again.

As expected for Lake Challa with its steep crater walls and a very small catchment area, sediments in the lake basin comprise a dominant proportion of autochthonous components.

Diatoms (as the main source for biogenic silica) are strongly linked with the dry and windy season between June and September. During these episodes of maximum wind stress, the structure of the temperature profile suggests mixing with a sharp increase in nutrient availability. This enhanced nutrient availability promotes diatom blooms, which are preserved in the light layer in the varves. Therefore, the amount of biogenic silica can be used to reflect wind strength or duration of the windy season derived from the intensity of the mixing process.

Furthermore, (Wolff, chapter 2) reported, that during the stratified period (October-May), Fe2+ and Mn2+ get enriched in the anoxic deep water. During an overturn event (~June-September), the dissolved Mn and Fe precipitate by oxygenation. This signal is recorded in the Mn/Fe ratio. Mn/Fe maxima that coincide with distinct light diatom rich layer deposited during the overturn events in the dry season. Accordingly, we apply the Mn/Fe intensity ratio to trace changes in redox conditions driven by change in wind strength and duration.

Wolff in chapter 2 also demonstrates that the siliclastic matter, represented by Al/Ti, deposited during the dry/windy season occurring in light layer is clearly enriched in the high Al/Ti ratio and reflects avoure input and therefore wind strength and duration of the windy season too.

In contrast, autochthonous calcite and organic- and siliclastic matter are main components of the dark layer, which typically represents the two rain seasons (November-December and March-May) and the brief dry season (January-February). Therefore, TOC can be used to describe the trend of the dark organic rich layer.

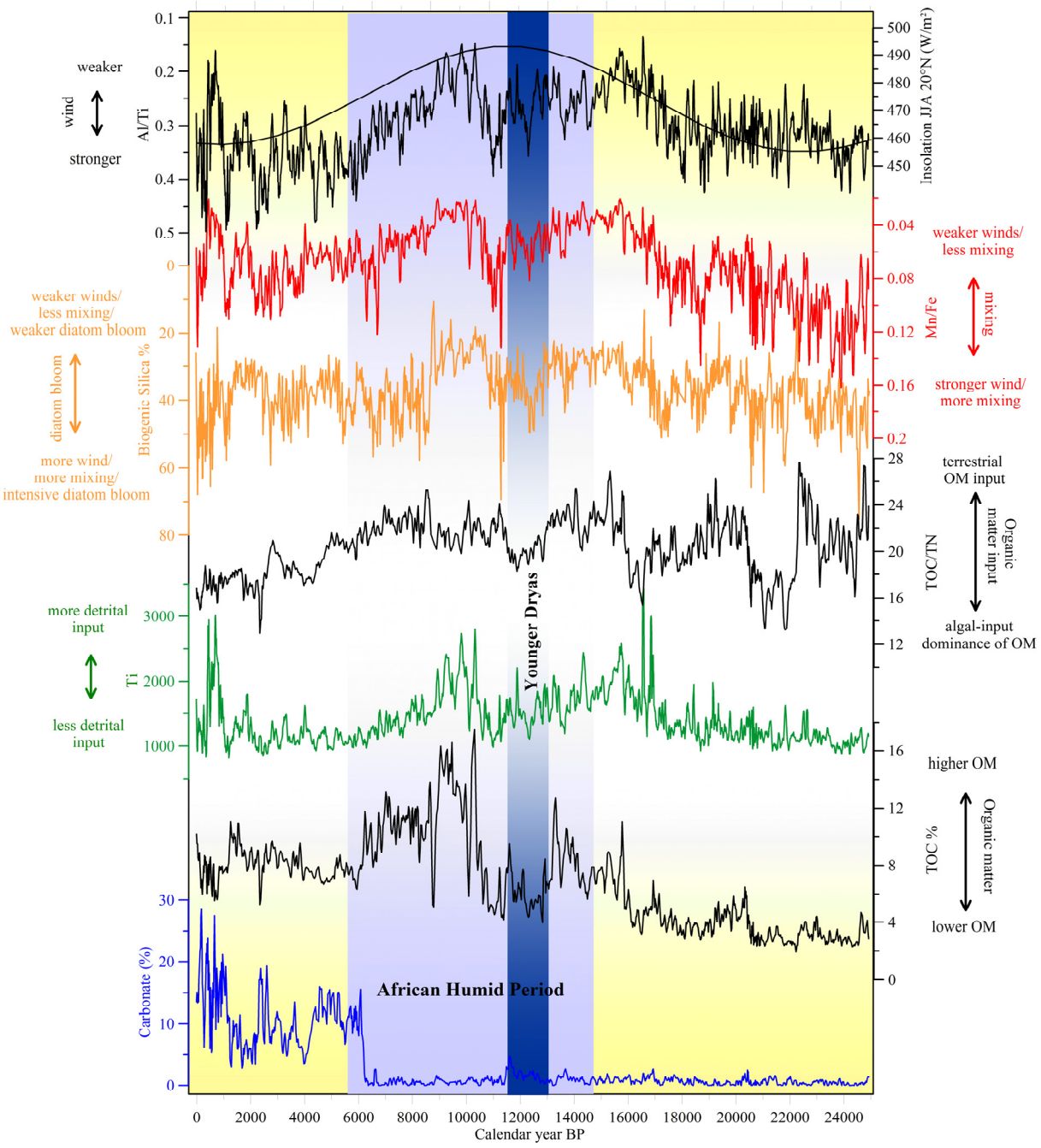

Fig. 5-2: Comparison of selected geochemical records from Lake Challa with JJA Insolation at 20°N.

Limnology and Climatology of the last 25,000

In the previous sections, we discussed the applicability of different sediment characteristics as proxies for detrital input, and changes in lake-bottom redox conditions driven by changes in wind strength or –duration. Accordingly, elevated Mn/Fe ratios represent periods of less intense reducing conditions, and deeper or more prolonged seasonal mixing in relation to higher wind stress and/or lower lake level. Furthermore, windspeed is the trigger for lake mixing. An indication about windspeed and/or length of the windy season is indicated by the Al/Ti ratio. Higher input of Al (higher al/ti) ratios indicate more dust input controlled by higher or longer windy season during the dry and windy period (June-September). Therefore, the Al/Ti and Mn/Fe ratios can used to describe wind speed and duration of the windy season of the past. These interpretations are backed with geochemical (TOC, biogenic Silica) data. Higher amounts of TOC are mainly attributed to a better preservation of OM under more stable water conditions, whereas increasing amounts of bSi are interpreted to reflect higher nutrient availability in response to stronger mixing (Wolff, chapter2; chapter 3) elevated TOC/TN values are interpreted to reflect a higher proportion of terrestrial plant material relative to authigenically produced OM from phytoplankton. These interpretations are in agreement with many lake studies (Lamb et al., 2004; Talbot and Lærdal, 2000; Tierney and Russell, 2007) and with the other presented parameters. Mutual dilution may have some effect on TOC and bSi variability, but changes in TOC in the range of 2 to 8 % are unlikely to be the only cause for bSi changes of 10 to 20 %; high diatom production and high total algal productivity need not be correlated. High TOC concentrations additionally tend to be accompanied by high S intensities (Wolff, chapter 2; Fig. 2-6), underlining the anoxic conditions which promote preservation of organic-rich sediments. By combining interpretation of Mn/Fe, AL/Ti with bSi, carbonate and TOC concentrations as well as TOC/TN ratios, we develop a picture of changing limnological conditions in Lake Challa since the last glacial period (25–2 kyr BP) and evaluate its potential as a new palaeoclimate archive for tropical East-Africa. At the beginning of the record under full-glacial conditions, Mn/Fe and Al/Ti rise to a maximum, whereas TOC content and TOC/TN values fall to minimum values, between 25 and ~24.5–23.5 kyr BP. At the same time, bSi content is relatively high, carbonates are absent, and Ti is low. These observations point to an evolution towards well-mixed lake conditions (stronger winds) during a period of reduced detrital input.

Carbonates are either not preserved or were not precipitating during this time. In modern Lake Challa, the formation of endogenic calcite is related to the activity of photosynthetic organisms during the warm and rainy southern hemisphere spring and summer months when the lake is stratified (Wolff, chapter 2 and chapter 3). Accordingly, a reduction in nutrient input, in the length of the stratified season or in temperature are possible explanations for the observed changes in sediment composition. Within the error of the age model this period is contemporaneous with Heinrich event 2, a period of cool temperatures over Greenland (Grootes et al., 1993), especially cool and dry conditions (Allen et al., 1999) and probably intensified atmospheric circulation (Cacho et al., 2001) in Europe, and generally cooler and more windy conditions reported from other East African archives (Brown et al., 2007; Gasse, 2000; Johnson, 2002). Between 23.5 and 22.3 kyr BP, increased TOC/TN values consistently indicate higher input from the catchment. The importance of sediment delivery and new nutrient input from the catchment is further underlined by high BIT indices during this period (Verschuren et al., 2009). Whether high erosion rates were caused by increased run-off or decreased vegetation cover cannot be decided here. In the following period (22.0–20.6 kyr BP), reduced TOC/TN indicates less allochthonous input. Whereas steadily decreasing Mn/Fe ratios argue for an increasingly stable water column, and mixing was still strong enough to sustain high diatom productivity and promote OM decomposition. Between 20.6 and 19 kyr BP, variability and values of Mn/Fe and Al/Ti are generally lower and bSi are reduced, whereas TOC and TOC/TN are relatively

high. Following this argumentation, these observations indicate a decrease in mixing (weaker winds), thereby decreasing diatom productivity and increasing OM preservation. As TOC/TN values are relatively high, this stabilisation was possibly caused by higher lake levels during a humid period with enhanced input of allochthonous organic matter. An abrupt return to more turbulent and oxidizing conditions occurred around 19 kyr BP which lasted until ~17 kyr BP. This period coincides with indications for lower lake levels from seismic-reflection data and decreased BIT data (Moernaut et al., 2010; Verschuren et al., 2009). Reported paleosols from Lake Victoria (Stager et al., 2002; Talbot and Lærdal, 2000) as well as other indications for generally dry conditions in tropical East Africa (Gasse, 2000) support the conclusion that drier conditions and lower lake levels caused generally less stratified conditions in Lake Challa (Wolff chapter 2 and 3), which favoured diatom productivity and Mn absorption, reduced OM preservation and Fe-sulphide formation.

From ~17 to 15.8 kyr BP, decreasing Mn/Fe and Al/Ti ratios, decreasing bSi and partly increasing TOC and Ti concentrations point to the establishment of a more stable lake stratification, culminating in a phase of enhanced OM preservation, and probably sulphide precipitation as well, from ~15.8 to 13.3 kyr BP. This period broadly coincides with the onset of the "African Humid Period" (deMenocal et al., 2000) and generally more humid conditions documented in many archives of tropical and subtropical Africa (Gasse, 2000). Around lakes on Mount Kenya, humidity rose abruptly after ~14.3 kyr BP (Street-Perrott et al., 2007). At Lake Masoko the development of semi-deciduous forest indicates increasingly humid conditions (Garcin, 2007), and in Lake Malawi the proportion of C4 plants decreased (Castaneda et al., 2007). The generally more humid conditions and resulting higher lake levels in Lake Challa probably favoured more intense reducing conditions at the lake bottom. It also fostered vegetation growth around the lake, which may have diminished soil erosion and input of allochthonous materials, as indicated by decreasing TOC/TN. Between 13.3 and 12.8 kyr BP, TOC content in sediments from Lake Challa is decreasing. Simultaneously, bSi, Mn/Fe and Al/Ti rise, indicating a destabilisation of the water column with reduced OM preservation and higher diatom productivity due to more intense or longer mixing seasons. These conditions prevailed until ~10.7 kyr BP, but seem to be composed of two main phases from ~12.8 to 11.7 kyr BP and from ~11.4 to 10.7 kyr BP. The former interval corresponds to the Younger Dryas (YD) period which is in many locations from tropical Africa associated with an abrupt reduction in humidity (Gasse et al., 2008; Weldeab et al., 2005) and with indications for stronger winds or changes in the dominance of north- vs. Southeasterly monsoonal winds (Gasse et al., 2008; Johnson, 2002).

Seismic-reflection and BIT data indicate more arid conditions around Lake Challa (Verschuren et al., 2009). In summary, reported observations seem to indicate a general reorganization of atmospheric circulation during the YD period which appears to be recorded as increased mixing in Lake Challa. The second, apparently even more pronounced mixing period in Lake Challa ~11.4 to 10.7 kyr BP occurs contemporaneously with a period of increased high-latitude temperature variability, including the 'Preboreal Oscillation' (Fig 6.9) (Walker et al., 1999). With the exception of one geochemical record from Lake Tanganyika reporting a coincident deepening of the oxycline there between ~12 and 10 kyr BP (Felton et al., 2007), no other tropical East African climate record shows evidence for especially dry or windy conditions in the earliest Holocene. However, indications for a delayed onset of early Holocene humid conditions associated with the intensification of the Indian South-West Monsoon are reported from north-eastern subtropical Africa (Garcin, 2007), from cave deposits in Oman (Fleitmann et al., 2003) and from sediment profiles of the Arabian Sea (Schulz et al., 1998).

Also records from the Asian and American Monsoon regions show strong variability between ~11.4 and 10.7 kyr BP with similar, though usually less pronounced, conditions as during the YD period: a weakened South-West Monsoon (Wang et al., 2005; Wang et al., 2001) and intensified North-East Monsoon (Haug et al., 2001; Hughen, 1996; Yancheva, 2007). These observations argue for a global

perturbation of the (northern hemisphere) monsoon system between ~11.4 and 10.7 kyr BP. After ~10.7 kyr BP, conditions in Lake Challa stabilised until ~8.8 kyr BP: TOC contents reach maximum values; in parallel, Mn/Fe and Ti/Fe ratios are at a minimum as are bSi concentrations; TOC/TN level off around 22. These observations indicate more intense or a longer season of stratified lake water conditions which probably resulted from more humid conditions with higher lake levels and now fully interglacial temperatures around Challa. The onset of these conditions occurs (within the error of the age models) contemporaneously with beginning stalagmite formation in a cave in Oman (Fleitmann et al., 2003) and maybe also with the formation of the ice cap on Mount Kilimanjaro (Thompson et al., 2002), considering that its basal age of ~11.7 kyr BP was assumed by comparison with a stalagmite from Soreq Cave/Israel). Observed humid conditions at Challa are further in agreement with recordings of a humid early Holocene in Lake Tanganyika (Felton et al., 2007; Tierney et al., 2008) and Lake Victoria (Talbot and Lærdal, 2000), as well as in other North- (Gasse, 2000) and West-African (Weldeab et al., 2005) records, documenting the widespread moisture increase in tropical and subtropical northern Africa in response to increased northern hemisphere insolation after the end of the last glacial period.

After ~8.8 kyr BP, Mn/Fe ratios show a generally increasing trend until ~2.2 kyr BP. This trend is accompanied by slightly increasing Al/Ti ratios, decreasing TOC concentrations, decreasing TOC/TN, generally high bSi concentrations, indicating a continued destabilisation of the Lake Challa water column over the course of the Holocene. This development is consistent with records from Asia (Wang et al., 2005; Yancheva, 2007) NE Africa/Arabia (Fleitmann et al., 2003) and the south American subtropics (Haug et al., 2001) which show a decline of the summer/increase of the winter monsoon intensity (Fig. 5-3). A southward shift in the mean position of the ITCZ in response to decreasing northern hemisphere insolation (Fig. 5-2) is a probable forcing mechanism (Yancheva, 2007). Noteworthy, however, is the early start of destabilisation in Lake Challa ~8.8 kyr BP when compared with the records mentioned above (Fig. 5-3). This may be a specific equatorial characteristic as Lake Challa is the most southern location of the cited monsoon records. The general Holocene trend is overlain by several abrupt events or shifts to inferred increased water-column mixing ~8.8–8.2 kyr BP, 6.6–6.3 kyr BP, 4.0 kyr BP, 2.2 kyr BP and 1.2–1.0 kyr BP. These events have been described from many climate and historical archives as periods of low monsoonal rainfall (Fleitmann et al., 2003; Gupta, 2003; Haug et al., 2001; Thompson et al., 2002). Their global expression, origin and link to changes in the North-Atlantic and in solar variability are currently under discussion.

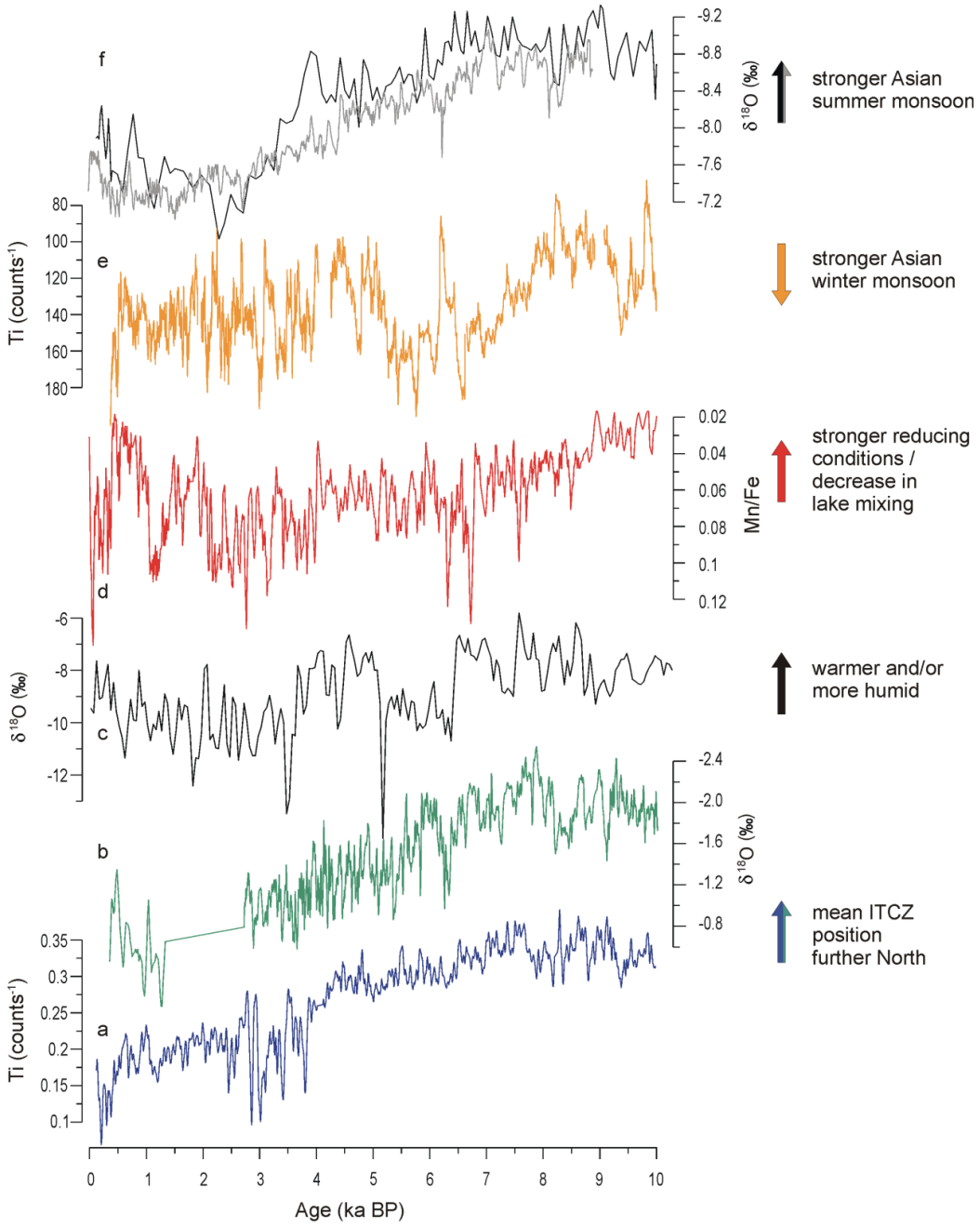

Fig. 5-3: Comparison of different monsoon records: (a) the Ti intensity record of a core from Cariaco basin (10°42' N, 65°10' W) (5-point running average) (Haug et al., 2001); (b) stable oxygen isotope record from a stalagmite from Qunf Cave, southern Oman (17°10 N, 54°18 E, black curve, 3-point running average) (Fleitmann et al., 2003); (c) the stable oxygen isotope record from Mount Kilimanjaro ice core KNIF3 (3°04.6 S; 37°21.2 E; 5893 m above sea level) (Thompson et al., 2002); (d) the Mn/Fe ratio of sediments from Lake Challa (3-point running average); (e) the Ti intensity record of sediments from Lake Huguang-Maar, China (21°9'N, 110°17'E) (Yancheva, 2007); (f) and two stable oxygen isotope records of stalagmites from Dongge Cave, China (25°17'N, 108°5'E) (grey line represents a 7-point running average after (Wang et al., 2005), black after (Yuan et al., 2004).

6 Summary

6.1 Synthesis

Lake sediments are often used to understand past climate variations. In most studies the interpretation of the sediments is based on hypothetical assumptions. As yet, only little is known about sedimentation processes from in-situ rocks to the deposited sediments and the interaction between climate signals and accumulated sediments. Therefore, I studied microfacies and geochemical data from a monthly cleared sediment trap and compared them with a broad range of limnological, meteorological, and geological parameters to characterize the impact of sedimentation processes from the origin to the deposition and their interaction with the waterbody. The characterization of different sediment components and their relation to the seasonal climate pattern gives important insights into past climatic changes on the hydrological cycle and its influence on lake ecosystems.

Here, I present a summary of the most important results of this work, with special focus on how sediment trap material can indicate climate changes and how climate and ENSO-related rainfall variability changed during the last 25,000 years.

6.2 Sediment trap samples

Analyzing the Lake Challa sediments reveals a dark/light lamination. Based on microscopic inspection, the dark layers are mainly composed of amorphous organic matter and fine-grained siliclastics. Furthermore, they show single silt-sized calcite crystals, which are imbedded in a fine-grained matrix. The light layers are primarily composed of diatoms. Variations in the thickness of a dark/light couplet are controlled by the thickness of the light diatom rich layer. The relation between the two layers and their components and its linkage to seasonally changing lake and climate conditions can be achieved by studying a monthly cleared sediment trap, which was deployed in the lake in November 2006. Monthly settling particle samples reveal a sediment input of three components: autogenic formed calcite, organic matter, and diatoms. With this method I confirmed that the diatoms are the dominant component in the total particle input. Their input occurred primarily during the dry and windy season (June-October) when lake productivity is enhanced because of wind-induced upwelling of nutrient rich water from deep waters. In contrast, calcite precipitation occurred during the southern hemisphere summer (November-March), followed by a small input of organic matter and less lithogenic material driven by rainfall during the ‘long rain’ season (March-May). This sediment trap program lasted 3 years and is still ongoing. It provides fundamental information for the claim that dark/light couplets reflect seasonal delivery to sediments of diatom-rich particles during the windy months and diatom-poor material (calcite and organic matter/lithogenic material) during the wet season. Furthermore, the sediment trap samples confirm the annual origin of the dark/light couplets and demonstrate that this varve-thickness is strongly linked to the duration and strength of the windy-dry season. Therefore, thicker varves represent windier and drier years, whereas thinner varves reflect years with less wind and more rainfall. El Niño (La Niña) events are associated with wetter (drier) conditions in east Africa and decreased (increased) surface wind speeds. Therefore the thicknesses of

these dark/light couplets (varve) indicate variations in humidity and ENSO dynamics. These results are supported by geochemical analyses of the sediment trap samples. Wind induced mixing leads to higher Mn/Fe and Si/Al ratios, which are based on the chemical precipitation of Mn during overturn events and a larger diatom bloom with enhanced nutrient availability, respectively. Al/Ti ratios show the link between an external dust signal and the internal lake mixing response. Therefore, the results of the geochemical analyses of the sediment trap samples provide an excellent proxy for wind intensity and duration.

6.3 El Niño Southern Oscillation

Rainfall in East Africa is tightly linked to the El Niño Southern Oscillation (ENSO), with more rainfall during El Niño years and severe droughts in La Niña years. Wind speeds show the inverse pattern with an intensified windy season during La Niña years in contrast to reduced conditions in El Niño years. As known from sediment trap samples (*section 6.2*), the thickness of the dark/light couplets (varve) can be used to reconstruct variations in rainfall and wind patterns and therefore ENSO dynamics. During episodes of extended wind stress, the Lake Challa water column is more turbulent and promotes diatom blooms based on an enhanced nutrient availability. Therefore, thicker varves indicate years with longer or intensified wind conditions (La Niña event in East Africa). In contrast thinner varves show a more stratified water column in which nutrient availability is limited and prevents an enhanced diatom bloom (El Niño event). One aim of this thesis was to reconstruct the pattern and timing of late-Glacial and Holocene moisture balance fluctuations.

From the existing 25,000 year long composite profile, two periods of climatic interest were chosen: (1) the last 3,000 years, which are based on a varve chronology anchored to ^{210}Pb-series data and accelerator mass spectrometry ^{14}C dates and represent warmer conditions, and (2) the glacial period between approximately 18,500 and 21,000 years BP, which are based on varve counting controlled by ^{14}C dates and representing cooler conditions. Our reconstructions show that interannual ENSO-related rainfall variability has undergone major changes and transitions during the last 3,000 years with strongly muted variability between 300 BC and 300 AD. This is in good agreement with ENSO proxy data from Ecuador (Moy et al., 2002). An increase in variability is observed for the period 400 AD - 750 AD. The gradual decline in variability during the Medieval Climate Anomaly ended abruptly around 1300 AD. A second - but less prominent - phase of variance reduction occurred during the Little Ice Age (1400 AD - 1750 AD). However, during cold late glacial conditions, the varve thickness record indicates an overall reduction in wind and rainfall variability on ENSO time scales. Only around 20,100 BP - 20,300 BP slightly increased variability can be observed (Fig. 6-1). Our interpretation reflects that warmer climate causes greater climate variability and an increase of extreme events.

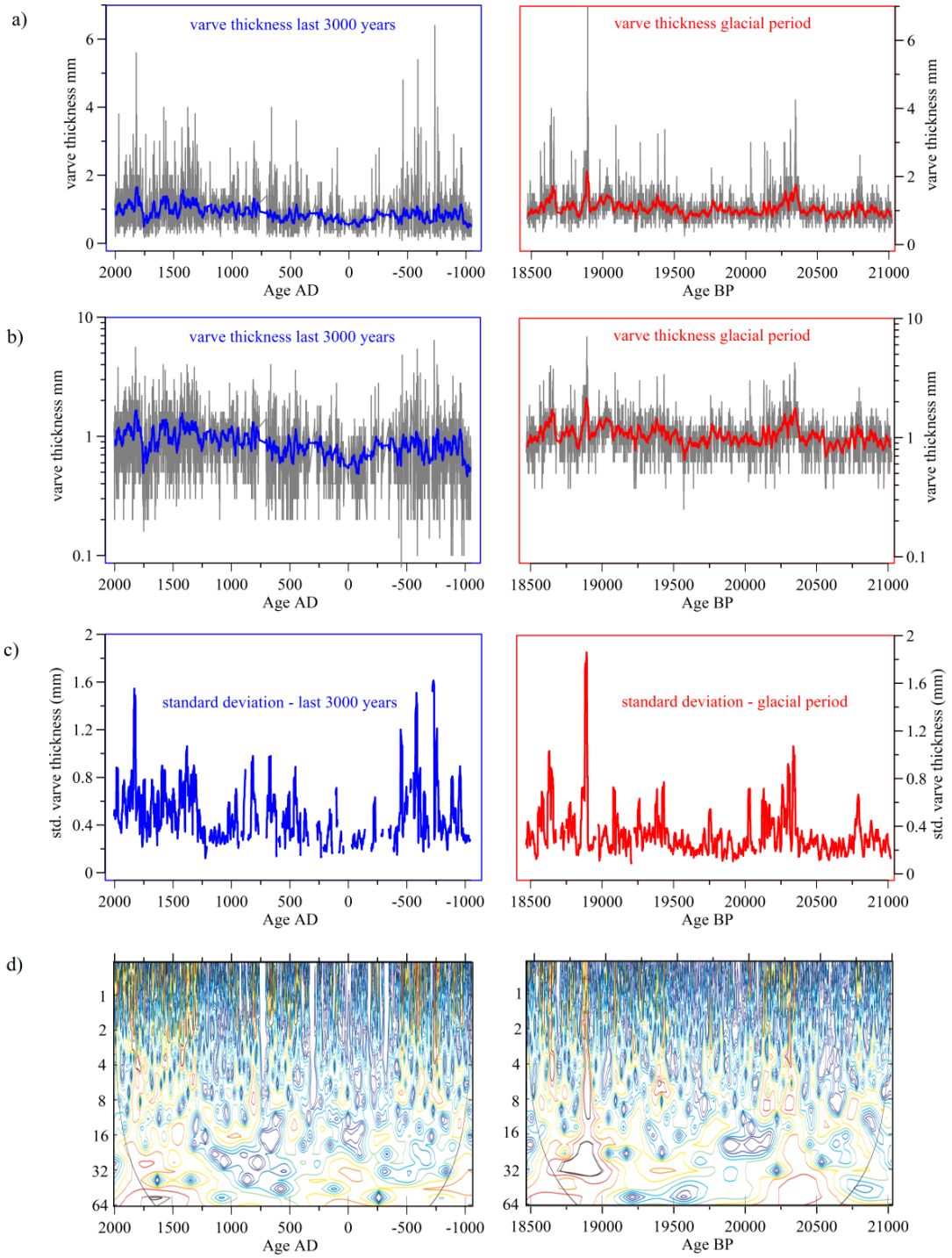

Fig. 6-1: Varve thickness time series for the last 3,000 years and between 18,500-21,000 years BP on linear (a) and logarithmic (b) scales, and the corresponding standard deviation (c, 15-year moving average). Panels (d) show the results of wavelet analysis with areas inside the black line indicating that the amplitude of frequency variation in varve thickness is significant at the 95% level.

6.4 The last 25,000 years

The transition from the cold conditions of the last glacial period into warmer conditions of modern times is documented in the Lake Challa sediments and supports a fundamental control of orbital insolation on equatorial East Africa (Verschuren et al., 2009). Based on seasonal components within sediment trap samples, Mn/Fe ratio can be used as an indicator of deeper and/or longer mixing, driven by an intensified and/or longer windy season. Similar changes in wind stress can be also observed in the Al/Ti ratio. Accordingly, higher Al/Ti ratio indicate stronger and/or a longer windy season. Given the modern control of seasonal ITCZ location on wind and rain in the region of Lake Challa and the inverse relation between the two (Fig. 3-6), Mn/Fe and Al/Ti ratios can be used as an indicator for changes in wind- or rainfall variations. Taken into account that modern climatological data confirm a broad relationship between existing ENSO indices and rainfall and wind speed in East Africa, Mn/Fe and Al/Ti can be additionally used to describe changes in ENSO pattern over the last 25,000 years. The Mn/Fe ratio in sediments from Lake Challa indicates an increasing intense and/or longer mixing period after ~14 kyr BP and a reversal again after ~11 kyr BP (Fig. 5-2). These changes in mixing and wind stress are supported by Al/Ti ratio and biogenic silica contents. The low Al/Ti and Mn/Fe ratios in this period are related to the 'African Humid Period' and can be also interpreted as a more El Niño like conditions during this period. During the Last Glacial Maximum, the Lake Challa records indicate generally drier conditions in comparison with stronger winds and enhanced diatom blooms. These findings are most probably related to lower tropical land- and sea-surface temperature as compared to modern control on temperature-rainfall and wind. This agrees with simulations using coupled ocean-atmosphere models predicting cooling and less summer precipitation in tropical Africa (Bush and Philander, 1998; Ganopolski et al., 1998). Following our interpretation of chapter 3, this period is might be related to a more La Niña like environment. During the Holocene, abrupt changes of extremely large amplitudes occurred. As reflected by rapid changes in wind and rainfall dynamics, which are might be driven by changes in ENSO dynamics, our results suggest an increase in ENSO variability (see chapter 3) during the last 3,000 years.

6.5 Quo Vadis? – East African climate in the future

The results of my thesis show a less variable climate in East Africa during colder periods and suggest a strong sensitivity of winds and the hydrological cycle to larger scale climate conditions. The proxy-derived coupling of mean hydro-climate conditions and variability in East Africa is further supported by the analysis of a series of Coupled General Circulation model experiments conducted with the NCAR CCSM3 model for the Last Glacial Maximum, pre-industrial, modern conditions, and conditions that represent a doubling of pre-industrial CO_2 levels (Otto-Bliesner et al., 2006; Yeager et al., 2006).

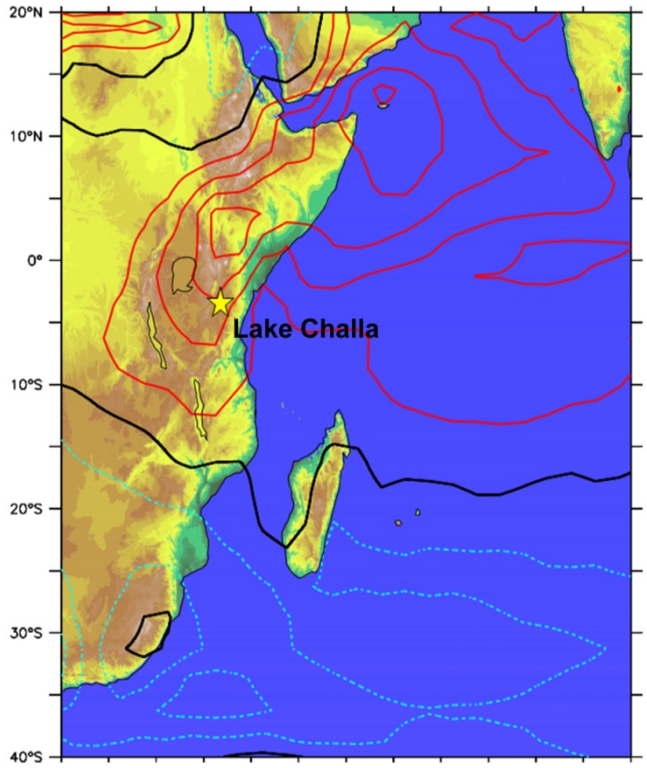

Fig. 6-2: Simulated percentage change in annual mean rainfall between pre-industrial climates and projected climate for the period 2070-2100 (following the IPCC A1B greenhouse gas emission scenario) using the multimodel ensemble mean of 23 climate model projections, obtained from the Coupled Model Intercomparison Project 3. Contour interval is 5% and red contours indicate an increase in projected rainfall towards the end of the 21st century and cyan contours indicate a reduction of the simulated rainfall. The black contour line represents zero change in rainfall. The region of Lake Challa will receive more rainfall.

The model simulations document an increase of long-term mean rainfall and interannual rainfall variability with increasing temperatures (Fig. 3-10; Fig. 6-2). This is in general agreement with my results derived from the varve record (Fig. 3-10). Warming increases the capacity of the atmosphere to hold moisture, which leads to an increase of mean precipitation in areas of the present-day ITCZ. Establishing an intensified ITCZ in warmer climates (East Africa) also implies that a stronger gradient can be shifted meridionally because of the seasonal migration of the ITCZ and its interannual variability. A future projected increase in the interannual variability of rainfall and extreme ENSO events in equatorial eastern Africa may bring further environmental stress to a region with reduced capacity to adapt to the mounting adverse effects of global climate change.

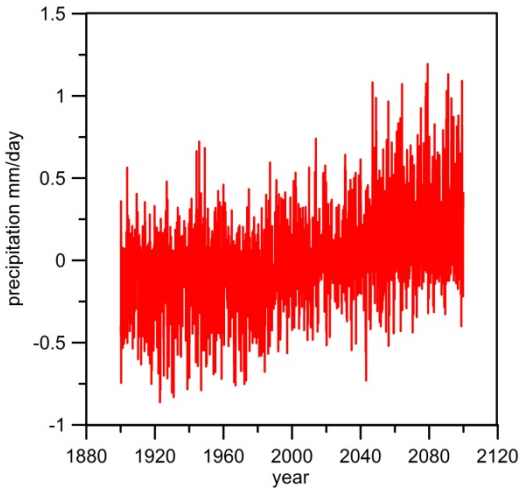

Fig. 6-3: Simulated changes in monthly mean rainfall for the period 1900-2100 (simulation based on observed greenhouse gas emission variations (1900-2000) and projected data (2000-2100) following the IPCC A1B greenhouse gas emission scenario) using the multimodel ensemble mean of 23 climate model projections, obtained from the Coupled Model Intercomparison Project 3. Anomalies based on differences from period 1981-2010. The region of Lake Challa will receive more rainfall.

6.6 Conclusion

In combination, microscopic analysis of laminated lake sediments from Lake Challa and sediment trap samples of the last three years provide climatic information in monthly resolution on annual to millennial time scale. The accumulation of light/dark couplets of the laminated lake sediments are of seasonal nature indicating annually laminated sediments (varves), which can be linked to seasonal and annual changes in lake and climate conditions. The thickness of the varves from Lake Challa sediments can be used to reconstruct the intensity of rainfall, wind stress and therefore ENSO dynamics. The results provide evidence that wind and rainfall extremes at ENSO timescales were weaker and less frequent under glacial conditions in contrast to higher variability during warmer conditions of the Holocene period. The transition from the cold Last Glacial period into warmer modern conditions is documented in µXRF data at decadal resolution. Especially, Mn/Fe and Al/Ti ratios demonstrate a strong imprint of orbitally induced changes in insolation. Abrupt changes during the Holocene are most probably related to the evolution of the tropical atmosphere-ocean circulation that is importantly coupled with ENSO dynamics.

7 References

Allen, J. R. M., Brandt, U., Brauer, A., Hubberten, H. W., Huntley, B., Keller, J., Kraml, M., Mackensen, A., Mingram, J., Negendank, J. F. W., Nowaczyk, N. R., Oberhansli, H., Watts, W. A., Wulf, S. and Zolitschka, B. 1999. Rapid environmental changes in southern Europe during the last glacial period. *Nature* 400, 740-743.

Balistrieri, L. S., Murray, J. W. and Paul, B. 1994. The geochemical cycling of trace elements in a biogenic meromictic lake. *Geochimica et Cosmochimica Acta* 58, 3993-4008.

Barker. 2001. A 14.000 year Oxygen Isotope Record from Diatom Silica in two Alpine lakes on Mt. Kenya. *Science* 292, 4.

Bear, L. M. 1955: Geology of the Taveta Area, Explanation of Degree Sheet 64 N.E. and 64 S.E. In Kenya, G. S. o., editor, *Report No. 32*, Nairobi: Government Printer.

Berger, A. and Loutre, M. F. 1991. Insolation Values for the Climate of the Last 10000000 Years. *Quaternary Science Reviews* 10, 297-317.

Black, E., Slingo, J. and Sperber, K. R. 2003. An observational study of the relationship between excessively strong short rains in coastal East Africa and Indian Ocean SST. *Monthly Weather Review* 131, 74-94.

Brown, E. T., Johnson, T. C., Scholz, C. A., Cohen, A. S. and King, J. W. 2007. Abrupt change in tropical African climate linked to the bipolar seesaw over the past 55,000 years. *Geophysical research letters* 34, doi:10.1029/2007GL031240.

Bush, A. B. G. and Philander, S. G. H. 1998. The role of ocean-atmosphere interactions in tropical cooling during the last glacial maximum. *Science* 279, 1341-1344.

Cacho, I., Grimalt, J. O., Canals, M., Sbaffi, L., Shackleton, N. J., Schonfeld, J. and Zahn, R. 2001. Variability of the western Mediterranean Sea surface temperature during the last 25,000 years and its connection with the Northern Hemisphere climatic changes. *Paleoceanography* 16, 40-52.

Castaneda, I. S., Werne, J. P. and Johnson, T. C. 2007. Wet and arid phases in the southeast African tropics since the Last Glacial Maximum. *Geology* 35, 823-826.

Clark, P. U., Dyke, A. S., Shakun, J. D., Carlson, A. E., Clark, J., Wohlfarth, B., Mitrovica, J. X., Hostetler, S. W. and McCabe, A. M. 2009. The Last Glacial Maximum. *Science* 325, 710-714.

Conley, D. J. and Schelske, C. L. 2002: Biogenic Silica. In Smol, J. P., Birks, H. J. B., Last, W. M., Bradley, R. S. and Alverson, K., editors, *Tracking Environmental Change Using Lake Sediments*: Springer Netherlands, 281-293.

Cullen, N. J., Mölg, T., Kaser, G., Hussein, K., Steffen, K. and Hardy, D. R. 2006. Kilimanjaro Glaciers: Recent areal extent from satellite data and new interpretation of observed 20th century retreat rates. *Geophysical research letters* 33.

Damsté, J. S. S., Ossebaar, J., Abbas, B., Schouten, S. and Verschuren, D. 2009. Fluxes and distribution of tetraether lipids in an equatorial African lake: Constraints on the application of the TEX86 palaeothermometer and BIT index in lacustrine settings. *Geochimica et Cosmochimica Acta* 73, 4232-4249.

Davison, W. 1993. Iron and manganese in lakes. *Earth-Science Reviews* 34, 119-163.

Dean, W. E. 1974. Determination of carbonate and organic matter in calcareous sediments and sedimentary rocks by loss on ignition; comparison with other methods. *Journal of Sedimentary Research* 44, 242-248.

deMenocal, P., Ortiz, J., Guilderson, T., Adkins, J., Sarnthein, M., Baker, L. and Yarusinsky, M. 2000. Abrupt onset and termination of the African Humid Period:: rapid climate responses to gradual insolation forcing. *Quaternary Science Reviews* 19, 347-361.

Dittrich, M. and Koschel, R. 2002. Interactions between calcite precipitation (natural and artificial) and phosphorus cycle in the hardwater lake. *Hydrobiologia* 469, 49-57.

Downie, C. and Wilkinson, P. 1972: *The Geology of Kilimanjaro*. Sheffield: The Department of Geology, The University of Sheffield.

Eggermont, H., Russell, J., Schettler, G., Van Damme, K., Bessems, I. and Verschuren, D. 2007. Physical and chemical limnology of alpine lakes and pools in the Rwenzori Mountains (Uganda–DR Congo). *Hydrobiologia* 592, 151-173.

Felton, A. A., Russell, J. M., Cohen, A. S., Baker, M. E., Chesley, J. I., Lezzar, K. E., McGlue, M. M., Pigati, J. S., Quade, J., Stager, J. C. and Tiercelin, J. J. 2007. Paleolimnological evidence for the onset and termination of glacial aridity from Lake Tanganyika, Tropical East Africa. *Palaeogeography Palaeoclimatology Palaeoecology* 252, 405-423.

Fleitmann, D., Burns, S. J., Mudelsee, M., Neff, U., Kramers, J., Mangini, A. and Matter, A. 2003. Holocene Forcing of the Indian Monsoon Recorded in a Stalagmite from Southern Oman. *Science* 300, 1737-1739.

Ganopolski, A., Rahmstorf, S., Petoukhov, V. and Claussen, M. 1998. Simulation of modern and glacial climates with a coupled global model of intermediate complexity. *Nature* 391, 351-356.

Garcin. 2007. Abrupt resumption of the African Monsoon at the Younger Dryas - Holocene climatic transition. *Quarternary Science Reviews*, 15.

Gasse. 2002. Kilimanjaro`s Secrets Revealed. *Science* 298, 2.

Gasse, F. 2000. Hydrological changes in the African tropics since the Last Glacial Maximum. *Quaternary Science Reviews* 19, 189-211.

Gasse, F., Chalie, F., Vincens, A., Williams, M. A. J. and Williamson, D. 2008. Climatic patterns in equatorial and southern Africa from 30,000 to 10,000 years ago reconstructed from terrestrial and near-shore proxy data. *Quaternary Science Reviews* 27, 2316-2340.

Gasse, F., Ledee, V., Massault, M. and Fontes, J.-C. 1989. Water-level fluctuations of Lake Tanganyika in phase with oceanic changes during the last glaciation and deglaciation. *Nature* 342, 57-59.

Goddard, L. and Graham, N. E. 1999. Importance of the Indian Ocean for simulating rainfall anomalies over eastern and southern Africa. *J. Geophys. Res.* 104, 19099-19116.

Grootes, P. M., Stuiver, M., White, J. W. C., Johnsen, S. and Jouzel, J. 1993. Comparison of Oxygen-Isotope Records from the Gisp2 and Grip Greenland Ice Cores. *Nature* 366, 552-554.

Gupta. 2003. Abrupt changes in the Asian southwest monsoon during the Holocene and their links to the North Atlantic Ocean. *Nature* 421, 4.

Gupta, A. K., Anderson, D. M. and Overpeck, J. T. 2003. Abrupt changes in the Asian southwest monsoon during the Holocene and their links to the North Atlantic Ocean. *Nature* 421, 354-357.

Hastenrath, S. and Polzin, D. 2004. Dynamics of the surface wind field over the equatorial Indian Ocean. *Quarterly Journal of the Royal Meteorological Society* 130, 503-517.

Hastenrath, S., Polzin, D. and Camberlin, P. 2004. Exploring the Predictability of the 'Short Rains" at the Coast of East Africa. *International Journal of climatology* 24, 1333-1343.

Haug, G. H., Hughen, K. A., Sigman, D. M., Peterson, L. C. and Rohl, U. 2001. Southward Migration of the Intertropical Convergence Zone Through the Holocene. *Science* 293, 1304-1308.

Held, I. M. and Soden, B. J. 2006. Robust responses of the hydrological cycle to global warming. *Journal of Climate* 19, 5686-5699.

Hopmans, E. C., Weijers, J. W. H., Schefuß, E., Herfort, L., Sinninghe Damsté, J. S. and Schouten, S. 2004. A novel proxy for terrestrial organic matter in sediments based on branched and isoprenoid tetraether lipids. *Earth and Planetary Science Letters* 224, 107-116.

Hughen. 1996. Rapid climate changes in the tropical atlantic region during the last deglaciation. *Nature* 380, 4.

IAEA. 1992: Statistical treatment of data on environmental isotopes in precipitation.

Johnson. 2002. A high resolution Paleoclimate Record spanning the past 25,000 years in southern east africa. *Science* 296, 4.

Johnson, T. C., Brown, E. T., McManus, J., Barry, S., Barker, P. and Gasse, F. 2002. A High-Resolution Paleoclimate Record Spanning the Past 25,000 Years in Southern East Africa. *Science* 296, 113-132.

Justino, F. and Peltier, W. R. 2008. Climate anomalies induced by the arctic and antarctic oscillations: Glacial maximum and present-day perspectives. *Journal of Climate* 21, 459-475.

Kalnay, E., Kanamitsu, M., Kistler, R., Collins, W., Deaven, D., Gandin, L., Iredell, M., Saha, S., White, G., Woollen, J., Zhu, Y., Chelliah, M., Ebisuzaki, W., Higgins, W., Janowiak, J., Mo, K. C., Ropelewski, C., Wang, J., Leetmaa, A., Reynolds, R., Jenne, R. and Joseph, D. 1996. The NCEP/NCAR 40-year reanalysis project. *Bulletin of the American Meteorological Society* 77, 437-471.

Kaplan, A., Cane, M. A., Kushnir, Y., Clement, A. C., Blumenthal, M. B. and Rajagopalan, B. 1998. Analyses of global sea surface temperature 1856-1991. *J. Geophys. Res.* 103, 18567-18589.

Kaser. 2004. Modern glacier retreat on kilimanjaro as evidence of climate change:observations and facts. *International Journal of climatology* 24, 10.

Kaser, G. K., G., Molg, T., Cullen, N. J., Hardy, D. R. and Winkler, M. 2010. Is the decline of ice on Kilimanjaro unprecedented in the Holocene? *Holocene* 20, 1079-1091.

Kiladis, G. N. and Diaz, H. F. 1989. Global Climatic Anomalies Associated with Extremes in the Southern Oscillation. *Journal of Climate* 2, 1069-1090.

Kutzbach, J. E. and Street-Perrott, F. A. 1985. Milankovitch forcing of fluctuations in the level of tropical lakes from 18 to 0 kyr BP. *Nature* 317, 130-134.

Lamb, A. L., Leng, M. J., Umer Mohammed, M. and Lamb, H. F. 2004. Holocene climate and vegetation change in the Main Ethiopian Rift Valley, inferred from the composition (C/N and [delta]13C) of lacustrine organic matter. *Quaternary Science Reviews* 23, 881-891.

Latif, M., Dommenget, D., Dima, M. and Grötzner, A. 1999. The role of Indian Ocean sea surface temperature in forcing east African rainfall anomalies during December-January 1997/98. *Journal of Climate* 12, 3497-3504.

Leng, M. J. and Barker, P. A. 2006. A review of the oxygen isotope composition of lacustrine diatom silica for palaeoclimate reconstruction. *Earth-Science Reviews* 75, 5-27.

Leng, M. J. and Sloane, H. J. 2008. Combined oxygen and silicon isotope analysis of biogenic silica. *Journal of Quaternary Science* 23, 313-319.

Levi, C., Labeyrie, L., Bassinot, F., Guichard, F., Cortijo, E., Waelbroeck, C., Caillon, N., Duprat, J., de Garidel-Thoron, T. and Elderfield, H. 2007. Low-latitude hydrological cycle and rapid climate changes during the last deglaciation. *Geochemistry Geophysics Geosystems* 8, -.

McGee, D., Broecker, W. S. and Winckler, G. 2010. Gustiness: The driver of glacial dustiness? *Quaternary Science Reviews* 29, 2340-2350.

Mckenzie, J. M., Mark, B. G., Thompson, L. G., Schotterer, U. and Lin, P. N. 2010. A hydrogeochemical survey of Kilimanjaro (Tanzania): implications for water sources and ages. *Hydrogeology Journal* 18, 985-995.

Meyer, H., Schonicke, L., Wand, U., Hubberten, H. W. and Friedrichsen, H. 2000. Isotope studies of hydrogen and oxygen in ground ice - Experiences with the equilibration technique. *Isotopes in Environmental and Health Studies* 36, 133-149.

Milne, I. 2007: Climate and Environmental change inferred from diatom communities in Lake Challa (Kenya/Tanzania). Kingston: Queen's University, 100.

Moernaut, J., Verschuren, D., Charlet, F., Kristen, I., Fagot, M. and De Batist, M. 2010. The seismic-stratigraphic record of lake-level fluctuations in Lake Challa: Hydrological stability and change in equatorial East Africa over the last 140 kyr. *Earth and Planetary Science Letters* 290, 214-223.

Mölg, T., Hardy, D. R., Cullen, N. J. and Kaser, G. 2005: Tropical glaciers in the context of climate change and society: Focus on Kilimanjaro (East Africa). In Earth and Atmospheric Science, U. o. I., editor, *Contribution to Wengen 2004 Workshop: Mountain Glaciers and Society*, Innsbruck, 28.

Moy, C. M., Seltzer, G. O., Rodbell, D. T. and Anderson, D. M. 2002. Variability of El Niño/Southern Oscillation activity at millennial timescales during the Holocene epoch. *Nature* 420, 162-165.

Nicholson, S. E. 1996: A Review of Climate Dynamics and Climate Variability in Eastern Africa. In Johnson, T. C. and Odada, E. O., editors, *The Limnology, Climatology and Paleoclimatology of the East African Lakes*, Amsterdam: Gordon and Breach, 25-56.

Nicholson, S. E. 2000. The nature of rainfall variability over Africa on time scales of decades to millenia. *Global and planetary Change* 26, 137-158.

Nowaczyk, N. R., Minyuk, P., Melles, M., Brigham-Grette, J., Glushkova, O., Nolan, M., Lozhkin, A. V., Stetsenko, T. V., Andersen, P. M. and Forman, S. L. 2002. Magnetostratigraphic results from impact crater Lake El'gygytgyn, northeastern Siberia: a 300 kyr long high-resolution terrestrial palaeoclimatic record from the Arctic. *Geophysical Journal International* 150, 109-126.

Otto-Bliesner, B. L., Brady, E. C., Clauzet, G., Tomas, R., Levis, S. and Kothavala, Z. 2006. Last Glacial Maximum and Holocene Climate in CCSM3. *Journal of Climate* 19, 2526-2544.

Paillard, D., Labeyrie, L. and Yiou, P. 1996. Macintosh Program performs time-series analysis. *Eos Transactions. AGU* 77, 379.

Parkhurst, D. L. and Appelo, C. A. J. 1999. User's guide to PHREEQC (Version 2)-a computer program for speciation, batch-reaction, one-dimensional transport, and inverse geochemical calculations. *U.S. Geological Survey, Water-Resources Investigations Report* 312.

Parry, M. L. and Intergovernmental Panel on Climate Change. Working Group II., editors. 2007: *Climate change 2007 : impacts, adaptation and vulnerability : contribution of Working Group II to the fourth assessment report of the Intergovernmental Panel on Climate Change*. Cambridge, U.K. ; New York: Cambridge University Press.

Payne, B. R. 1970. Water Balance of Lake Chala and its Relation to Groundwater from Tritium and stable isotope data. *Journal of Hydrology* 11, 11.

Petters, S. W. 1991: *Regional Geology of Africa*. Berlin - Heidelberg: Springer-Verlag.

Pilskaln, C. H. and Johnson, T. C. 1991. Seasonal Signals in Lake Malawi Sediments. *Limnology and Oceanography* 36, 544-557.

Rasmussen, S. O., Andersen, K. K., Svensson, A. M., Steffensen, J. P., Vinther, B. M., Clausen, H. B., Siggaard-Andersen, M. L., Johnsen, S. J., Larsen, L. B., Dahl-Jensen, D., Bigler, M., Rothlisberger, R., Fischer, H., Goto-Azuma, K., Hansson, M. E. and Ruth, U. 2006. A new Greenland ice core chronology for the last glacial termination. *Journal of Geophysical Research-Atmospheres* 111.

Rayner, N. A., Parker, D. E., Horton, E. B., Folland, C. K., Alexander, L. V., Rowell, D. P., Kent, E. C. and Kaplan, A. 2003. Global analyses of sea surface temperature, sea ice, and night marine air temperature since the late nineteenth century. *Journal of Geophysical Research-Atmospheres* 108.

Richardson, J. L. and Dussinger, R. A. 1986. Paleolimnology of mid-elevation lakes in the Kenya Rift Valley. *Hydrobiologia* 143, 167-174.

Röhl, U. and Abrams, L. J. 2000: High-resolution, downhole, and nondestructive core measurements from sites 999 and 1001 in the Caribbean Sea: Application to the late Paleocene Thermal Maximum. In Leckie, R. M., Sigurdsson, H., Acton, G. D. and Draper, G., editors, *Proceedings of the Ocean Drilling Program, Scientific Results*, College Station,TX, USA: Ocean Drilling Program, 191-203.

Ropelewski, C. F. and Halpert, M. S. 1987. Global and Regional Scale Precipitation Patterns Associated with the El Niño/Southern Oscillation. *Monthly Weather Review* 115, 1606-1626.

Ropelewski, C. F. and Jones, P. D. 1987. An Extension of the Tahiti-Darwin Southern Oscillation Index. *Monthly Weather Review* 115, 2161-2165.

Rozanski, K., Araguasaraguas, L. and Gonfiantini, R. 1992. Relation between Long-Term Trends of O-18 Isotope Composition of Precipitation and Climate. *Science* 258, 981-985.

Russell, J. M. and Johnson, T. C. 2005. A high-resolution geochemical record from Lake Edward, Uganda Congo and the timing and causes of tropical African drought during the late Holocene. *Quaternary Science Reviews* 24, 1375-1389.

Russell, J. M., Verschuren, D. and Eggermont, H. 2007. Spatial complexity of 'Little Ice Age' climate in East Africa: sedimentary records from two crater lake basins in western Uganda. *The Holocene* 17, 183-193.

Saji, N. H., Goswami, B. N., Vinayachandran, P. N. and Yamagata, T. 1999. A dipole mode in the tropical Indian Ocean. *Nature* 401, 360-363.

Schettler, G. and Albéric, P. 2008. Laghi di Monticchio (Southern Italy, Region Basilicata): genesis of sediments—a geochemical study. *Journal of Paleolimnology* 40, 529-556.

Schulz, H., von Rad, U. and Erlenkeuser, H. 1998. Correlation between Arabian Sea and Greenland climate oscillations of the past 110,000 years. *Nature* 393, 54-57.

Shanahan, T. M., Overpeck, J. T., Anchukaitis, K. J., Beck, J. W., Cole, J. E., Dettman, D. L., Peck, J. A., Scholz, C. A. and King, J. W. 2009. Atlantic Forcing of Persistent Drought in West Africa. *Science* 324, 377-380.

Simmons, A., Uppala, S., Dee, D. and Kobayashi, S. 2007. ERA-Interim: New ECMWF reanalysis products from 1989 onwards. *ECMWF Newsletter* 110, 25-35.

Sonzogni, C., Bard, E. and Rostek, F. 1998. Tropical sea-surface temperatures during the last glacial period: A view based on alkenones in Indian Ocean sediments. *Quaternary Science Reviews* 17, 1185-1201.

Stager, J. C. and Mayewski, P. A. 1997. Abrupt early to mid-Holocene climatic transition registered at the equator and the poles. *Science* 276, 1834-1836.

Stager, J. C., Mayewski, P. A. and Meeker, L. D. 2002. Cooling cycles, Heinrich event 1, and the desiccation of Lake Victoria. *Palaeogeography, Palaeoclimatology, Palaeoecology* 183, 169-178.

Street-Perrott, F. A., Barker, P. A., Swain, D. L., Ficken, K. J., Wooller, M. J., Olago, D. O. and Huang, Y. 2007. Late Quaternary changes in ecosystems and carbon cycling on Mt. Kenya, East Africa: a landscape-ecological perspective based on multi-proxy lake-sediment influxes. *Quaternary Science Reviews* 26, 1838–1860.

Talbot, M. R. and Lærdal, T. 2000. The Late Pleistocene - Holocene palaeolimnology of Lake Victoria, East Africa, based upon elemental and isotopic analyses of sedimentary organic matter. *Journal of Paleolimnology* 23, 141-164.

Talling, J. F. 1966. The Annual Cycle of Stratification and Phytoplankton Growth in Lake Victoria (East Africa). *Internationale Revue der gesamten Hydrobiologie und Hydrographie* 51, 545-621.

Talling, J. F. and Talling, I. B. 1965. The Chemical Compositions of African Lake Waters. *Internationale Revue der gesamten Hydrobiologie und Hydrographie* 50, 421-463.

Taylor, S. R. 1964. Abundance of chemical elements in the continental crust: a new table. *Geochimica et Cosmochimica Acta* 28, 1273-1285.

Thompson, L. 2003. Tropical Glacier and Ice Core Evidence of Climate Change on Annual to Millenial Time Scales. *Climate Change* 59, 19.

Thompson, L. 2006. Abrupt tropical change: Past and present. *PNAS* 103, 8.

Thompson, L. G., Mosley-Thompson, E., Davis, M. E., Henderson, K. A., Brecher, H. H., Zagorodnov, V. S., Mashiotta, T. A., Lin, P.-N., Mikhalenko, V. N., Hardy, D. R. and Beer, J. 2002. Kilimanjaro Ice Core Records: Evidence of Holocene Climate Change in Tropical Africa. *Science* 298, 589-593.

Tierney, J. E. and Russell, J. M. 2007. Abrupt climate change in southeast tropical Africa influenced by Indian monsoon variability and ITCZ migration. *Geophysical research letters* 34.

Tierney, J. E., Russell, J. M., Huang, Y., Damste, J. S. S., Hopmans, E. C. and Cohen, A. S. 2008. Northern Hemisphere Controls on Tropical Southeast African Climate During the Past 60,000 Years. *Science* 322, 252-255.

Torrence, C. and Compo, G. P. 1998. A Practical Guide to Wavelet Analysis. *Bulletin of the American Meteorological Society* 79, 61-78.

Trauth, M. H., Maslin, M. A., Deino, A. L., Junginger, A., Lesoloyia, M., Odada, E. O., Olago, D. O., Olaka, L. A., Strecker, M. R. and Tiedemann, R. 2010. Human evolution in a variable environment: the amplifier lakes of Eastern Africa. *Quaternary Science Reviews* 29, 2981-2988.

Trenberth, K. E. 1997. The Definition of El Niño *Bulletin of the American Meteorological Society* 78, 2771-2777.

Tudhope, A. W., Chilcott, C. P., McCulloch, M. T., Cook, E. R., Chappell, J., Ellam, R. M., Lea, D. W., Lough, J. M. and Shimmield, G. B. 2001. Variability in the El Nino-Southern Oscillation Through a Glacial-Interglacial Cycle. *Science* 291, 1511-1517.

Verschuren, D., Laird, K. R. and Cumming, B. F. 2000. Rainfall and drought in equatorial east Africa during the past 1,100 years. *Nature* 403, 410-414.

Verschuren, D., Sinninghe Damste, J. S., Moernaut, J., Kristen, I., Blaauw, M., Fagot, M. and Haug, G. H. 2009. Half-precessional dynamics of monsoon rainfall near the East African Equator. *Nature* 462, 637-641.

Vuille, M., Werner, M., Bradley, R. S., Chan, R. Y. and Keimig, F. 2005. Stable isotopes in East African precipitation record Indian Ocean zonal mode. *Geophys. Res. Lett.* 32.

Walker, M. J. C., Bjorck, S., Lowe, J. J., Cwynar, L. C., Johnsen, S., Knudsen, K. L., Wohlfarth, B. and Grp, I. 1999. Isotopic 'events' in the GRIP ice core: a stratotype for the Late Pleistocene. *Quaternary Science Reviews* 18, 1143-1150.

Wang, Y., Cheng, H., Edwards, R. L., He, Y., Kong, X., An, Z., Wu, J., Kelly, M. J., Dykoski, C. A. and Li, X. 2005. The Holocene Asian Monsoon: Links to Solar Changes and North Atlantic Climate. *Science* 308, 854-857.

Wang, Y. J., Cheng, H., Edwards, R. L., An, Z. S., Wu, J. Y., Shen, C.-C. and Dorale, J. A. 2001. A High-Resolution Absolute-Dated Late Pleistocene Monsoon Record from Hulu Cave, China. *Science* 294, 2345-2348.

Wani, S. P., Sreedevi, T. K., Rockström, J. and Ramakrishna, Y. S. 2009: *Rainfed Agriculture – Past Trends and Future Prospects*. Wallingford: CABI.

Weldeab, S., Schneider, R. R., Kolling, M. and Wefer, G. 2005. Holocene African droughts relate to eastern equatorial Atlantic cooling. *Geology* 33, 981-984.

Wetzel, R. G. 1983: *Limnology*. New York: Saunders College Publishing.

Yancheva. 2007. Influence of the intertropical convergence zone on the East Asian monsoon. *Nature* 445, 4.

Yeager, S. G., Shields, C. A., Large, W. G. and Hack, J. J. 2006. The low-resolution CCSM3. *Journal of Climate* 19, 2545-2566.

Yuan, D. X., Cheng, H., Edwards, R. L., Dykoski, C. A., Kelly, M. J., Zhang, M. L., Qing, J. M., Lin, Y. S., Wang, Y. J., Wu, J. Y., Dorale, J. A., An, Z. S. and Cai, Y. J. 2004. Timing, duration, and transitions of the Last Interglacial Asian Monsoon. *Science* 304, 575-578.

8 Appendix

Table A. 8-1: Hydrochemical data set from Lake Challa a) 23 August 2007, 6 pm, b) 28 November 2007.

a)

depth (m)	Na (mg/l)	K (mg/l)	Ca (mg/l)	Mg (mg/l)	Fe (mg/l)	Mn (mg/l)	Sr (mg/l)	Ba (mg/l)	F (mg/l)	Cl (mg/l)
0	19.3	5.8	19.2	21.2	0.008	0.001	0.228	0.006	0.20	9.9
5	20.2	6.4	19.8	22.2	0.010	0.003	0.235	0.007	0.27	9.8
10	19.8	6.2	19.6	22.3	0.006	0.002	0.233	0.006	0.31	9.8
15	19.5	6.1	19.5	22.1	0.007	0.001	0.229	0.006	0.30	9.7
20	19.4	5.9	19.4	22.3	0.005	0.001	0.228	0.006	0.27	9.9
30	20.0	6.1	20.2	23.3	0.044	0.002	0.236	0.008	0.28	9.8
40	19.6	5.8	19.9	23.3	0.006	0.001	0.232	0.006	0.27	9.8
50	19.0	6.1	22.7	22.7	0.032	0.091	0.235	0.009	0.23	9.6
60	19.2	5.9	31.3	23.9	0.070	0.104	0.264	0.010	0.32	9.1
70	18.8	6.2	36.7	23.5	0.065	0.111	0.272	0.011	0.26	9.3
80	18.7	5.7	38.4	24.2	0.070	0.112	0.279	0.011	0.25	8.8

depth (m)	DIC (mg/l)	H_2CO_3* (mg/l)	HCO_3^- (mg/l)	CO_3^{2-} (mg/l)	SO_4 (mg/l)	SRP (mg/l)	NPOC (mg/l)	NH_4 (mg/l)	NO_3 (mg/l)	Si (mg/l)	TDS (mg/l)
0	38.4	0.25	37.55	0.559	3.1	<0.005	6.7	<0.025	0.28	20.7	138.3
5	38.2	0.25	37.37	0.556	3.2	<0.005	3.9	<0.025	<0.2	20.6	140.8
10	38.2	0.26	37.40	0.532	3.4	<0.005	3.0	<0.025	<0.2	20.9	140.9
15	38.4	0.28	37.63	0.511	2.8	<0.005	2.8	<0.025	<0.2	20.5	139.2
20	37.5	0.41	36.80	0.332	3.2	<0.005	2.8	<0.025	1.5	20.8	140.5
30	38.3	0.47	37.54	0.302	3.3	<0.005	1.8	<0.025	2.0	20.6	144.2
40	38.8	0.62	37.95	0.238	3.0	<0.005	1.5	<0.025	<0.2	21.1	141.9
50	41.9	1.91	39.91	0.087	2.0	0.029	1.5	0.77	2.1	21.6	149.2
60	48.0	4.36	43.64	0.048	1.2	0.160	1.6	2.32	0.34	24.9	167.0
70	53.0	5.92	47.06	0.042	1.2	0.288	1.8	3.97	0.51	28.4	182.4
80	53.8	7.36	46.43	0.034	<0.3	0.325	1.7	4.43	<0.2	28.4	183.5

b)

depth (m)	Na (mg/l)	K (mg/l)	Ca (mg/l)	Mg (mg/l)	Fe (mg/l)	Mn (mg/l)	Sr (mg/l)	Ba (mg/l)	F (mg/l)	Cl (mg/l)
0	22.4	6.7	21.7	22.8	<0.01	0.001	0.256	0.005	0.25	10.3
10	22.2	6.6	21.5	22.7	<0.01	0.001	0.256	0.005	0.31	10.4
20	21.4	6.4	21.1	22.3	<0.01	0.001	0.254	0.005	0.31	10.1
40	21.0	6.3	22.0	21.9	<0.01	0.006	0.248	0.006	0.28	9.4
60	20.8	6.5	33.4	22.3	0.01	0.103	0.284	0.010	0.30	9.2
80	21.8	6.7	21.7	22.9	<0.01	0.002	0.259	0.005	0.31	10.3
90	21.0	6.9	22.3	22.1	<0.01	0.006	0.252	0.006	0.23	9.8
95	21.8	6.9	22.4	22.6	0.014	0.004	0.256	0.006	0.27	10.3

depth (m)	DIC (mg/l)	H_2CO_3* (mg/l)	HCO_3^- (mg/l)	CO_3^{2-} (mg/l)	SO_4 (mg/l)	SRP (mg/l)	NH_4 (mg/l)	NO_3 (mg/l)	Si (mg/l)	TDS (mg/l)
0	40.0	0.06	37.71	2.224	2.9	n.a.	<0.025	0.09	21.2	148.7
10	40.0	0.06	37.51	2.426	3.2	<0.005	<0.025	<0.2	22.5	149.6
20	39.0	0.09	37.38	1.562	2.6	<0.005	<0.025	<0.2	20.4	144.0
40	39.1	0.53	38.27	0.281	2.9	<0.005	<0.025	<0.2	21.8	145.0
60	45.7	1.71	43.84	0.117	1.8	0.138	<0.025	9.3	26.0	175.8
80	40.6	0.06	38.22	2.360	3.1	<0.005	<0.025	0.18	20.4	148.3
90	39.7	0.63	38.81	0.243	2.7	<0.005	0.19	<0.2	20.3	147.5
95	39.9	0.24	39.06	0.652	2.7	<0.005	<0.025	<0.2	20.7	148.1

n.a.: not analysed

Table A. 8-2: Results from XRF analyses of selected source rocks and corresponding soil samples (all collected within 30 km around Lake Challa). Element ratios refer to mass ratios calculated from the oxide content (wt. % / wt .%).

sample description	SiO_2	TiO_2	Al_2O_3	Fe_2O_3	MnO	MgO	CaO	Na_2O	K_2O	P_2O_5	H_2O	CO_2	Σ	Ca/Al	Si/Al	Mn/Fe	Ti/Al	Fe/Al	Mn/Al	Mg/Al	Al2O3/TiO2
unweathered grits (Challa)	35.9	4.0	9.7	14.2	0.21	8.5	15.9	1.5	0.7	0.9	2.7	4.7	99.1	2.2	3.3	0.017	0.47	1.9	0.03	1.0	2.4
weathered grits (crater rim)	39.9	4.3	11.0	15.5	0.23	8.5	11.0	1.4	2.1	1.1	3.6	0.7	99.4	1.4	3.2	0.017	0.44	1.9	0.03	0.9	2.6
soil on grits (crater rim)	38.1	4.2	11.0	14.0	0.21	8.3	11.3	0.4	1.1	0.8	6.0	4.0	99.4	1.4	3.1	0.016	0.43	1.7	0.03	0.9	2.6
local lava (crater rim)	40.7	3.3	11.1	12.9	0.19	12.2	13.0	1.8	0.7	0.6	2.2	0.6	99.3	1.6	3.2	0.016	0.33	1.5	0.03	1.3	3.4
soil on lava (crater rim)	41.2	4.0	11.7	14.7	0.22	7.2	9.9	1.9	1.8	0.9	3.6	2.3	99.4	1.1	3.1	0.016	0.39	1.7	0.03	0.7	2.9
pumice peaces (crater rim)	39.4	3.3	11.8	13.4	0.20	12.5	13.5	0.6	0.5	0.6	3.2	0.5	99.5	1.6	3.0	0.017	0.32	1.5	0.03	1.2	3.5
soil on pumice (crater rim)	38.3	3.8	11.2	13.5	0.20	10.5	9.8	0.8	0.8	0.6	5.3	4.6	99.4	1.2	3.0	0.016	0.39	1.6	0.03	1.1	2.9
unweathered basalt	44.9	3.8	15.2	14.1	0.19	5.3	8.3	3.3	1.7	0.7	1.8	0.2	99.5	0.7	2.6	0.015	0.28	1.2	0.02	0.4	4.0
unweathered basalt (foot of Challa)	45.5	3.8	16.1	13.6	0.19	4.6	8.7	3.3	1.5	0.8	1.3	0.1	99.5	0.7	2.5	0.015	0.27	1.1	0.02	0.3	4.3
soil on basalt	40.5	4.3	13.1	17.2	0.24	7.7	8.2	1.7	1.4	0.7	3.1	1.3	99.4	0.8	2.7	0.015	0.37	1.7	0.03	0.7	3.0
sand of pool in rivine*	34.0	4.7	16.1	17.9	0.25	3.3	4.5	0.3	0.8	0.9	9.0	7.8	99.5	0.4	1.9	0.016	0.33	1.5	0.02	0.2	3.4
sand/clay from dry river bed (foot of Challa)	33.2	5.4	17.6	22.1	0.30	2.8	1.6	0.1	0.3	0.5	10.1	5.5	99.5	0.1	1.7	0.015	0.35	1.7	0.03	0.2	3.3
fsp rich gneiss (Reata Mt.)	75.4	0.1	12.6	1.74	0.07	0.2	0.9	2.0	5.8	0.0	0.7	0.1	99.7	0.1	5.3	0.046	0.01	0.2	0.01	0.0	90.9
soil on fsp rich gneiss	60.0	1.6	13.4	6.91	0.11	1.1	2.5	1.9	3.3	0.2	3.1	5.6	99.6	0.3	4.0	0.017	0.13	0.7	0.01	0.1	8.4
banded gneiss (Reata Mt.)	77.3	0.1	12.4	0.70	0.00	0.0	0.6	3.2	4.8	0.0	0.7	0.0	99.9	0.1	5.5	0.002	0.00	0.1	0.00	0.0	234.5
soil on banded gneiss	58.0	1.7	17.2	8.78	0.15	1.0	3.1	2.6	2.2	0.2	3.2	1.5	99.5	0.2	3.0	0.019	0.11	0.7	0.01	0.1	9.9
soil from Challa	37.2	4.2	16.7	15.8	0.24	3.2	7.2	0.7	1.2	0.7	7.1	5.2	99.5	0.6	2.0	0.017	0.29	1.3	0.02	0.2	3.9
soil from Challa village	41.2	4.0	17.3	15.5	0.25	3.0	4.1	0.2	1.1	0.7	8.3	3.8	99.5	0.3	2.1	0.018	0.26	1.2	0.02	0.2	4.4
UCC (Rudnick& Gao(2004)		0.6	15.4	2.0	0.10	2.5	3.6	3.3	2.8	0.2											

Table A. 8-3: Trap deployment periods, main components of sediment trap samples and results from ICP-AES analysis for selected elements.

a)

Date	sample desciption			Al	Al_2O_3	Siliclastic	Be	Ca	Fe	K	La	Mg	Mn	Na	P	S	Sc	Sr	Ti	TiO_2	V
	calcite	organic	diatoms	(µg/g)	%	%	(µg/g)	(µg/g)	(µg/g)	(µg/g)	(µg/g	(µg/g)	(µg/g)	(µg/g)	(µg/g)	(µg/g)	(µg/g)	(µg/g)	(µg/g)	%	(µg/g)
30.12.2006	x			29624	5.6	35.9	0.3	280339	12214	1533	DL	18469	250	993	1953	2127	2	845.7	2716	0.5	14
10.02.2007	x			40945	7.7	49.6	0.1	320964	2673	446	1.4	15245	44	373	3692	1471	0	833.6	530	0.1	4
28.02.2007	x			22020	4.2	26.7	0.1	306882	6794	816	3.7	16339	86	582	905	1579	1	835.0	1288	0.2	9
31.03.2007	x			18878	3.6	22.9	0.4	212233	12111	1784	9.8	12463	205	544	2248	3530	2	604.6	2469	0.4	27
30.04.2007		x		n.a.	n.a.	n.a.	n.a.	n.a.	n.a.	n.a.	n.a.	n.a.	n.a.	n.a.	n.a.	n.a.	n.a.	n.a.	n.a.	n.a.	n.a.
04.06.2007		x	x	20974	4.0	25.4	1	34524	19913	2788	19.5	8952	221	1455	4106	7503	5	258	4633	0.8	37
30.06.2007		x	x	17308	3.3	21.0	0.8	64292	18319	2388	15.4	9029	1675	766	5124	7625	4	339.3	4092	0.7	29
31.07.2007		x		n.a.	n.a.	n.a.	n.a.	n.a.	n.a.	n.a.	n.a.	n.a.	n.a.	n.a.	n.a.	n.a.	n.a.	n.a.	n.a.	n.a.	n.a.
24.08.2007			x	23787	4.5	28.8	0.5	29823	22815	2825	14.9	8390	8515	2146	5870	4294	4	214.0	4731	0.8	40
28.09.2007			x	17921	3.4	21.7	0	3792	7742	1001	5.3	2264	263	415	2584	3544	2	44	1706	0.3	17
30.10.2007			x	21317	4.0	25.8	1	46818	20028	4654	17.8	11266	346	2397	5302	7345	4	430	4448	0.7	32
01.12.2007	x			n.a.	n.a.	n.a.	n.a.	n.a.	n.a.	n.a.	n.a.	n.a.	n.a.	n.a.	n.a.	n.a.	n.a.	n.a.	n.a.	n.a.	n.a.
31.12.2007	x			n.a.	n.a.	n.a.	n.a.	n.a.	n.a.	n.a.	n.a.	n.a.	n.a.	n.a.	n.a.	n.a.	n.a.	n.a.	n.a.	n.a.	n.a.
30.01.2008	x			16719	3.2	20.3	0.7	53871	18389	3764	17.5	7895	401	1496	4426	7506	4	501.6	4142	0.7	35
29.02.2008		x	x	18580	3.5	22.5	1	73528	26167	3861	23.0	10002	442	1453	4576	6857	6	524	5834	1.0	52
31.03.2008		x	x	21400	4.0	25.9	4.4	6718	114902	3552	123.3	4886	1114	743	7677	1075	35	123.5	30209	5.0	162
30.04.2008		x		19372	3.7	23.5	4.3	9844	102416	3181	122.3	4943	465	556	5984	1011	34	146.9	28908	4.8	189

n.a.: not analysed; DL: under Detection limit; *: CaCO3+MgCO3; **without TOC/P<60

Appendix

b)

Date	Y	Zr	CaCO3*	Al2O3/TiO2	La/Y	Mn/Fe	Ti/Fe	TOC	IOC	Mn/Ti	Fe/Ti	Al/Ti	Ca/Sr	CaCO3(Ca/Al)	Al/Fe	TOC **	P**	S**	Ti/Al**	Fe/Al **
	(µg/g)	(µg/g)						%						Ca/Al=0.25						
30.12.2006	3	5	76.5	12.4		0.02	0.22	7.01	9.3	0.09	4.5	10.91	331.5	68.1	2.4	7.01	1953	2127	0.09	0.41
10.02.2007	2	2	85.6	87.5	0.9	0.02	0.20	5.98	10.5	0.08	5.0	77.22	385.0	77.5	15.3					
28.02.2007	2	24	82.4	19.4	1.5	0.01	0.19	6.35	10.1	0.07	5.3	17.10	367.5	75.2	3.2	6.35	905	1579	0.06	0.31
31.03.2007	6	52	57.4	8.7	1.7	0.02	0.20	15.16	7.6	0.08	4.9	7.64	351.0	51.8	1.6	15.16	2248	3530	0.13	0.64
30.04.2007	n.a.	n.a.	n.a.	n.a.	n.a.	n.a.	n.a.	22.55	3.6	n.a.	n.a.	n.a.	n.a.	n.a.	n.a.					
04.06.2007	7	85	12	5.1	3.0	0.01	0.23	31.14	1.2	0.05	4.3	4.53	133.6	7.3	1.1	31.14	4106	7503	0.22	0.95
30.06.2007	5	70	19.2	4.8	3.1	0.09	0.22	27.37	3.6	0.41	4.5	4.23	189.5	15.0	0.9	27.37	5124	7625	0.24	1.06
31.07.2007	n.a.	n.a.	n.a.	n.a.	n.a.	n.a.	n.a.	28.30	1.5	n.a.	n.a.	n.a.	n.a.	n.a.	n.a.					
24.08.2007	5	64	10.4	5.7	3.3	0.37	0.21	DL	DL	1.80	4.8	5.03	139.4	6.0	1.0					
28.09.2007	2	4	2	11.9	2.5	0.03	0.22	10.70	1.1	0.15	4.5	10.50	86.6	DL	2.3	10.70	2584	3544	0.10	0.43
30.10.2007	6	14	16	5.4	2.8	0.02	0.22	17.19	1.1	0.08	4.5	4.79	108.9	10.4	1.1	17.19	5302	7345	0.21	0.94
01.12.2007	n.a.	n.a.	n.a.	n.a.	n.a.	n.a.	n.a.	n.a.	n.a.	n.a.	n.a.	n.a.	n.a.	n.a.	n.a.					
31.12.2007	n.a.	n.a.	n.a.	n.a.	n.a.	n.a.	n.a.	19.77	1.9	n.a.	n.a.	n.a.	n.a.	n.a.	n.a.					
30.01.2008	6	12	16.2	4.6	2.8	0.02	0.23	21.21	2.0	0.10	4.4	4.04	107.4	12.4	0.9	21.21	4426	7506	0.25	1.10
29.02.2008	10	26	22	3.6	2.4	0.02	0.22	16.79	3.9	0.08	4.5	3.18	140.4	17.2	0.7	16.79	4576	6857	0.31	1.41
31.03.2008	41	445	3.4	0.8	3.0	0.01	0.26	2.68	0.4	0.04	3.8	0.71	54.4	0.3	0.2					
30.04.2008	38	442	4.2	0.8	3.2	0.00	0.28	3.00	0.8	0.02	3.5	0.67	67.0	1.2	0.2					

n.a.: not analysed; DL: under Detection limit; *: CaCO3+MgCO3; **without TOC/P<60

Appendix

c)

Date	sample desciption			Al	Al_2O_3	Siliclastic	Be	Ca	Fe	K	La	Mg	Mn	Na	P	S	Sc	Sr	Ti	TiO_2	V
	calcite	organic	diatoms	(µg/g)	%	%	(µg/g)	(µg/g)	(µg/g)	(µg/g)	(µg/g	(µg/g)	(µg/g)	(µg/g)	(µg/g)	(µg/g)	(µg/g)	(µg/g)	(µg/g)	%	(µg/g)
31.05.2008		x	x	18733	3.5	22.7	3.0	30367	65363	6997	75.2	8563	1096	3511	6591	5764	22	262.8	17872	3.0	125
30.06.2008		x	x	23440	4.4	28.4	0.5	42336	12421	1233	12.6	5207	5377	394	2593	2928	4	179.2	2681	0.4	16
31.07.2008		x	x	17678	3.3	21.4	0.1	2605	2947	651	1.9	1525	425	721	2077	2852	1	26.9	342	0.1	10
31.08.2008			x	17181	3.2	20.8	0.1	1573	1491	230	0.7	761	81	201	1124	2345	0	13.4	177	0.0	7
30.09.2008			x	23446	4.4	28.4	0.3	9397	16472	1468	10.5	7351	227	810	1639	2617	4	150.3	3829	0.6	27
31.10.2008			x	21040	4.0	25.5	0.4	13372	14467	1917	11.6	4740	269	824	2239	3205	4	133.3	3295	0.5	19
30.11.2008	x		x	33247	6.3	40.3	0.2	253670	4601	503	4.4	9808	70	332	899	1074	1	620.2	1010	0.2	6
20.12.2008	x			28041	5.3	34.0	2.1	199522	102416	2591	60.4	12491	221	873	3793	1955	17	601.0	14811	2.5	75
30.01.2009	x			26821	5.1	32.5	0.5	241298	18023	1951	DL	13083	171	713	2108	2305	4	670.2	4118	0.7	33
28.02.2009	x	x	x	26414	5.0	32.0	0.6	178219	18173	2231	DL	11549	226	1161	1711	2325	4	649.5	3928	0.7	23
30.03.2009		x	x	16906	3.2	20.5	1.0	64195	28250	3682	23.1	8343	429	1183	2411	4696	7	272.2	6149	1.0	47
30.04.2009		x	x	18194	3.4	22.0	0.5	51327	15517	1950	10.0	5536	529	896	2567	5083	3	282.5	3431	0.6	22
30.05.2009		x	x	17980	3.4	21.8	0.5	103595	13592	2028	8.4	8221	275	1051	2679	6658	3	526.3	2951	0.5	20
30.06.2009	x	x	x	21144	4.0	25.6	1.0	16430	28809	3123	25.3	7601	459	1318	4372	8308	7	178.1	6622	1.1	52
30.07.2009	x	x	x	17690	3.3	21.4	1.3	44376	39203	3762	34.5	10057	6834	1657	12045	7755	9	318.2	8713	1.5	54
31.08.2009			x	17788	3.4	21.5	1.2	25017	34978	3688	29.4	8894	15090	1609	6404	9837	8	233.6	7207	1.2	50
30.09.2009			x	18031	3.4	21.8	0.6	5943	17007	1956	11.7	3455	1906	738	3200	5272	4	70.3	3382	0.6	23
30.10.2009			x	17591	3.3	21.3	0.3	119717	8628	1201	7.7	5994	323	518	1937	3353	2	303.7	1725	0.3	13
30.11.2009	x		x	17797	3.4	21.6	0.2	224177	7013	1056	5.7	10189	119	464	1308	2233	2	516.9	1408	0.2	10
27.12.2009	x		x	26531	5.0	32.1	0	318134	4113	519	3.3	14451	132	355	2273	1444	1	726	902	0.2	5
30.01.2010	x			35979	6.8	43.6	0.2	321879	5556	873	4.4	16175	171	367	2256	1206	1	711.2	1260	0.2	6

n.a.: not analysed; DL: under Detection limit; *: CaCO3+MgCO3; **without TOC/P<60

Appendix

d)

Date	Y (µg/g)	Zr (µg/g)	CaCO3*	Al2O3/TiO2	La/Y	Mn/Fe	Ti/Fe	TOC %	IOC	Mn/Ti	Fe/Ti	Al/Ti	Ca/Sr	CaCO3(Ca/Al) Ca/Al=0.25	Al/Fe	TOC **	P**	S**	Ti/Al**	Fe/Al **
31.05.2008	26	50	10.6	1.2	2.8	0.02	0.27	11.4	2.4	0.06	3.7	1.05	115.6	6.4	0.3					
30.06.2008	5	5	12.4	9.9	2.6	0.43	0.22	7.7	3.3	2.01	4.6	8.74	236.2	9.1	1.9	7.7	2593	2928	0.11	0.53
31.07.2008	1	4	1.2	58.5	1.6	0.14	0.12	5.0	0.8	1.24	8.6	51.62	96.8	DL	6.0	5.0	2077	2852	0.02	0.17
31.08.2008	1	3	0.7	109.7	1.0	0.05	0.12	4.9	1.1	0.46	8.4	96.82	117.4	DL	11.5	4.9	1124	2345	0.01	0.09
30.09.2008	4	14	4.9	6.9	2.8	0.01	0.23	5.7	0.5	0.06	4.3	6.12	62.5	0.9	1.4	5.7	1639	2617	0.16	0.70
31.10.2008	4	12	5.0	7.2	2.8	0.02	0.23	10.1	0.4	0.08	4.4	6.39	100.3	2.0	1.5	10.1	2239	3205	0.16	0.69
30.11.2008	3	9	66.9	37.3	1.5	0.02	0.22	7.5	8.5	0.07	4.6	32.93	409.0	61.2	7.2	7.5	899	1074	0.03	0.14
20.12.2008	20	93	54.3	2.1	3.1	0.00	0.14	9.1	4.1	0.01	6.9	1.89	332.0	48.0	0.3	9.1	3793	1955	0.53	3.65
30.01.2009	7	11	64.9	7.4		0.01	0.23	8.2	7.5	0.04	4.4	6.51	360.0	58.5	1.5	8.2	2108	2305	0.15	0.67
28.02.2009	6	10	48.6	7.6		0.01	0.22	10.1	7.6	0.06	4.6	6.73	274.4	42.8	1.5	10.1	1711	2325	0.15	0.69
30.03.2009	9	19	19.0	3.1	2.5	0.02	0.22	19.7	1.3	0.07	4.6	2.75	235.8	15.0	0.6	19.7	2411	4696	0.36	1.67
30.04.2009	5	51	14.8	6.0	2.1	0.03	0.22	24.9	4.9	0.15	4.5	5.30	181.7	11.7	1.2	24.9	2567	5083	0.19	0.85
30.05.2009	5	7	28.8	6.9	1.6	0.02	0.22	25.8	2.8	0.09	4.6	6.09	196.8	24.7	1.3	25.8	2679	6658	0.16	0.76
30.06.2009	8	11	6.8	3.6	3.2	0.02	0.23	29.9	3.3	0.07	4.4	3.19	92.2	2.8	0.7	29.9	4372	8308	0.31	1.36
30.07.2009	11	10	14.6	2.3	3.2	0.17	0.22	23.6	1.7	0.78	4.5	2.03	139.5	10.0	0.5					
31.08.2009	10	14	9.4	2.8	3.0	0.43	0.21	25.6	0.5	2.09	4.9	2.47	107.1	5.1	0.5	25.6	6404	9837	0.41	1.97
30.09.2009	5	5	2.7	6.0	2.5	0.11	0.20	17.9		0.56	5.0	5.33	84.6	0.4	1.1	17.9	3200	5272	0.19	0.94
30.10.2009	4	3	32.0	11.5	2.0	0.04	0.20	12.0	4.6	0.19	5.0	10.19	394.2	28.8	2.0	12.0	1937	3353	0.10	0.49
30.11.2009	3	5	59.6	14.3	2.0	0.02	0.20	8.3	6.2	0.08	5.0	12.64	433.7	54.8	2.5	8.3	1308	2233	0.08	0.39
27.12.2009	2	3	85	33.3	1.7	0.03	0.22	6.1	9.0	0.15	4.6	29.42	438.5	77.7	6.5	6.1	2273	1444	0.03	0.16
30.01.2010	3	12	86.1	32.4	1.7	0.03	0.23	5.1	9.3	0.14	4.4	28.56	452.6	78.1	6.5					

n.a.: not analysed; DL: under Detection limit; *: CaCO3+MgCO3; **without TOC/P<60